Investigation of Cellular Compartmentation of Brain Energy Metabolism using Genetically Encoded FRET Sensors

---

Dissertation

zur

Erlangung der naturwissenschaftlichen Doktorwürde

(Dr. sc. nat.)

vorgelegt der
Mathematisch-naturwissenschaftlichen Fakultät

der

Universität Zürich
von

Philipp Mächler

von Zürich

Promotionskomitee

Prof. Dr. Markus Rudin

(Vorsitz der Dissertation)

Prof. Dr. Bruno Weber

(Leitung der Dissertation)

Prof. Dr. med. Alfred Buck

Prof. Dr. Hanns Ulrich Zeilhofer

Zürich, 2016

List of content

Summary

Glucose is the main energy substrate for the mammalian brain. On a cellular level, however, lactate has been discussed as an alternative energy substrate for neurons since the astrocyte neuron lactate shuttle (ANLS) was hypothesized more than two decades ago. As brain energy metabolism is known to be highly dependent on neuronal activity *in vivo*, its properties should ideally be investigated in an intact organism with a sufficiently high temporal and spatial resolution. Specifically, measurements of concentrations and fluxes of the main metabolites glucose, lactate and pyruvate in single cells would allow to model the cellular compartmentation of brain energy metabolism.

To follow cellular metabolite levels in the living mouse, the glucose sensors *FLIPΔ6,* the lactate sensor *Laconic* and the pyruvate sensor *Pyronic* were expressed using adeno-associated viral vectors and recorded with two-photon laser scanning microscopy (*TPLSM*). In a first part of my MD-PhD project, astrocytic and neuronal *FLIPΔ6* signals were correlated to increasing blood and extracellular glucose levels, identifying the blood brain barrier as a main rate limiting transport obstacle and showing early saturation of glucose accumulation in neurons. Sensory stimulation induced only minor and variable changes on cellular glucose levels, while electrical intracortical stimulation induced a decrease of glucose signals in astrocytes but not in neurons. In the second part of my MD-PhD project, simultaneous *Laconic* measurements in astrocytes and neurons were used. We used intravenous pyruvate injections to trans-accelerate the efflux of lactate from brain-cells and found a lactate deprivation in astrocytes but not in neurons. Additionally, intravenous ammonium chloride injections allowed to increase brain lactate levels in order to saturate *Laconic*, what occurred at lower signal increases in astrocytes than in neurons. Both pronounced trans-acceleration and earlier saturation in astrocytes compared to neurons indicate higher baseline lactate levels in astrocytes, as it is expected from net-producers of lactate. Cortical microstimulation revealed a fast astrocytic lactate dip, followed by a large increase of astrocytic and neuronal lactate levels, which might indicate an active transport of lactate towards neurons during increased neuronal activation. The neuronal NH^{+}_{4} production during activation was mimicked by intravenous ammonium chloride that lead to astrocytic and neuronal lactate accumulation.

Altogether the combination of metabolic sensors with TPLSM was well suited to follow transients of astrocytic and neuronal glucose, lactate and pyruvate signals in the living mouse. More pronounced glucose transients and higher lactate levels in astrocytes compared to neurons support the ANLS hypothesis.

Zusammenfassung

Glukose ist das hauptsächliche Energiesubstrat für das Gehirn von Säugetieren. Auf zellulärer Ebene wird jedoch Laktat als alternatives Energie-tragendes Substrat für Neuronen gehandelt, seit vor mehr als zwei Jahrzehnten der Astrocyten-Neuronen Laktat Shuttle (ANLS) postuliert wurde. Da bekannt ist, dass der Energie-Stoffwechsel des Gehirn stark von der neuronalen Aktivität abhängt, sollte dessen Eigenschaften optimalerweise im intakten Organismus untersucht werden und zwar mit einer ausreichend hohen zeitlichen und örtlichen Auflösung. Messungen von Konzentrationen und Umsatzraten der zentralen Stoffwechselprodukte Glukose, Laktat und Pyruvat in einzelnen Zellen würden eine genauere Modellierung der zellulären Kompartimentierung des Energiestoffwechsels des Gehirns erlauben.

Um die zellulären Spiegel von Stoffwechselprodukten in der lebendigen Maus zu untersuchen, wurden der Glukose Sensor *FLIPΔ6*, der Laktat Sensor *Laconic* und der Pyruvat Sensor *Pyronic* mit Hilfe von adeno-assozierten, viralen Vektoren zell-spezifisch exprimiert und mittels Zweiphotonenmikroskopie (TPLSM) aufgenommen. In einem ersten Teil meines MD-PhD-Projektes wurden astrozytäre und neuronale *FLIPΔ6* Signale mit ansteigenden Glukose Spiegeln im Blut und im Extrazellulärraum korreliert, womit die Blut-Hirn-Schranke als hauptsächliches Fluss-limitierendes Transport-Hindernis identifiziert und eine frühe Saturierung der Glukose-Akkumulation in Neuronen gezeigt wurde. Sensorische Stimulation induzierte nur minimale und variable Änderungen der zellulären Glukosespiegel, während elektrische intrakortikale Stimulation ein Absinken der Glukose Signale in Astrozyten aber nicht in Neuronen bewirkte.

In einem zweiten Teil meines MD-PhD-Projektes wurden simultane *Laconic*-Messungen in Astrozyten und Neuronen verwendet. Wir nutzten intravenöse Pyruvat-Injektionen, um den Laktat-Export aus Hirnzellen zu trans-accelerieren und fanden einen Laktatentzug in Astrozyten aber nicht in Neuronen. Zudem erhöhten wir die Laktat-Spiegel des Gehirns durch intravenöse Ammoniumchlorid-Injektionen um damit *Laconic* zu sättigen, was in Astrozyten bei einem kleineren Signalanstieg stattfand als in Neuronen. Zusammengenommen können die verstärkte Trans-acceleration und frühere Saturierung in Astrozyten verglichen mit Neuronen mit einem höheren Basis-Laktatspiegel in Astrozyten erklärt werden, wie es von einem Netto-Laktatproduzent zu erwarten ist. Experimente mit kortikaler Mikrostimulation zeigten eine schnelle astrozytäre Laktat-Senke, welche von einem grossen Anstieg von astrozytären und neuronalen Laktatspiegeln gefolgt wurde. Dies könnte auf einen aktiven Transport von Laktat in Richtung Neuronen während verstärkter neuronaler Aktivierung hinweisen.

Die neuronale NH^+_4 Produktion wärend Aktivierung wurde durch intravenöse Ammoniumchlorid-Injektionen imitiert, was ebenfalls zu einer astrozytären und neuronalen Laktat-Akkumulation führte.

Zusammenfassend kann geschlossen werden, dass die Kombination von metabolischen Sensoren mit TPLSM es erlaubte, Transienten von astrozytären und neuronalen Glukose-, Laktat- und Pyruvat-Konzentrationen in der lebendigen Maus mit zellulärer Auflösung zu messen. Verstärkte Glukose-Transienten und höhere Laktat-Spiegel in Astrozyten verglichen mit Neuronen unterstützen die ANLS Hypothese.

Introduction

Brain energy metabolism

Scientific field and its significance

About 10% of the cardiac output, 20% of the whole body oxygen and 25% of the glucose utilization are appointed to the brain, although it represents only 2% of the body mass[1]. This high energetic turnover of brain tissue makes our central computational organ extremely vulnerable to failure of glucose and oxygen supply: few minutes of oxygen or glucose depletion in the blood compartment induce a loss of consciousness. On a cellular level, neurons are the main consumers of energy mostly for membrane repolarization and postsynaptic processes involved in signal transmission, which is often located far away from the cell body[2]. Therefore, it is likely that other highly abundant cell types in the 'glia' of brain might play an essential role in supporting the energetically demanding neurons. The term 'glia' was coined in 1858 by Rudolf Virchow reflecting the instance that he regarded 'glia' as a connective substance forming a 'Nervenkitt' in which neuronal elements are embedded[3]. After the identification of cellular elements of the neuroglia, the term 'astrocyte' was proposed by Michael von Lenhossek based on the star-like appearance in the Golgi staining[4] and later on categorized into 'fibrous' and 'protoplasmic' astrocytes[5–7]. Consequently, modern neuroscience has identified a variety of possible functions of astrocytes such as the controlling of synaptic genesis and functioning, the role as stem cells and even influencing cognition[5]. Concerning neuroenergetics, roles in neurovascular interactions and metabolic blood-brain-exchange have been suggested, because of their close morphological relationship with neurons and vessels[8]. However, there is still no consent to the physiological relevance of astrocytes in general and to their role for a proper energy supply of the neurons specifically. The conservation of astrocytes over many species and their increased densities and volumes in humans in comparison to other mammals such as rodents[9,10] suggest an important role for brain physiology.

Astrocyte metabolism is altered in a variety of highly prevalent brain pathologies such as Alzheimer's Disease (reactive astrocytes, intracellular Aβ protein accumulation), depression (prefrontal cortex with reduced astrocyte density), epilepsy (astrogliosis) or stroke (downregulation of astrocytic glutamate transporters and gap junction proteins)[11]. In the context of this work, the neuropsychiatric syndrome called hepatic encephalopathy (HE) is of special interest: An acute or chronic failure of the liver to detoxify intestinal ammonia leads to its accumulation in the brain tissue, where it is a substrate of astrocytic glutamine synthetase[12]. Consecutively, brain glutamine, reactive oxygen species (ROS) and lactate levels rise inducing brain edema up to a fatal tentorial herniation[13]. Astrocytes are the only

brain cells with a significant energy storage in the form of glycogen, which is neuroprotective during acute hypoglycemia, a common and life threatening side effect of insulin therapy of diabetes[14].

Localized changes of brain perfusion and metabolism have been used successfully to detect physiological and pathological processes non-invasively in the human brain. 'Functional hyperemia' describes the highly dynamic increase in cerebral blood perfusion accompanying neuronal activation[15]. This neurovascular coupling (NVC) is the theoretical basis to create detailed maps of neuronal activity by displaying hemodynamic changes and forms the basis for many heavily used non-invasive neuroimaging methods. Functional magnetic resonance imaging (fMRI) takes advantage of the differences in the magnetic properties of oxygenated and deoxygenated hemoglobin. This so called 'blood oxygenation level-dependent' contrast measured by fMRI reflects the activity-induced spatiotemporal increase of blood volume and blood flow, which exceed the elevated needs of the local oxidative metabolism[16,17]. Another metabolic phenomenon used for functional brain studies is the tight association of local glucose consumption with neuronal activity[18]. For this purpose, positron emission tomography (PET) together with ^{18}F-fluorodeoxyglucose (FDG) has been mainly used for the measurement of glucose utilization as an important surrogate marker of neuronal activity. Additionally, the characteristic changes of FDG-PET signals in pre-symptomatic stages of Alzheimer's Disease might lead to an early diagnostic and progression marker[19]. The most common diagnostic use of FDG-PET is the metabolic characterization of malignant tumors, which prefer aerobic glycolysis over oxidative phosphorylation, a phenomenon called after its discoverer Warburg[20]. This enables anabolic metabolism and proliferation also in hypoxic tumor cells and thereby provides the energy substrate lactate for hypoglycemic but oxygenated tumor cells, an effect that is especially prominent in the fatal astrocyte-derived cancer glioblastoma[21].

Astrocyte morphology

The term astrocyte is used for a heterogeneous group of cells in the central nervous system, with the main classifications into 'protoplasmic astrocytes' in the grey matter, 'fibrous astrocytes' in the white matter, 'Bergmann glia' in cerebellum, 'Müller glia' in the retina and 'radial glia' during developmental neurogenesis[22]. However, many other less accepted classifications have been suggested based on different progenitor cells, differentiation potentials, gene expression patterns, electrophysiological properties, interactions with neurons and reactivity in astrogliosis[23]. Astrocytes close to the dura mater and the ventricular endothelium have a distinct morphology with processes covering the brain outer surface. In rodents, the processes of protoplasmic astrocytes cover the whole cortex volume with

almost non-overlapping territories, while in primates[10,24,25]. The usage of mouse models to investigate astrocyte metabolism imposes limitations to translational validity, as cortical astrocytes in primates are several-fold larger, have more small processes and additionally long fibers with varicosities[9]. Cortical neurons are not only organized in distinguishable layers depending on the depth below the surface, but they are also topically organized into receptive fields, which has been well characterized in the rodents barrel cortex[26]. Similarly, a pronounced electrochemical coupling of neighboring astrocytes within barrels has been observed[27].

Astrocytes and neurovascular coupling

Increased neuronal activity is followed by an increase of local blood perfusion, a phenomenon that is called 'neurovascular coupling' and that is the basis of the BOLD-fMRI signal, which has been widely used to functionally map brain regions[28]. Astrocytes have large-diameter vascular processes called 'endfeet', which cover most of the vascular surface[29], suggesting a role in controlling vascular diameter. These endfeet are expressing specific proteins, such as aquaporin 4 channels, Connexin 43 and partially glial fibrillary acid proteins (GFAP). Recent *in vitro* preparations like brain slices and isolated retina preparations allowed by using single-cell electrophysiology, microscopy and pharmacological manipulations the identification of numerous vasoactive agents implicated in functional hyperemia[8]. Vasodilation and -constriction following neuronal activity could be reproduced by elevating the intracellular Ca^{2+} in astrocytes[30,31]. Several other mediators, such as metabolites of the cyclooxygenase-1 (COX) and the cytochrome P450 ω-hydroxylase pathways, lactate, adenosine, adenosine-3-phosphate, eicosanoids (20-HETE, EET), carbon monoxide, oxygen, H^+, NO, astrocytic and smooth muscle potassium channels (K_{Ca}, K_{ir}) have been identified[14,15].

Between different astrocytes and between processes of the same astrocyte a high density of gap junctions has been found[32]. Connexins (Cx's) display the molecular constituents of gap junctions. So far twenty-one Cx's have been identified, whereby Cx30 and Cx43 are the main Cx's in astrocytes. Gap junctions allow passage of ions and small molecules up to 1.2 kDa including glucose, lactate, K^+, Ca^{2+} and second messengers[33]. Through these connections astrocytes form functional networks, which enable neuroglial and gliovascular interactions, whereas the extent of this coupling is varying between different brain regions and different astrocytic subpopulations[34]. Additionally, astrocytic Ca^{2+} waves have been shown to propagate between perivascular astrocytes via electrical synapses formed by gap junctions. Astrocytic networks might also support the delivery of energetic metabolites from blood vessels to distal neurons[35]. However, the main transport limiting barrier for energy substrates are not

cellular membranes within the brain tissue but rather the blood brain barrier formed by vascular endothelial cells, which chemically isolate the central nervous system from the rest of the body[36,37].

Astrocytes and neurometabolic coupling

In this chapter, the potential role of astrocytes in the local increase of brain energy metabolism as it can be measured with FDG-PET is discussed. Beside the above-mentioned endfeet, astrocytes have thin processes which cover most of the synapses and dendrites in a distinct area, forming more than a million so called 'tripartite synapses' each[15]. Therefore, astrocytic processes are perfectly positioned for the removal of glutamate that has been synaptically released by neurons upon neuronal activity. After intracellular conversion to glutamine by the enzyme glutamine synthase, which is found exclusively in astrocytes[38], glutamine is transferred back to neurons. This 'recycling' process of glutamate is known as the 'glutamate-glutamine cycle'[1,39]. Initially, astrocytes were considered to support neuronal homeostasis by clearing synaptically released glutamate and potassium and thereby sharing the metabolic workload of neuronal signal transmission[40]. With the so-called 'astrocyte-neuron lactate shuttle' (ANLS) hypothesis a more active metabolic support for neurons by the astrocytes has been suggested: Upon neuronal activity, glutamate is co-transported into astrocytes with Na^+, activating the Na^+/K^+-ATPase which stimulates the astrocytic glycolysis to produce lactate, which could then be transported into neurons as the preferred energy substrate (for scheme see Figure i-1)[41]. Partial support for the ANLS hypothesis has come from various *in vitro* and *in vivo* experiments, which are discussed in the section 'Publication I' of this thesis and elsewhere[42]. However, there is still an ongoing controversy under what conditions and to what extent such a lactate transfer actually occurs in the living mammal[43,44].

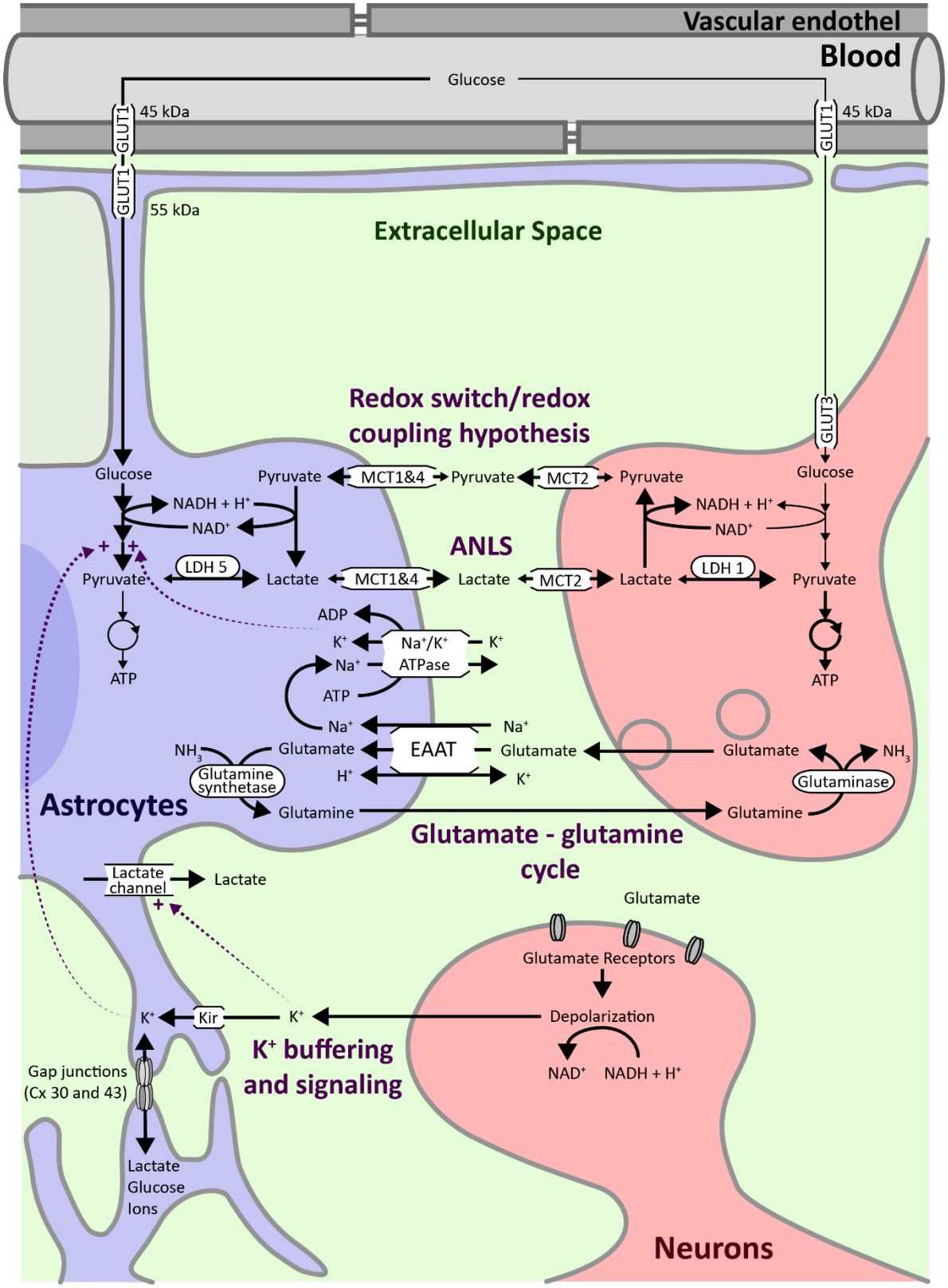

Figure i-1: Concepts of metabolic cooperation between astrocytes and neurons at the tripartite synapse. According to the astrocyte-neuron lactate shuttle (ANLS) hypothesis, glucose from the blood is preferentially transported into astrocytes using glucose transporters (GLUT). In astrocytes, glucose gets metabolized to lactate, which can then be transported towards neurons using monocarboxylate transporters (MCT), where lactate can be converted into pyruvate by lactate dehydrogenase (LDH) and fuel mitochondrial adenosine triphosphate (ATP) production[45]. The kinetic properties of GLUT, MCT

and LDH isoforms expressed in the different compartments are discussed in the following sections. Neuronal glutamate released into the synaptic cleft is mainly taken up by astrocytes using excitatory amino acid transporters (EAATs, human EAAT-2 corresponds to the glutamate transporter 1 (GLT-1) in rodents). The coupled Na^+ influx into astrocytic activates the Na^+/K^+-ATPase, which increases astrocytic ADP and potassium concentrations and thereby activates astrocytic glycolysis[11]. Glutamate in astrocytes is converted into glutamine using glutamine synthetase, shuttled into neurons and converted back to glutamate by neuronal glutaminase to close the glutamate-glutamine cycle[45]. Presynaptically released glutamate can activate ionotropic and metabotropic glutamate receptors at the postsynapse, which induce depolarization of neuronal membranes and oxidation of neuronal NAD^+/NADH-redox states. Excess neuronal NAD^+ can be shuttled into astrocytes according to the redox switch/redox coupling hypothesis by exchanging neuronal pyruvate for astrocytic lactate using MCTs[46]. Potassium released from activated neurons can be imported and buffered in astrocytic networks by gap junctional coupling of connexin (Cx) 30 and 43 expressing astrocytes. Additionally, extracellular potassium has been proposed to activate astrocytic lactate export via a lactate channel[47].

The high glucose uptake of the mammalian brain can be explained by the energy needs for neuronal signaling mostly because of the expensive generation of excitatory postsynaptic potentials (EPSP) via glutamate receptors[48] and the neuronal resting homeostasis[49]. The most universal intracellular energy rich substrate used by neurons is adenosine triphosphate (ATP), which can be converted into adenosine diphosphate, monophosphate and other phosphate group donors as energetic coenzymes[1]. The metabolic steps from one glucose molecule to the production of 30 to 36 ATP molecules can be clustered into glycolysis, the tricarboxylic acid (TCA) cycle and oxidative phosphorylation, with additional branches for glycogenesis and the pentose phosphate pathway (PPP)[44]. The following sections will provide a short overview of the steps, which are most relevant for the understanding of the work presented in this thesis. A selection of metabolic pathways involved in ATP production is illustrated in Figure i-2.

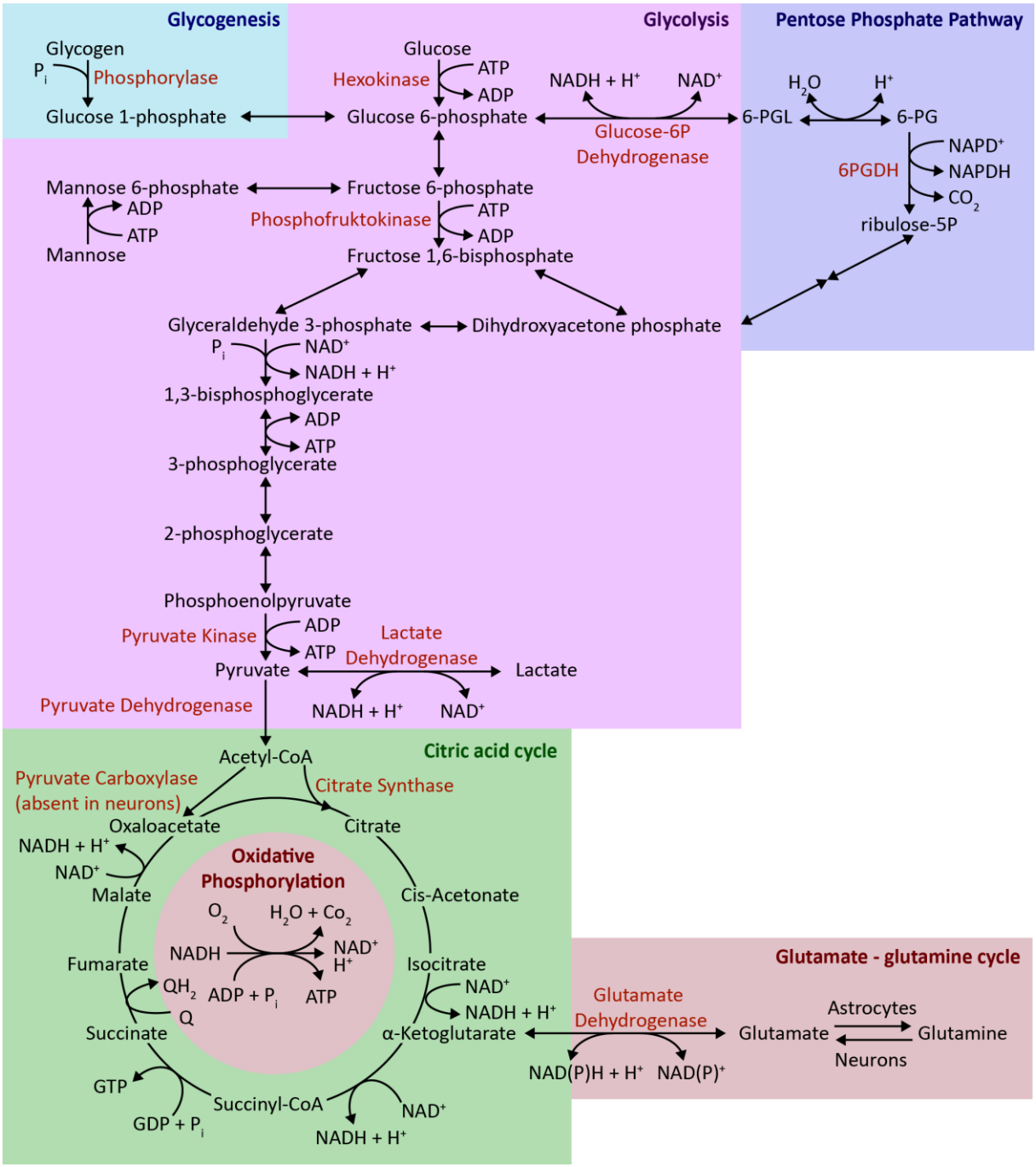

Figure i-2: Selection of pathways involved in cortical generation of the energy rich substrate ATP out of glucose. Glycolysis describes the anaerobic degradation of glucose to pyruvate and lactate. Glycogenesis allows the storage of glucose in the form of glycogen, which has been found to a limited extent in astrocytes but not in neurons[50]. The pentose phosphate pathway describes an alternative metabolic route for glucose, which is important for anaplerosis and the formation of scavengers to antagonize oxidative stress. The enzyme pyruvate dehydrogenase links pyruvate to the citric acid cycle via acetyl-CoA, which can either enter oxidation via citrate synthase or fill up the tricarboxylic backbone via pyruvate carboxylase (in astrocytes but not in neurons[51]. Alpha-ketoglutarate can be converted to glutamate, an important neurotransmitter that astrocytes provide to neurons as glutamine, forming the glutamate-glutamine cycle. The reducing agents (such as NADH) produced by glycolysis and the citric acid cycle can then be used for the oxidative phosphorylation of ADP to ATP in mitochondria.

Glucose uptake

Blood glucose needs to pass the blood brain barrier (BBB) formed by vascular endothelial cells, in order to be taken up into the brain tissue. As glucose uptake depends over a large range on its blood concentration and diffusion of the hydrophilic glucose molecule over membranes is limited, a low affinity transporter must be responsible[33]. Glucose transporters (GLUT's) belong to the solute carrier superfamily of membrane transporters, whereby the isoform GLUT-1 (55 kDa) has been localized to the vascular endothelium in the brain[52]. The glucose uptake via GLUT-1 across the BBB has been shown to be rate liming in a quantitative model of brain glucose utilization[53]. GLUT's are functionally symmetrical so that the direction of glucose flux depends solely on substrate concentration gradients as described by Michaelis-Menten kinetic equation (see equation E-1, with the transporter and substrate specific Michaelis-Menten constant K_m, and the maximal rate v_{max}). The affinities for glucose differ between GLUT serotypes: Astrocytes express the low-affinity transporter GLUT-1 (45 kDa, K_m of 5-8 mM) and neurons the high affinity transporter GLUT-3 (K_m of 1-2 mM)[54,55], which makes neurons more efficient glucose importers at low substrate levels but also earlier saturated at higher concentrations[49]. The uniporters can not only transport glucose, but also mannose, galactose and dehydroascorbate, which can all contribute to trans-accelerated exchange (for explanation see Figure i-3)[49].

$$\text{rate} = \text{v} = \frac{d[\text{P}]}{dt} = \frac{[\text{S}]^* \text{v}_{\text{max}}}{\text{K}_\text{m} + [\text{S}]}$$

Equation E-1: Michaelis-Menten kinetic model.

Glucose metabolism

The glucose influx into brain tissue depends not only on blood glucose levels but is also highly correlated to glucose phosphorylation, indicating a high v_{max} of the rate limiting enzyme hexokinase[50]. Phosphorylated glucose (glucose-6-P) is not transported across cellular membranes and can either enter glycolysis, glycogenesis or the PPP. Glycolysis results in two pyruvate molecules and the conversion of two ADP and two NAD^+ into ATP and NADH, respectively. The glycogen content of brain tissue depends on cellular glucose levels and is relatively low compared to muscles or liver tissue and mostly restricted to astrocytes[56]. The increased glycogen phosphorylase activity (creating glucose-6-P and glucose-1-P) and the consecutive lactate buildup during increased neuronal firing led to the hypothesis, that astrocytic glycogen might still support neuronal energy needs especially during acute

hypoglycemia[50,57]. The PPP converts glucose-6-P into ribulose-5-phosphate coupled to the conversion of two $NADP^+$ into NADPH, both used for anaplerosis, which is most prominent in the neonatal brain[58]. The second anaplerotic reaction is the conversion of pyruvate into oxaloacetate catalyzed by pyruvate carboxylase (PC), which shows substrate competition with the pyruvate analogue oxamate[54]. PC is expressed in astrocytes but not in neurons so that the neurotransmitters glutamate and GABA can only be produced in astrocytes before being shuttled into neurons[59]. Pre-synaptically released glutamate can increase astrocytic glucose uptake[60] and glycolysis[61,62]. Synaptic and axonal signaling leads to an increase of extracellular potassium, which in turn activates astrocytic glycolysis[61]. This effect depends on the Na^+/HCO_3^- cotransporter NBCe1 via astrocytic membrane depolarization and intracellular alkanization[63]. Astrocytic glycolysis has been shown to be inhibited by the downstream product lactate resulting in a negative feedback mechanism[64].

Pyruvate and lactate dehydrogenase

In the adult brain glucose is fully oxidized over extended time periods, whereby most ATP (ca. 93%) is generated in mitochondria using the TCA cycle and consecutively oxidative phosphorylation (OXPHOS)[61]. Mitochondria are transported along dendrites and axons[65] and are therefore found at high densities at the pre- and post-synapse[66]. OXPHOS is linked to glycolysis via the pyruvate dehydrogenase (PDH) catalyzed conversion of pyruvate into acetyl coenzyme A, which can then enter the TCA cycle to produce succinate and NADH, the reducing substrates for OXPHOS. Indeed, exogenous pyruvate has been shown to have the capacity to enter the TCA cycle as an energy substrate for the brain, but it also induced seizures[67]. The epileptogenicity of venous pyruvate could be reproduced in our mouse model (data not shown) and has recently been shown to depend on lactate dehydrogenase (LDH) activity[68]. LDH has four subunits (which can be either muscle type M or hearth type H) and catalyzes the reversible reaction from pyruvate to lactate coupled to the conversion of NADH to NAD^+. This coupling leads to a close correlation between the lactate/pyruvate and the NADH/NAD^+ ratio[69], which makes cellular NADH/NAD^+ redox states a central regulator of the directionality of intercellular lactate fluxes[70]. Indeed, cytoplasmic and mitochondrial calcium transients are regularly followed by increased NAD(P)H autofluorescence[71]. In hippocampal brain tissue slices, the initial dip of NADH fluorescence during electrical stimulation could be collocated with neurons and the delayed overshoot with astrocytes[72]. This finding led to the postulation of the redox switch/redox coupling hypothesis, which makes the direction of the lactate shuttle dependent on cytoplasmic redox states and suggests an exchange of astrocytic lactate with neuronal pyruvate in order to transfer oxidative equivalents produced in active neurons towards astrocytes[46].

Neurons express the isoform LDH-1, which consists of four H subunits and prefers the reaction towards pyruvate due to pyruvate inhibition, while astrocytes also express LDH-5, which consist of four M subunits and favors lactate production[73]. LDH-5 activity increases during alkalization as it happens in astrocytes during increased activity[74,75], what is further supporting the ANLS hypothesis[76].

Lactate transport

Even if glucose is the main energetic compound taken up by human brain tissue, systemic lactate can fuel ATP production in the adult brain and is therefore a suitable energy-rich substrate[77], even though lactate uptake might be only relevant under hyperlactataemic conditions[78] such as during physical activity[79,80]. On a cellular level, brain cells are exposed to substantially lower levels of glucose and higher levels of lactate than cells in blood plasma[81]. As already described beforehand, lactate can link glycolysis and OXPHOS over different cellular compartments via lactate-shuttles[82]. Indeed, cultured astrocytes export lactate as long as their pH is alkaline[83], which is produced from glucose and glycogen[84]. Mitochondrial and cellular lactate shuttles depend on the lactate transport over monocarboxylate transporters (MCTs)[85]. The expression of different MCT serotypes in the main cellular compartments of the cortex favors astrocytic export and neuronal import of lactate: Astrocytes express the low affinity transporters MCT1 and MCT4, while neurons express the high affinity transporter MCT2[86], notably at the postsynaptic density[87]. This distribution is similar to lactate exporting fast twitch muscle fibers (MCT4) and lactate importing slow twitch muscle fibers (MCT1)[88].
For the present study, we used the trans-acceleration property of MCT, which has previously been well characterized in MCT-1 positive erythrocytes (see figure i-3)[89]. Despite trans-accelerated exchange, MCT mediated lactate transport can hardly explain the possibility of lactate flux across astrocytic cell membranes against a concentration gradient, which led to the postulation of the existence of a so far unknown potassium-dependent lactate channel[47].

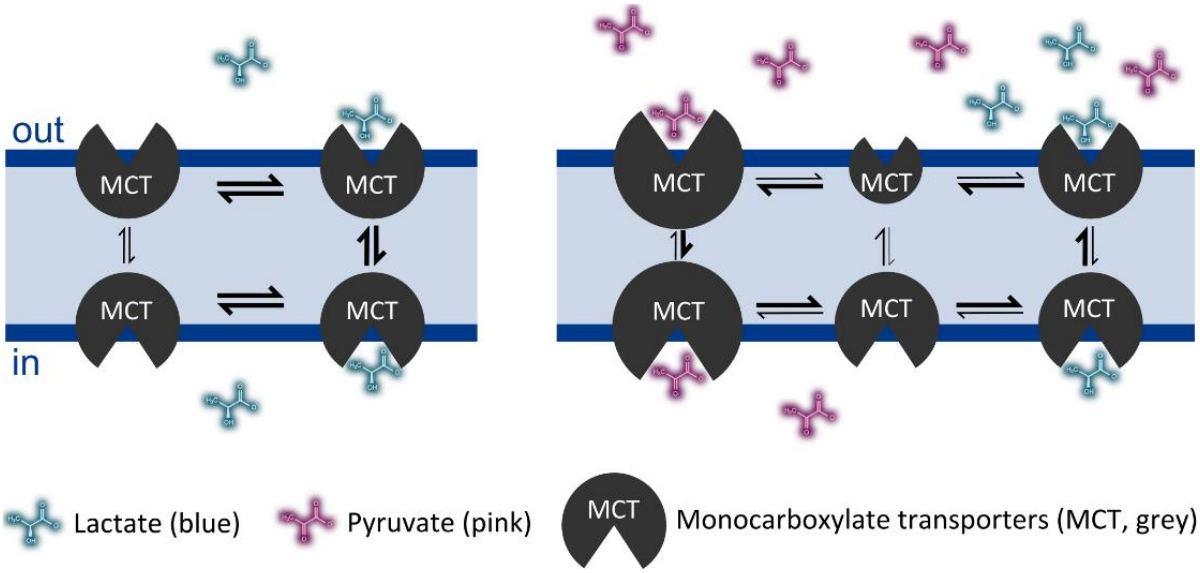

Figure i-3: Scheme of trans-accelerated exchange at Monocarboxylate transporters (MCT). MCTs (grey) transport lactate (blue) and pyruvate (pink) across cell membranes, what can be described as probabilities of different states of the MCTs (diameter of MCT symbol). Physiological lactate concentrations are significantly higher than pyruvate concentrations (left panel). Both substrates compete for the same binding site and binding increases the efficiency of translocation of the binding site. Each substrate enhances the transport of substrates situated at the opposite side of the membrane, a phenomenon called trans-acceleration[90]. Therefore, an increase of extracellular pyruvate enhances the transport of lactate out of the cell (right).

It is still controversial if a lactate shuttle as proposed by the ANSL is relevant at resting conditions or only during increased neuronal activity[91] or pathological conditions such as brain trauma[92]. Increased neuronal activity leads to a local rise of brain lactate concentrations. Several mechanisms have been proposed for the lactate surge, which might act synergistically: AMPA receptors have been shown to be involved[65], but also the activation of GLUT1 by Na^+-glutamate cotransporters[60] and the stimulation of the Na^+-HCO_3^- cotransporter NBCe1[63], soluble adenylyl cyclase[93] and a lactate channel[47] by extracellular potassium. NH_4^+ released by active neurons might additionally prevent astrocytic mitochondria from oxidizing pyruvate via mitochondrial acidification[94,95]. This phenomenon is clinically relevant in HE, where intestinal NH_4^+ induces a LDH-dependent brain lactate rise and consecutive brain edema[96].

Lactate signaling

Upon neuronal activity, astrocytes release not only lactate, but also second messengers and chemical gliotransmitters like glutamate, D-Serine or ATP as part of the 'tripartite synapse'[97]. Therefore, L-lactate might be an additional gliotransmitter, which affects signal transmission in a relatively large

area[98]. More specifically, lactate was proposed as a volume transmitter that increases neuronal cAMP via the lactate receptor GPR81 and affects cellular NADH/NAD^+ redox states[99]. In the brainstem region locus coeruleus, astrocytic lactate and exogenous lactate could activate via a not yet identified receptor noradrenergic neurons and evoke arousal[100]. In the ventromedial hypothalamus, counter-regulatory catecholamine and glucagon secretion has been shown to respond to hypoglycemia[101] and low lactate levels[102]. In a hippocampal slice preparation, astrocytic lactate was either constricting or dilating arterioles[31]. Surprisingly, astrocytic lactate release in the hippocampus seems to be essential for long-term memory formation[103]. The physiological relevance of lactate signaling in different brain regions will finally depend on the actual lactate concentrations during baseline and neuronal activity[104]. Whether astrocytic lactate is linked to astrocytic calcium transients or the associated astrocytic oxygen sensitivity is another unresolved issue[105].

Methods

In this method section the basic principles of the methods used in the present work are introduced and their limitations are compared with the most relevant alternative approaches available to investigate brain energy metabolism. More specific method sections including immunohistochemical stainings to control for cell type specific sensor expression and inflammatory response, intrinsic optical imaging to map the primary somatosensory cortex[106] and extracellular enzymatic lactate and glucose electrodes[107,108] are provided in the corresponding publication sections.

Two-photon laser scanning microscopy

TPLSM can image several hundred micrometers deep into strongly scattering brain tissue by assigning scattered fluorescence to its original coordinates of nonlinear excitation at a defined point in time[109]. The key feature of nonlinear excitation as it has been predicted in the year 1931[110] is the relatively low absorption cross section (measured in units of Goeppert-Mayer), what allows excitation only with sufficiently high photon density, as it can be achieved in the focal point of a converging (pulsed) laser beam[111]. Frame scans of a focal plane can be achieved by laser-scanning with galvo-mirrors and temporally coordinated fluorescence detection with photomultiplier-tubes and specialized software[112].

In the present work, data were acquired using a custom-built two-photon laser scanning microscope[113] equipped with a 20x water immersion objective (NA 0.95, Olympus, Japan) and the acquisition software Scanimage[114]. The two fluorescence detection channels (CFP (Brightline HC 475/64 nm) and YFP (Brightline HC 542/50 nm); Semrock Inc., Rochester NY, USA) were used. For excitation a tunable pulsed laser (MaiTai eHP DS, Spectra-Physics, Santa Clara CA, USA) at 870 nm wavelength was used guided through an IR filter HC 770/SP and a dichroic mirror HC BS 506.

For *in vivo* imaging of mouse brain surgical preparations are necessary, such as a chronic cranial window to increase depth penetration and a head fixation to reduce motion[115]. Nevertheless, emitted light can be absorbed by vascular hemoglobin, the tissue can pulsate due to the breathing or the heart beat and fluorophores can be bleached at higher laser powers[115]. The spatial resolution is limited by the point spread function of the microscope, the temporal resolution depends on the pixel dwell time and the achievable signal to noise ratio of a measurement depends on the signal amplitude of the sensor relatively to the background signal[113].

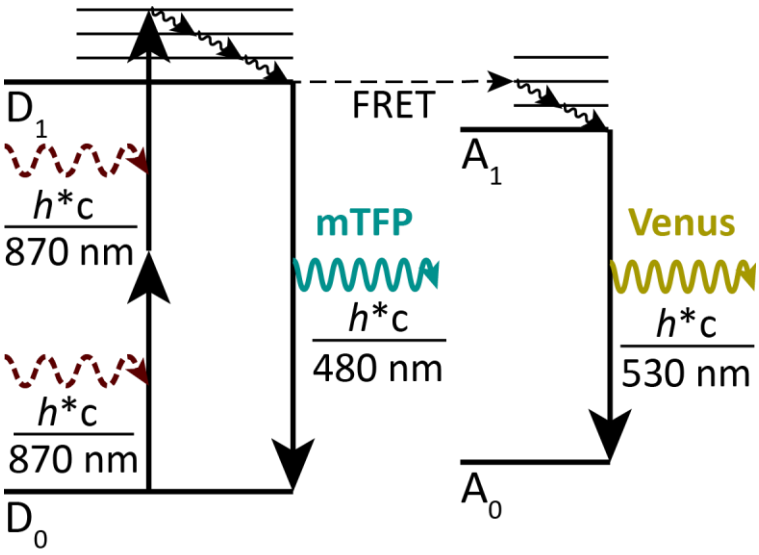

Figure i-4: Simplified Jablonski diagram illustrating the energy states of the FRET sensors *Laconic* and *Pyronic*. Pulsed laser light of 870 nm wavelength is used to induce mTFP fluorescence emission (peaking at about 480 nm) and via FRET Venus fluorescence emission (peaking at about 530 nm). Venus excitation is also directly induced by the 870 nm laser, as absorption spectra of two-photon excitation are broader than for single photon excitation[116]. The ground and excited electronic states of the donor (D_0 and D_1) and of the acceptor (A_0 and A_1, respectively) are indicated. *h* is the Planck constant and c is the speed of light.

The emitted light can be split into multiple channels of different wavelengths using dichroic mirrors and consecutive bandpass filters for simultaneous detection of multiple fluorophores. After bleach-through correction, this can be used to correlate signals from multiple fluorescent sensors, such as the red astrocyte morphology marker SR101 with vascular fluorescein isothiocyanate dextran or the green calcium indicator Oregon Green 488 BAPTA-1[117]. In the present work, sensors were used containing two fluorescent domains at the proteins C and the N termini, which can form a donor-acceptor pair capable of non-radiative dipole-dipole coupling called 'Fluorescent Resonance Energy Transfer' (FRET, Figure i-4). The FRET efficiency depends on the orientation and the distance between the two fluorophores[118]. These properties have been used to genetically construct sensors for specific substrates with core proteins that are known to change their conformation upon binding of the target substrate[119]. The binding of the substrate either increases or decreases the FRET efficiency and therefore affects the ratio of the emitted light from the donor and the acceptor fluorophore accordingly (Figure i-5). These substrate binding kinetics cause the ratio value to correlate with the concentration of the substrate ([S]) as described by Michaelis-Menten equation:

$$\Delta FRET = \frac{[S]^* \Delta FRET_{max}}{K_d + [S]}$$

Equation E-2: FRET sensor kinetics.

The key parameters for calibration of a FRET signal change (ΔFRET) are the maximal amplitude of the sensor ($\Delta FRET_{max}$) and the dissociation constant K_d:

$$[S] = \frac{K_d * \Delta FRET/\Delta FRET_{max}}{1 - \Delta FRET/\Delta FRET_{max}}$$

Equation E-3: Calibration of FRET sensors.

While the K_d for a given sensor can be characterized *in vitro*, the $\Delta FRET_{max}$ depends on multiple *in vivo* factors such as optical properties of the microscope, the quality of sensor expression or any signal offset such as background signal. It is therefore necessary to calibrate every region of interest (ROI) during an experiment to make conclusions about absolute substrate concentrations, ideally with two reference points on the *in vitro* calibration curve.

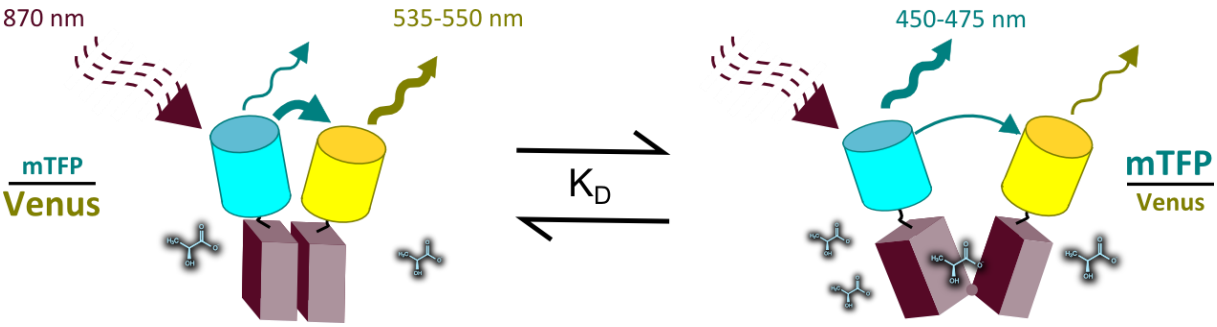

Figure i-5: Illustration of *Laconic* sensor functionality. An increase in lactate (molecule in blue) concentration changes the conformation of the sensor and orientates the yellow fluorescent protein (Venus; acceptor) domain away from to the cyan fluorescent protein (mTFP; donor) domain, what decreases the FRET efficiency indicated by the increase of the ratio mTFP/Venus.

FRET dyes for metabolism

The use of FRET dyes for intracellular neuronal calcium transients has been used successfully for functional measurements of neuronal cell population[120,121]. FRET dyes specific for energy substrates have mainly been used in cell cultures, such as the glucose sensor FLII[12]Pglu600μΔ6 (*FLIPΔ6*)[119]. *FLIPΔ6* was first characterized in COS-7 cells[122] and has been successfully applied in cell cultures[123]. *FLIPΔ6* can be calibrated in β-escin permeabilized cultured cells to estimate absolute concentrations[126]. In our hands, *FLIPΔ6* proved to be functional also in the *in vivo* situation: Under insulin induced hypoglycemia, increasing blood glucose within seconds from 0.5 mM to more than 20 mM induced a higher increase of *FLIPΔ6* signal in astrocytes than in neurons (Figure i-6). However, without the possibility to calibrate the sensor *in vivo*, it is not possible to determine whether this difference is due to different baseline glucose concentrations or different glucose accumulation in the two cell types. Another principal limitation of FRET dye signal interpretation is the fact, that metabolite concentrations rather than fluxes are measured. This can be demonstrated with electrical hind-paw stimulation experiments, which are known to increase the glucose uptake in the corresponding primary somatosensory cortex: *FLIPΔ6* indicated no changes of neuronal glucose levels and only minor and ambivalent changes of astrocytic glucose levels, reflecting the fact that free glucose concentrations are dependent on glucose uptake and intracellular glucose phosphorylation (Figure i-6).

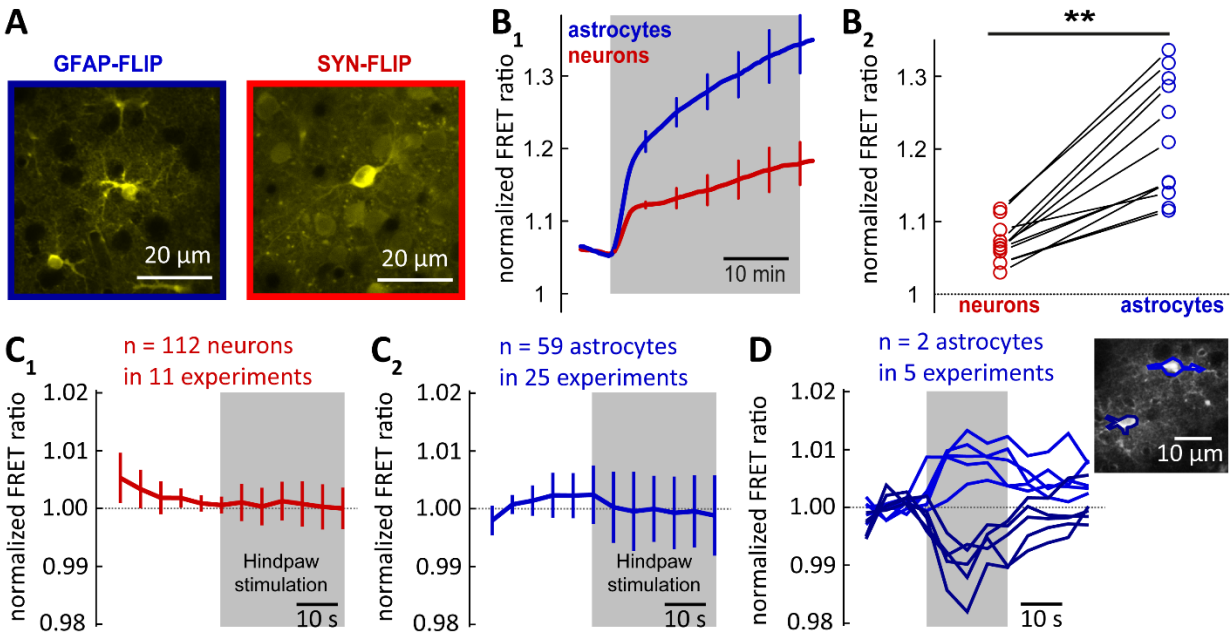

Figure i-6: Expression and dynamic changes of the glucose sensor *FLIPΔ6*. Under the control of the GFAP and synapsin (SYN) promotors, cell-type specific sensor expression for subsequent imaging of astrocytic and neuronal FLIP fluorescence, respectively, was possible (A). After 45 minutes of insulin infusion, a glucose infusion (B_1, single exemplary trial, glucose infusion indicated by grey bar) induced an increase in bot cell types. This increase was higher in astrocytes compared to neurons after 30 minutes (B_2, n = 12 trials, ** p > 0.01). Electrical hindpaw stimulation (400 µA, 4 Hz, 30 sec duration; gray bar) led to no overall changes in a population of neurons (C_1, mean ± SD) and astrocytes (C_2, mean ± SD). However, a minority of astrocytes showed transients during a 20 seconds hind-paw stimulation as shown here in the case of two exemplary neighboring astrocytes with changes in different directions - the transients were persistent over five individual imaging session on different days (D_2).

In cell cultures and brain slice preparations, the Inhibition-Transport-Method (ITM; Figure i-7) allowed measurements of single cell glucose consumption rates (or glycolytic rates) and GLUT transport rates[124] of cultured astrocytes and other cell types[125]. This led to the characterization of increased astrocytic glycolysis due to increased extracellular potassium and glutamate[61,63] and decreased glycolytic rates under increased lactate levels[64]. However, there is no successful application of this method in the intact animal so far.

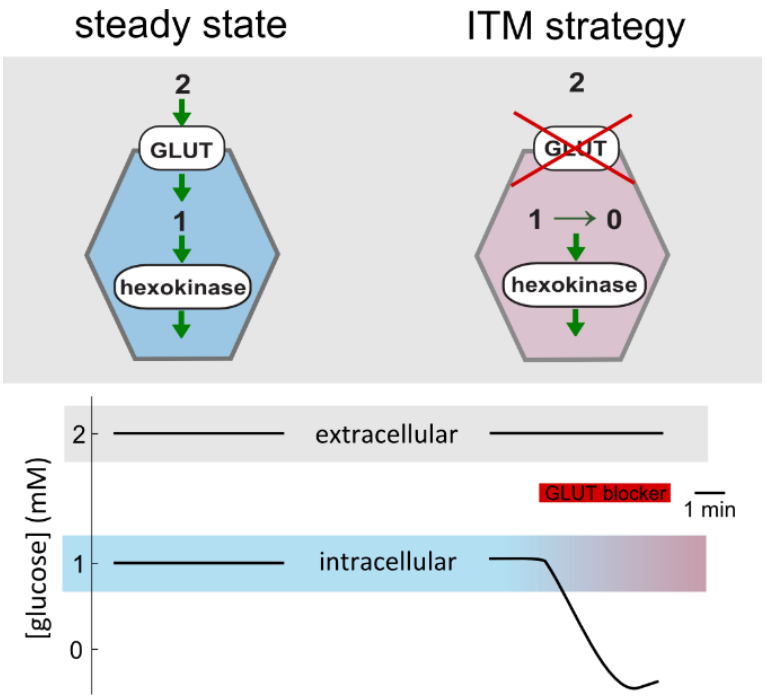

Figure i-7: Inhibition-Transport-Method (ITM) for glycolytic rate measurements with FLIPΔ6 in a cellular compartment. At steady state the intracellular concentration of glucose is kept at a constant level and is determined by glucose uptake via glucose transporters (GLUT) and phosphorylation by hexokinase (HK). In order to obtain an estimate of flux through HK, a possible strategy is to isolate the rate of metabolism by pharmacological elimination of the glucose uptake using the GLUT blocker Cytochalasin B. The V_{max} of hexokinase can be estimated from the decline in intracellular glucose concentration during the blockade of GLUT[125].

Another FRET sensor that has been used to investigate brain energy metabolism is the NAD^+-NADH redox state sensor *Peredox*, which showed a higher NAD^+/NADH ratio in cultured astrocytes compared to neurons[127]. FRET sensors have also been developed for glutamate[128] and glutamine[129]. Recently, a FRET sensor specific for lactate called *Laconic* has been constructed and allowed to follow intracellular lactate levels of cultured astrocytes and glioma cells using pyruvate-induced trans-accelerated export of lactate and to determine their net lactate consumption or production using the MCT blocker phloretin[130]. More recently, a FRET sensor specific for pyruvate called *Pyronic* was presented, which allowed the quantification of pyruvate transport, production and consumption in cultured HEK293 cells, astrocytes and neurons[131].

The plasmids coding for these sensor constructs can be cloned and loaded into adenoviral vectors for expression in target cell types using specific promoters. The astrocyte-specific construct included a minimal GFAP promoter (GFaABC1D, sGFAP; kindly provided by Dr. M. Brenner, Department of Neurobiology, University of Alabama)[132], a beta-globin intron and a poly-adenylation signal. The neuronal construct included a human synapsin-1 (SYN) promoter, a Woodchuck Hepatitis Virus post-

transcriptional regulatory element (WPRE) and a poly-adenylation signal[133,134]. The two plasmids were used to generate AAV serotype 6 (SYN construct) or AAV serotype 9 (GFAP constructs) viral particles by co-transfecting the shuttle plasmid with the pDP6 and pDF9 helper plasmids in HEK293-AAV cells (Agilent Technologies, Santa Clara, CA). Viral particles were isolated from the cell lysates, using iodixanol step gradients and HPLC purification on heparin-binding (AAV6) and ion exchange (AAV9) columns.

However, there are major obstacles with *in vivo* imaging of energy metabolites: First, despite the increased depth penetration of TPLSM, an invasive surgical preparation is necessary to access brain cortex optically. Second, awake TPLSM imaging has been established in our laboratory[121], but the necessary head-fixation and training of mice limits the use of pharmacological interventions and stimulation intensities. However, anaesthetic agents are known to influence brain energy metabolism; especially volatile halogenated anaesthetics such as isoflurane have been shown to significantly increase brain lactate levels[135,136]. But energy metabolite levels can also change with different physiological states of the brain, such as extracellular glucose[137] and lactate[138] levels during different sleep stages and wakefulness. Therefore, an appropriate anaesthesia is favorable for a first characterization of the sensors *FLIPΔ6*, *Laconic* and *Pyronic in vivo*.

To make conclusions about brain energy metabolism using these FRET dyes it is necessary to interfere with the steady states of a metabolic pathway with specific, reproducible and fast interventions such as electrical stimulation or pharmacological interventions. The compartmentation of neurometabolic coupling was investigated with peripheral electrical stimulation (e.g. at the contralateral hindpaw). The less physiological direct intracortical microstimulation was used to induce a stronger but still sparse neuronal response[139]. This method allowed to follow intracellular glucose and lactate concentrations during locally increased neuronal activity and to observe a reduction of the lactate peak when lactated dehydrogenase was blocked pharmacologically (Figure i-8). Other pharmacological interventions used in this work included the direct challenge with energy metabolites but also the blockage of transporters such as GLUT (Cytochalasin B, phloretin) or MCT (α-cyano-4-hydroxy-cinnamate, AR-C155858). Thereby, the BBB is a limiting factor for the convenient peripheral (subcutaneous, intraperitoneal or intravenous) administration of drugs. Direct intracortical air-pressure injection of drugs using a Picospritzer® is limited to very small injection volumes which are not reproducible enough for quantitative measurements which are needed for the ITM.

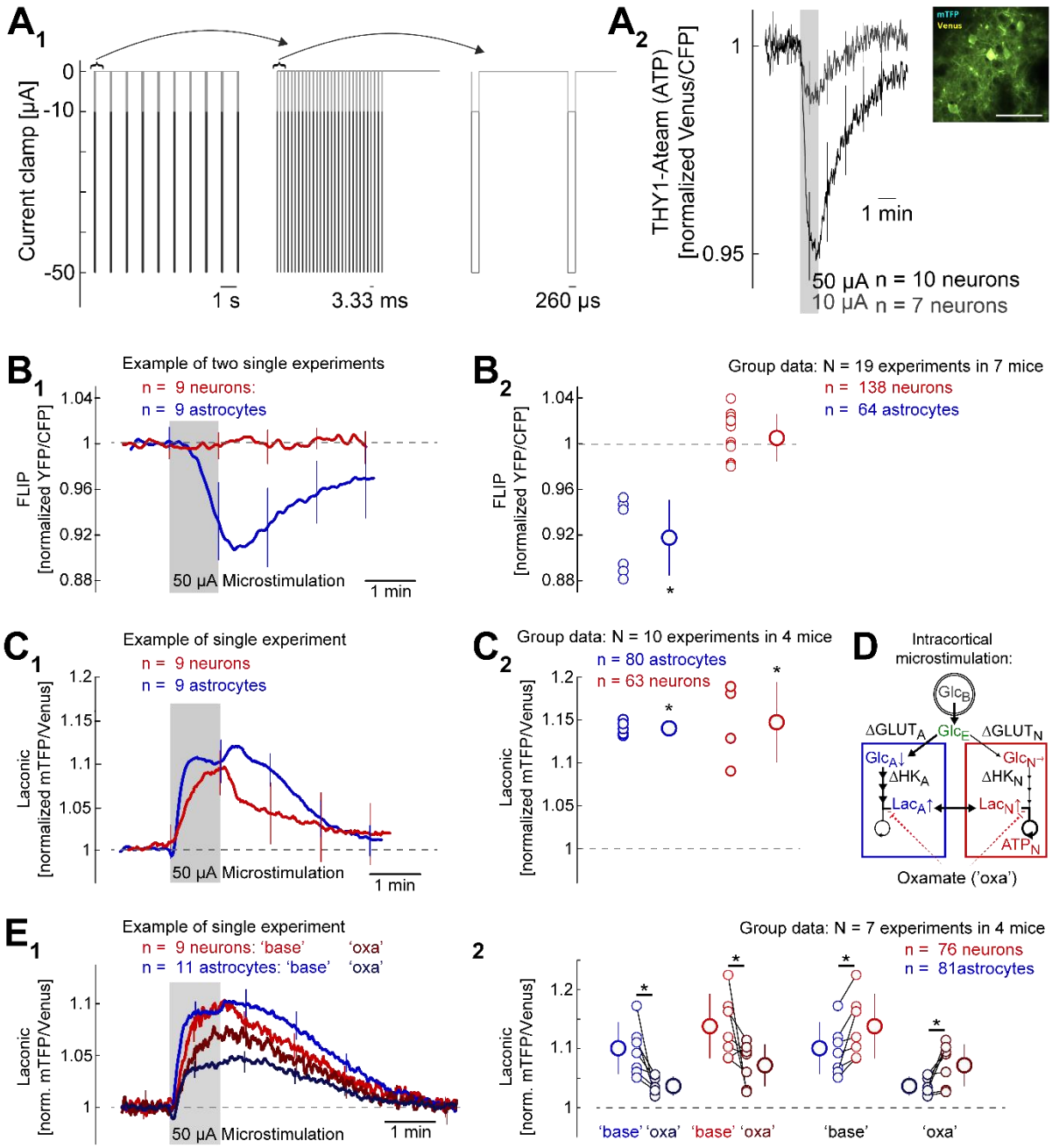

Figure i-8: Glucose and lactate concentration transients during intracortical electrical stimulation. A pipette was acutely inserted below a chronic cranial window. A stimulation train with currents of -10 µA or of -50 µA (A_1) induced a fast and transient decrease of neuronal ATP, indicating an acute disequilibrium of ATP production and consumption (A_2). Changes of astrocytic and neuronal glucose concentrations upon a stimulation of 50 µA are illustrated for a single experiment (B_1) and the whole set of experiments (B_2; astrocytes: 6 experiments in 3 animals; neurons: 13 experiments in 4 animals). The same stimulation induced an increase of astrocytic and neuronal lactate signals in a single experiment (C_1) and in the whole experimental group (C_2). The dip in astrocytic glucose and the increase of astrocytic lactate can be explained with a stronger stimulation-induced activation of astrocytic hexokinase activity (ΔHK_A) than glucose uptake ($\Delta GLUT_A$), while neuronal glucose uptake and consumption stay balanced (D). According to the ANLS, this lactate increase represents the shuttling of astrocytic lactate towards neurons, which is dependent on the conversion between pyruvate and

lactate by lactate dehydrogenase (LDH) activity in both cell types. Inhibition of LDH with the substrate analogon oxamate ('oxa', dark colors, 17 to 24 minutes after 500 mg per kg bodyweight oxamate infusion in 3 minutes) reduced the stimulation-induced lactate increase compared to baseline conditions ('base', bright colors) in an exemplary single experiment (E_1) and in the whole set of experiments (E_2 left, * $p < 0.05$ in paired t-test). In both conditions neuronal *Laconic* amplitudes were higher in neurons compared to astrocytes (E_2 right).

Aims of the current project

The established methods to investigate brain energy metabolism such as enzymatic quantifications, MRS or radiotracer methods have led to the postulation of a cellular compartmentation between neurons and astrocytes such as the ANLS hypothesis. However, the evidence for the controversial ANLS hypothesis is based on methods with key limitations: Measurements are invasive (post mortem concentrations[140], autoradiography[141]), lack of cellular resolution (microdilalysis[142,143], MRS[144], FDG-PET[145,146]), are *in silico* (modeling[2,147]), are *in vitro* (cell cultures, modeling), are indirect (immunohistochemistry) or require artificial labeling (6NBDG[143–145], 2NBDG[145,146] or IR2DG[41]).

More direct *in vivo* evidence for a cellular compartmentation of brain energy metabolism requires a method that combines cellular specificity, a sufficient spatial resolution, sub-second temporal resolution and a high enough signal to noise ratio that allow the detection of localized low-amplitude metabolite transients. TPLSM in combination with genetically encoded metabolite sensors in living mice holds the potential to fulfill these requirements, if the method can be optimized to achieve a signal quality sufficient to capture physiological transients. The complex nature of this new method makes it necessary to optimize TPLSM in mouse cortex for metabolic imaging while keeping the mouse in a physiological state: Interventions are needed to calibrate metabolic sensors for concentration measurements and to read out key metabolic rates in order to make statements about competing hypothesis of brain energy metabolism.

I) The first aim of this project was the implementation of the methodology to use TPLSM in combination with metabolite sensors for glucose, lactate and pyruvate in the intact brain.

II) The second aim was to compare the astrocytic with the neuronal glucose transport capacities, consumption rates and activity dependent transients: Therefore, the cellular accumulation of glucose

during increased supply, the glucose consumption rates using ITM and transients under increased neuronal activation were investigated, respectively.

III) The third aim was to calibrate the lactate sensor *Laconic in vivo* in order to compare astrocytic with neuronal lactate levels. Based on this calibration, lactate accumulation during increased blood lactate levels, neuronal activation (electrical somatosensory stimulation and direct intracortical stimulation) and metabolic conditions (ammonium chloride, anaesthesia) were investigated.

IV) The final aim of this project was to use the acquired data to draw conclusions regarding the ongoing debate over the cellular compartmentation of brain energy metabolism. Qualitative and quantitative models are needed to either support existing hypothesis or adjust them.

Publication I: Laconic

In vivo evidence for a lactate gradient from astrocytes to neurons

Philipp Mächler[1,2,6], Matthias T. Wyss[1,2,6], Maha Elsayed[3], Jillian Stobart[1,2], Robin Gutierrez[1,4], Alexandra von Faber-Castell[1], Vincens Kaelin[1], Marc Zuend[1,2], Alejandro San Martín[4], Ignacio Romero-Gómez[4], Felipe Baeza-Lehnert[4], Sylvain Lengacher[3], Bernard L. Schneider[3], Patrick Aebischer[3], Pierre J. Magistretti[3,5], L. Felipe Barros[4] and Bruno Weber[1,2]

[1]Institute of Pharmacology and Toxicology, University of Zurich, 8057 Zurich, Switzerland

[2]Neuroscience Center Zurich, University and ETH Zurich, 8092 Zurich, Switzerland

[3]Brain Mind Institute, École Polytechnique Fédérale de Lausanne, 1015 Lausanne, Switzerland

[4]Centro de Estudios Científicos, Valdivia 5110466, Chile

[5]Division of Biological and Environmental Sciences and Engineering, KAUST, Thuwal, KSA

Correspondence: bweber@pharma.uzh.ch

[6] These authors contributed equally to this work

Summary

The determination of lactate dynamics in brain tissue represents a challenge, partly because *in vivo* data at cellular resolution are not available. Here we monitored lactate in astrocytes and neurons of the primary somatosensory cortex of mice using the genetically-encoded FRET sensor *Laconic* in combination with two-photon laser scanning microscopy. An intravenous lactate injection rapidly increased the *Laconic* signal in both astrocytes and neurons, demonstrating high lactate permeability across the tissue. The signal increase was significantly smaller in astrocytes pointing to higher basal lactate levels in these cells, confirmed by a one-point in vivo calibration protocol.

Trans-acceleration of the monocarboxylate transporter with pyruvate was able to reduce intracellular lactate in astrocytes but not in neurons. Collectively, this data provides i*n vivo* evidence for a lactate gradient from astrocytes to neurons.

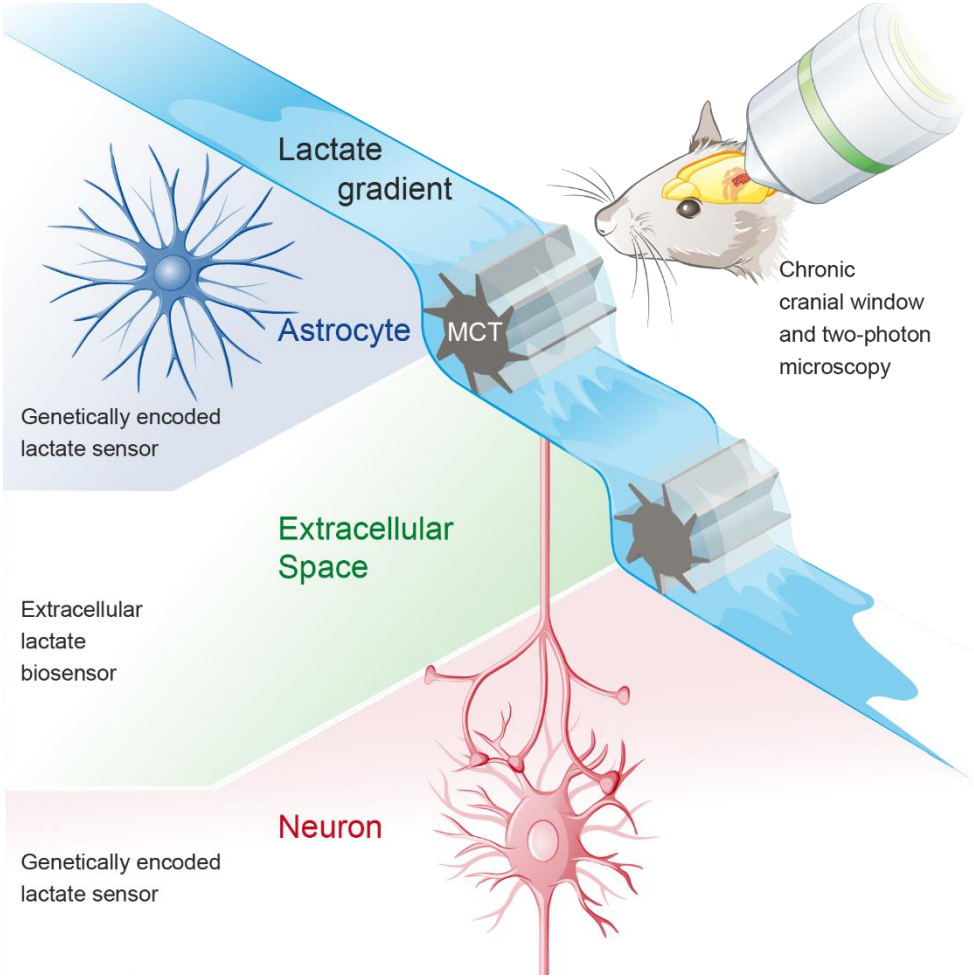

Introduction

The energy demand of mammalian brain tissue is met mainly by degradation of blood borne glucose. Classical experiments with radiolabeled substrates showed label incorporation into glutamate and glutamine in a manner suggestive of two separate tricarboxylic acid cycles, a 'large' and a 'small' compartment (Van den Berg et al., 1969), which were assigned to neurons and astrocytes respectively using immunohistochemical techniques (Martinez-Hernandez et al., 1977). The concept of compartmentation in brain energy metabolism gained new momentum with the postulation of the astrocyte neuron lactate shuttle model (ANLS). In the classical version of this hypothesis, glutamate transients are linked to a cellular compartmentation of lactate (Pellerin and Magistretti, 1994). Glutamate released from active neurons activates astrocytic glycolysis leading to production of lactate, which serves as an energy source for neurons. Increased brain lactate levels upon neuronal activation have been observed in several studies via different techniques (Hu and Wilson, 1997; Lin et al., 2010; Prichard et al., 1991; Sappey-Marinier et al., 1992). Also, L-lactate acts as a signaling molecule in certain mammalian brain regions (Mosienko et al., 2015; Tang et al., 2014; Yang et al., 2014). However, the cellular origin of lactate released during increased activity (Barros and Deitmer, 2010; Stobart and Anderson, 2013) and its significance as an energy substrate or signaling molecule remains largely unclear (Barros, 2013; Weber and Barros, 2015).

Experimental evidence from *in vitro* and *in vivo animal* studies demonstrate that lactate is able to sustain neuronal activity during glucose deprivation (Schurr, 2002; Wyss et al., 2011) and patients with non-penetrating traumatic brain injuries use peripheral lactate as brain energy substrates (for review see Glenn et al., 2015). Furthermore, lactate transport across cell membranes via monocarboxylate transporters (MCTs) is a facilitated transport (Halestrap and Wilson, 2012). Increased lactate production in one cell type and predominant lactate consumption in another cell type would therefore require a lactate concentration gradient from the 'producer' to the 'consumer'. Lactate dehydrogenase (LDH), located in mitochondria and the surrounding cytoplasm (Brooks et al., 1999), links lactate to oxidative metabolism, by catalyzing the conversion between lactate and pyruvate. The higher affinity for lactate of MCT and LDH isoforms expressed in neurons (MCT2 and LDH1) relative to the isoforms expressed in astrocytes (MCT1/4 and LDH5) supports an astrocytic production and neuronal consumption of lactate (Bittar et al., 1996; Debernardi et al., 2003; Laughton et al., 2000; Pierre and Pellerin, 2005). Inhibition of astrocytic production and neuronal consumption of lactate via LDH inhibition reduces epileptic neuronal activity, possibly due to neuronal ATP depletion (Sada et al., 2015). Moreover, the fast and transient lactate depletion in astrocytes during different *in vivo* and *in vitro* stimulation paradigms may represent the emptying of a lactate pool (Sotelo-Hitschfeld et al.,

2015). Taken together, these results suggest a lactate concentration gradient from astrocytes to neurons; however, *in vivo* evidence of such a cellular gradient is currently absent.

Here, we investigated cell-specific lactate reservoirs *in vivo* employing the recently developed genetically encoded biosensor *Laconic* (San Martín et al., 2013), which we specifically expressed in astrocytes and neurons. Through two-photon laser scanning microscopy (*2PLSM;* Denk et al., 1990), we show, for the first time, direct indication of an *in vivo* lactate gradient from astrocytes to neurons.

Results

Expression of Laconic and Pyronic *in vivo*

To evaluate the specificity of *Laconic* transients, a biosensor construct specific for pyruvate (‘*Pyronic’;* San Martín et al., 2014) was measured simultaneously with *Laconic*. Different adeno-associated viral (AAV) vectors, encoding either the *Laconic* or the *Pyronic* sensors, were injected in close distance to each other at the center of a craniotomy in the primary somatosensory cortex of mice (Figure 1A, S1A). The fluorescence of both sensors, driven by the short GFAP promoter, was located in the cytoplasm and showed the typical morphology of protoplasmic cortical astrocytes, including vascular end-feet and fine processes outlining dark non-fluorescent cells (Figure 1B). A similar fluorescence pattern was found throughout all imaged cortical layers, consistent with non-overlapping astrocytic domains in mice (Oberheim et al., 2009). Human synapsin promoter constructs induced cytoplasmic fluorescence in cells matching neuronal morphology, with dark nuclei and long ranging processes toward superficial or deeper structures, located more than 150 µm below the dura (Figure 1B). 2PLSM was restricted to layer 2/3 cells with a laser power above 20 mW to ensure stable FRET ratios (Figure S1F) and below 40 mW to prevent tissue damage and bleaching of the fluorescence. Immunohistochemical staining for GFAP, CD68 and fibrinogen revealed no increase in gliosis, microglial activity or blood-brain barrier leakage (Figures S1A-D).

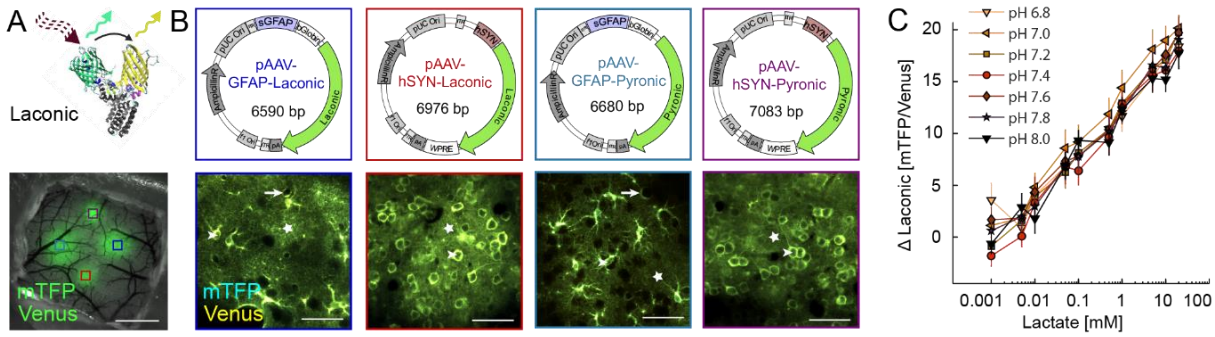

Figure 1. Expression of *Laconic* and *Pyronic in vivo*. (A top) 3D-Structure of the lactate sensor *Laconic*, which was excited with a pulsed laser (870 nm). Emission was collected for mTFP (450-475 nm) and for Venus (535-550 nm). (A bottom) The fluorescence (480 nm excitation, 505-565 nm emission, green) of four individual sensors was collected through a chronic cranial window preparation of the primary somatosensory cortex of a *C57BL/6* mice, scale bar: 1 mm. (B top) Serotype 6 adeno-associated viral vector (AAV6) with a *synapsin* promoter was used for neuronal expression, and serotype 9 vector (AAV9) with a *sGFAP* promoter for astrocytic expression. (B bottom) 2PLSM at 150 to 250 µm below the dura shows cell-type specific cytoplasmic sensor expression with nuclear exclusion (arrow heads), vascular end feet (arrows) and cellular processes (stars); scale bars: 50 µm. (C) The *in vitro* calibration curve of *Laconic* at 37°C shows substrate binding kinetics of lactate but no pH sensitivity. See also Figure S1A to E.

Laconic sensor functions are comparable *in vivo* and *in vitro*

L-lactate binding induces a conformational change of *Laconic* causing a decrease in fluorescent resonance energy transfer (FRET) efficiency which increases the ratio of mTFP (monomeric teal fluorescent protein) over Venus (Figure 1A). *In vitro* lactate application leads to two-site saturable *Laconic* kinetics without pH sensitivity (Figure 1C and S1F, San Martín et al., 2013). The functionality of the sensor *in vivo* was demonstrated with increasing doses of sodium-L-lactate injected via a tail vein catheter during 2PLSM. *Laconic* signals in neurons and astrocytes increased non-linearly with the intravenously injected lactate dose but did not respond to 500 mM saline injections (Figure 2A, S1E). The amplitudes of *Laconic* signal changes *in vivo* were of the same order of magnitude as *in vitro* cell culture, where *Laconic* signals can be explored at a much wider range of lactate concentrations (Figure 2B).

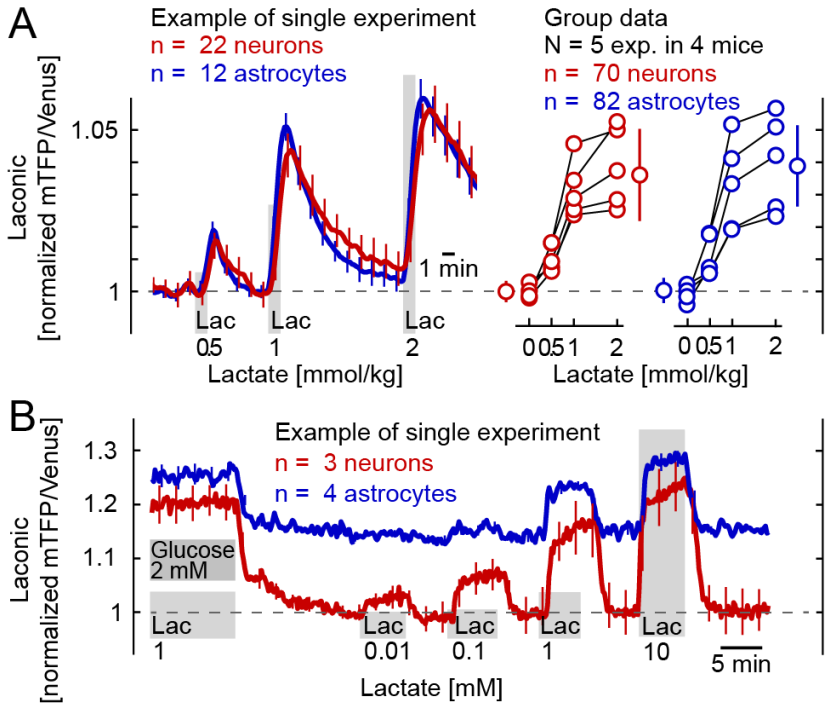

Figure 2. *Laconic* sensor functions *in vivo*. (A) *Laconic* signals increased both in astrocytes and neurons depending on the intravenously injected lactate dosage (Lac; 500 mM L-lactate solution; 0.5, 1 and 2 mmol per kg bodyweight; 0 mmol lactate was performed with 2 mmol per kg bodyweight of 500 mM sodium chloride solution). The standard deviations of cells in a single experiment (left) and of multiple independent experiments (right) are indicated (from 0 to 2 mmol/kg; normalization to individual baseline). See also Figure S1F, S1G, S3A and S3B. (B) Similarly, *Laconic* expressed in cultured astrocytes and neurons showed dose dependent signal increases. Data are normalized to pyruvate induced lactate depletion (see Figure S2D and S2E). Astrocytes but not neurons maintain sizable intracellular lactate levels even in a zero glucose and lactate medium, resulting in relatively low *Laconic* signal increases.

A single intravenous injection of lactate increases *Laconic* signal more in neurons than in astrocytes

To compare lactate accumulation in astrocytes and neurons, *Laconic* was simultaneously measured in neurons and astrocytes during short intravenous L-lactate infusions over three minutes (4 mmol/kg bodyweight), elevating blood lactate levels from 0.81 ± 0.26 mM to 17 ± 5.7 mM (Figure 3C). The *Laconic* signal increased more significantly in neurons than in astrocytes (5.7 ± 1.3% vs. 4.3 ± 1.3%, respectively; Figure 3A) with a rise in extracellular lactate levels of 0.27 ± 0.08 mM (Figure 3B). This discrepancy between neurons and astrocytes could reflect higher lactate accumulation in neurons at similar baseline lactate concentrations in both cell types. Alternatively, this difference could be attributed to lower baseline lactate concentrations in neurons, which would permit a greater upward dynamic range and sensitivity of *Laconic*.

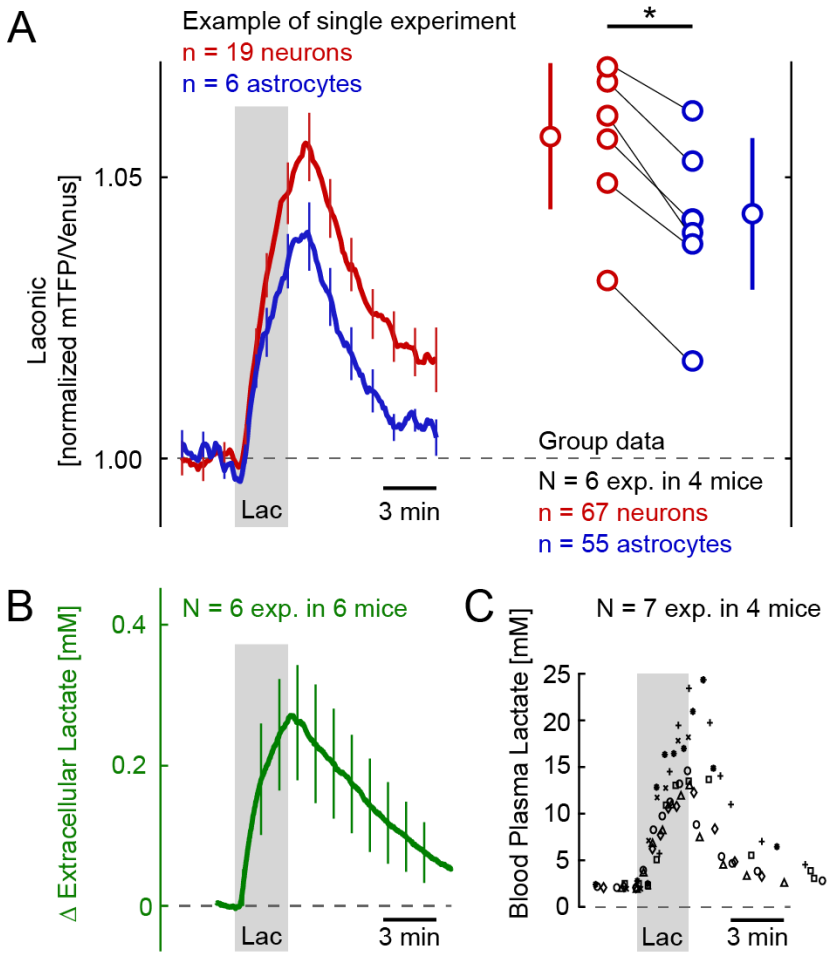

Figure 3. An intravenous injection of lactate increases *Laconic* signals more in neurons than in astrocytes. (A) Intravenous lactate infusions (4 mmol per kg bodyweight in 3 minutes, 500 mM solution) increased neuronal (5.7 ± 1.3%) more than astrocytic *Laconic* signal (4.3 ± 1.3%) in simultaneous recordings in one experiment (left) and over multiple recordings (right, normalization to individual baseline, mean on peak amplitudes, * = $p < 0.05$). See also Figure S3C. (B) The same lactate infusion protocol increased extracellular lactate (N = 6 animals, 0.27 ± 0.08 mM). (C) Blood lactate concentrations rose from 0.81 ± 0.26 mM to 17 ± 5.7 mM (N = 7 experiments). Data are represented as mean ± SD.

To distinguish between these two possibilities, the baseline lactate concentrations in astrocytes and neurons were compared by saturating *Laconic* in both cellular compartments. Ammonium chloride infusion over four minutes (2.5 mmol/kg bodyweight), which boosts cytosolic lactate concentration in brain cells by inhibiting mitochondrial pyruvate consumption (Lerchundi et al., 2015), increased *Laconic* signals in neurons and astrocytes (7.3 ± 1.3% vs. 7.4 ± 1.6%, respectively; Figure S1H). When ammonium chloride and L-lactate were simultaneously infused intravenously beforehand, additional

L-lactate application induced a significantly smaller increase of the *Laconic* signal in neurons (0.95 ± 0.62%, n = 53, $p < 0.05$, one-sample t-test) and astrocytes (0.57 ± 0.55%, n = 43 cells, $p < 0.05$, one-sample t-test) (Figure 4A) compared to the same lactate infusion in Figure 3 ($p < 10^{-7}$, two-sample t-test). However, extracellular lactate levels continued to increase with additional lactate infusion by 16 ± 10.7% of the total increase ($p < 0.05$, one-sample t-test) (Figure 4B). This suggests that ammonium chloride administration increased intracellular lactate concentrations to levels which saturated *Laconic*. Overall, a greater change in neuronal *Laconic* signal was observed (ΔFRET signal: 9.9 ± 2.4 %) compared to astrocytes (6.9 ± 2.0 %), supporting our hypothesis of lower baseline lactate levels in neurons (Figure 4A).

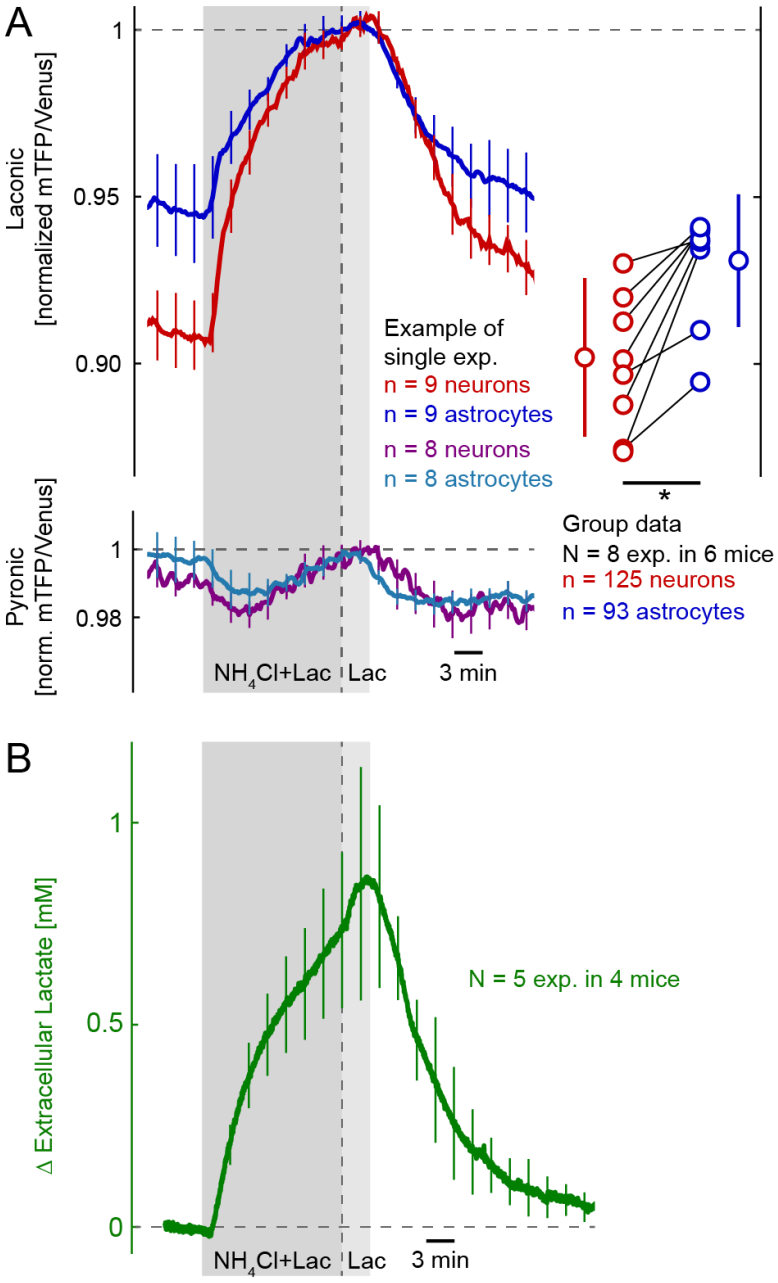

Figure 4. Baseline lactate levels in astrocytes and neurons can be compared by saturating *Laconic*. (A) Astrocytic and neuronal *Laconic* and *Pyronic* were simultaneously recorded during an intravenous infusion of ammonium chloride (4 mmol per kg bodyweight in 15 minutes, 500 mM solution) mixed with lactate (8 mmol per kg bodyweight in 15 minutes, 1 M solution), followed by a faster lactate injection (4 mmol per kg bodyweight in 3 minutes, 500 mM solution). *Pyronic* signals decreased during the ammonium chloride-lactate mix. In eight independent experiments, normalization to the saturation level of *Laconic* revealed lower baseline levels in neurons than in astrocytes (0.901 ± 0.024 vs. 0.931 ± 0.020, normalization to the three minutes after ammonium chloride stop, mean of baseline minima, * = $p < 0.05$). (B) Using the same infusion protocol, changes in extracellular lactate concentrations were measured in five trials. Extracellular lactate increased until the end of the infusion protocol by 0.87 ± 0.29 mM. Data are represented as mean ± SD. See also Figure S1H and S1I.

Pronounced trans-acceleration in astrocytes occurs at baseline

Pyruvate application has been used *in vitro* to decrease intracellular lactate levels in erythrocytes (Fishbein et al., 1988). This effect is based on a property of MCTs called trans-acceleration (Figure 5E), where the presence of extracellular monocarboxylates stimulates transporter substrate efflux. This process involves a facilitated conformational switch of the substrate binding site across the cell membrane when an adequate substrate is bound (Figure S2G, Garcia et al., 1994; Halestrap, 2013).

To test the capacity of intravenously applied pyruvate to produce a trans-acceleration-induced lactate efflux out of brain cells, extracellular brain lactate levels were measured with Pinnacle© biosensors (Figure S3D). Intravenous injection of 4 mmol/kg pyruvate over three minutes induced a transient increase of extracellular lactate levels of 0.084 ± 0.022 mM (Figure 5B), consistent with trans-acceleration of MCTs.

To compare trans-acceleration of MCTs in neurons and astrocytes, simultaneous measurements of *Laconic* and *Pyronic* during pyruvate application were performed. At baseline lactate levels, pyruvate decreased *Laconic* signal in astrocytes (-4.7 ± 1.5%), while signal in neurons was relatively unchanged (-0.6 ± 0.9%; Figure 5A). *Pyronic* showed only minor changes. However, after achieving higher intracellular lactate concentrations by the combined infusion of ammonium chloride and lactate, pyruvate administration was able to decrease *Laconic* signals in both astrocytes and neurons while increasing *Pyronic* signals in both cells (Figure 5C). Upon repeated i.v. injections of pyruvate, neuronal Laconic signal kept increasing, possibly due to the conversion of pyruvate to lactate (Gonzalez et al., 2005). Under these high lactate conditions, both astrocytes and neurons show trans-acceleration (Figure 5D), demonstrating that neuronal MCTs are also susceptible to pyruvate-driven efflux (Figure 5E). In a subset of recordings this lactate accumulation was absent in neurons, in which case a lactate depletion during pyruvate infusions could not be observed.

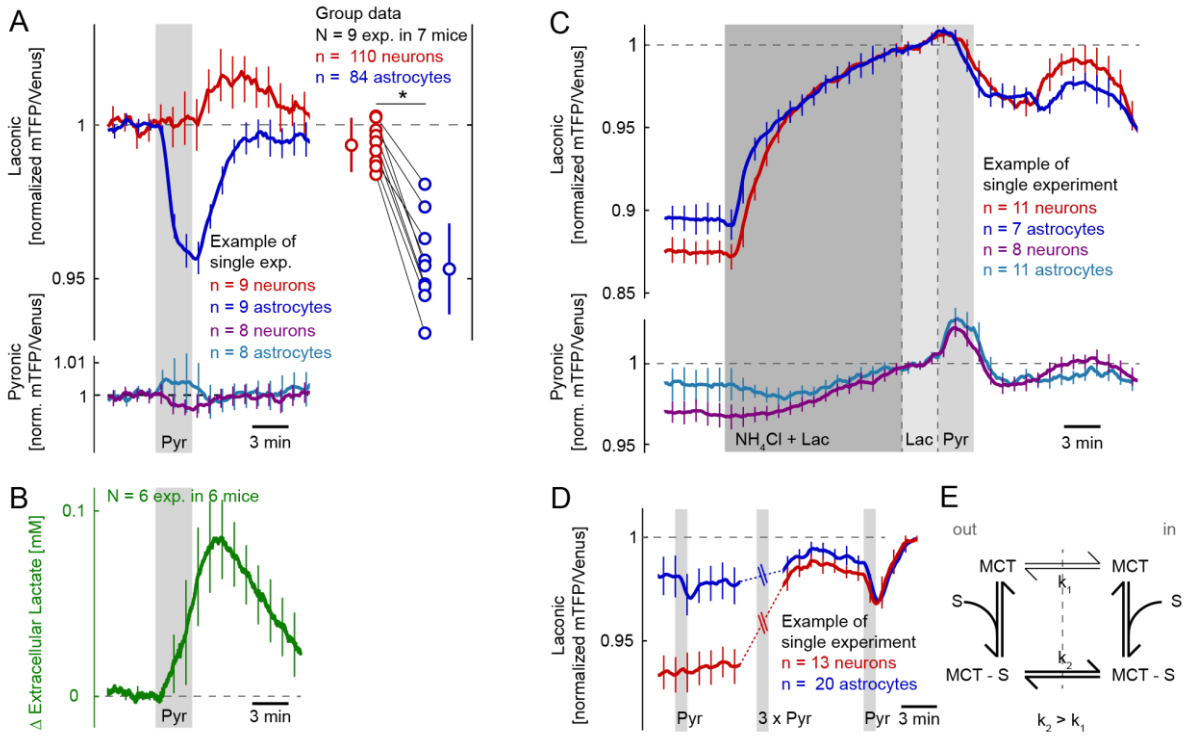

Figure 5. An intravenous injection of pyruvate decreases *Laconic* signals more in astrocytes than in neurons. (A) Intravenous pyruvate infusions (4 mmol per kg bodyweight in 3 minutes, 500 mM solution) decreased *Laconic* signal in astrocytes more than in neurons, while inducing only minor changes in *Pyronic* signal, as observed during simultaneous recordings in one experiment (left, normalization to individual baseline). Similar effects were observed over multiple recordings (right, normalization to individual baseline, maximum decrease of astrocytes was 4.7 ± 1.5 and of neurons 0.6 ± 0.9 %, * = $p < 0.05$). (B) The same pyruvate infusion protocol increased extracellular lactate (N = 6 animals, 0.084 ± 0.02 mM). (C) The *Laconic* saturation protocol (see figure 4) was followed by a pyruvate infusion, which induced a decrease of astrocytic and neuronal *Laconic* signal and an increase in *Pyronic* signal. Normalization to three minutes after cessation of ammonium chloride infusion. (D) In some trials repetitive pyruvate infusions increased *Laconic* signal in neurons, possibly due to conversion of pyruvate to lactate. With this artificially increased neuronal lactate levels, a pyruvate infusion (2 mmol per kg bodyweight in 1 minute, 500 mM solution) induced trans-acceleration also in neurons. Normalization to last minute of trace. (E) Trans-acceleration occurs at monocarboxylate transporters (MCT), because the substrate binding site of MCTs switches at a higher rate to the other side of the membrane when a substrate is bound (MCT – S; k_2) than without a substrate bound (MCT; k_1). Therefore, any substrate of MCT on one side of the membrane increases the rate of transport of another substrate in the opposite direction. Data are represented as mean ± SD. See also Figure S2.

Discussion

The compartmentation of brain energy metabolism is a subject of intense debate, fuelled by a lack of accurate *in vivo* intracellular lactate measurements in different cell populations. Here, we utilized the genetically encoded lactate sensor *Laconic* to observe the capacity of blood borne lactate to enter both

astrocytes and neurons and to approximate lactate concentrations in these cells. Whole brain tissue uptake of lactate from blood has previously been demonstrated *in vivo* (Cremer et al., 1979; Klein and Olsen, 1947; Wyss et al., 2011) and has been quantified in humans (Glenn et al., 2015; van Hall et al., 2009). We observed an accumulation of cellular and extracellular brain lactate during artificially increased blood lactate levels, which indicate a net uptake under these conditions and is in agreement with findings in humans (Boumezbeur et al., 2010; Quistorff et al., 2008; Rasmussen et al., 2011). The ability of neurons to take up lactate is an important prerequisite for the use of lactate as an energy substrate as suggested by the ANLS (Bélanger et al., 2011; Magistretti and Allaman, 2015), a concept that is still debated (Dienel, 2012 and references therein). Lactate has been shown to enter oxidative energy production in physiological resting conditions (Bouzier-Sore et al., 2006) and support neuronal activity under low-glucose conditions both *in vitro* (Tekkök et al., 2005) and *in vivo* (Herzog et al., 2013; Wyss et al., 2011).

We observed a greater neocortical *Laconic* signal increase in neurons than in astrocytes when blood lactate was elevated. This cell type difference was not due to altered *Laconic* sensitivity, as cumulative signal amplitudes were similar in both populations after decreasing intracellular lactate with pyruvate infusions and normalizing to the saturated sensor (Figure S1I). Therefore, baseline neuronal lactate levels could be lower where *Laconic* is more responsive. To evaluate this possibility, *Laconic* was saturated in both cellular compartments simultaneously using a mixture of lactate and ammonium (Provent et al., 2007), which revealed a higher maximal increase of neuronal *Laconic* and suggests a lower baseline lactate concentration in neurons than in astrocytes (Figure 6A).

We utilized the trans-acceleration property of MCTs (Brown and Brooks, 1994) by applying an inward pyruvate gradient to force the cells to release their lactate. The pronounced drop of astrocytic lactate and the negligible decrease in neurons is in agreement with higher resting lactate levels in astrocytes (Figure 6B). We can reject the following alternative explanations for the astrocyte-specific lactate drop: First, cell-type specific expression of isoforms in the brain has been reported with MCT1 mainly expressed in astrocytes and oligodendrocytes and MCT2 in neurons (Pellerin et al., 2005). We assessed the influence of MCT isoforms on trans-acceleration with a numerical model and demonstrated an almost linear dependency of the pyruvate-induced trans-acceleration on intracellular baseline lactate levels for both MCT1 and MCT2 (Figure S2A-C). However, the relatively higher affinity of MCT2 than MCT1 for pyruvate in our model would predict stronger trans-acceleration of MCT2, i.e. in neurons (Figure S2A-C). Also, trans-acceleration can be induced in cultured neurons (Figure S2E) and astrocytes (Figure S2F), where baseline lactate levels depend on the experimental conditions. The differential MCT isoform expression and kinetics can therefore not explain the predominant trans-acceleration in astrocytes.

Second, LDH diminishes lactate depletion caused by pyruvate uptake over time by transforming pyruvate into lactate. Intracellular lactate levels start to increase during pyruvate exposure if the rate of LDH-catalyzed conversion of pyruvate to lactate is high compared to lactate transport (Figure S2C) which may explain the delayed increase in lactate we observed following pyruvate infusion (Figure 5A). However, the lower NADH/NAD+ ratio in neurons compared to astrocytes (Hung et al., 2011) implies weaker conversion of pyruvate to lactate and is therefore unlikely to mask pyruvate induced lactate depletion in neurons.

Third, the brain vasculature is almost entirely covered by astrocytic endfeet (Mathiisen et al., 2010; McCaslin et al., 2011). Therefore, astrocytes are predominantly exposed to blood-borne pyruvate. The main transport limiting barrier for blood-borne pyruvate to enter brain tissue is MCT1 at the endothelial membranes and the fast diffusion within the tissue will expose all brain cells similarly (Halestrap, 2013; Miller and Oldendorf, 1986). Accordingly, we did not observe any temporal differences between astrocytic and neuronal lactate accumulation (Figure 2A and 3A). Additionally, buffering of lactate by *Laconic* is unlikely, because baseline lactate levels are higher (hundreds of µM instead of nM) and lactate transients are slower (multiple seconds instead of ms) than in the case of calcium dynamics, where buffering by the sensor is reported to be an issue (Grienberger and Konnerth, 2012). Finally, increasing lactate levels in neurons lead to trans-acceleration and lactate efflux in neurons similarly as in astrocytes (Figure 5C-D).

A higher resting state lactate level in astrocytes in comparison to neurons has significant implications for transcellular lactate exchange. Intracellular lactate accumulation driven by increased blood lactate and depletion during increased blood pyruvate is consistent with a facilitated transport of lactate via MCTs. The direction of a facilitated transport is determined by the concentration gradient, for which we found evidence to be from astrocytes to neurons as has been suggested by the ANLS (Pellerin and Magistretti, 1994) (Figure 6A). However, alternative lactate transport mechanisms have been suggested, such as via pannexins and connexins (Barros, 2013; Giaume et al., 2013) or an unknown potassium-dependent ion channel, which would allow active lactate transport even against a chemical concentration gradient during increased neuronal activity (Sotelo-Hitschfeld et al., 2015).

In addition, astrocytic lactate could provide a small but fast energy reserve; cultured astrocytes have been shown to preferentially export glucose-derived lactate rather than lactate derived from glycogen (Sickmann et al., 2005). Glycogen may serve as a slower energy pool, as astrocytic glycogen-derived lactate sustains neuronal function in rat optical nerve preparations for several minutes (Brown and Ransom, 2007).

Our data provide important information about lactate concentrations of the different cellular compartments, which are fundamental for the role of lactate as an activity dependent signaling

molecule (Mosienko et al., 2015). The transport of lactate from astrocytes to neurons has been shown to be necessary for the establishment of long-term memory (Suzuki et al., 2011) by inducing the expression of plasticity-related genes (Yang et al., 2014). Volatile halogenated anesthetics such as isoflurane are known to increase brain lactate levels (Boretius et al., 2013; Horn and Klein, 2010) and Fünfschilling and colleagues (Fünfschilling et al., 2012) reported a marked decrease in tissue lactate concentration in response to the discontinuation of isoflurane anesthesia, indicative of a substantial lactate exchange. In our study, we used injectable anesthetics to avoid elevated lactate levels, but our results can be used to interpret the direction of isoflurane-induced lactate exchange at the cellular level. It is important to note, however, that *Laconic* did not enable us to measure cellular or whole brain lactate transport or oxidation rates *in vivo*, as currently available pharmacological agents (such as the MCT blocker α-cyano-4-hydroxycinnamate) are neither fast (seconds) nor specific (limited side effects) enough.

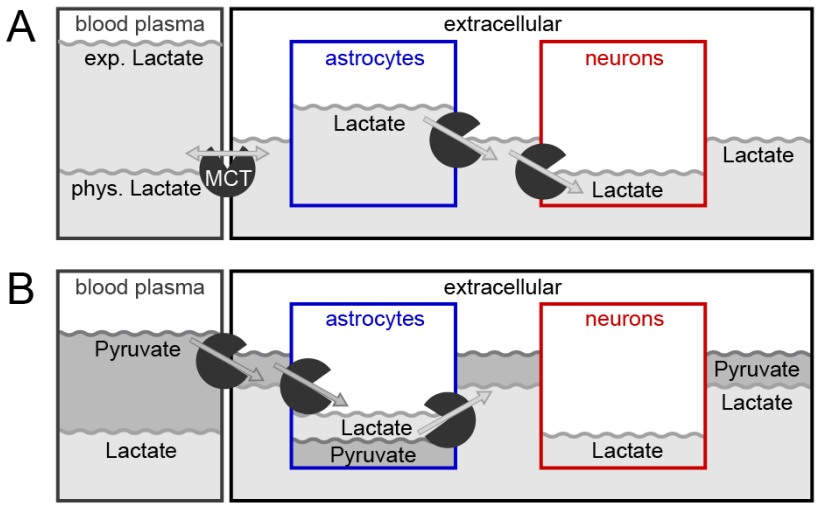

Figure 6. Model of lactate compartmentation. (A) Astrocytes accumulate lactate, which is transported along a concentration gradient via monocarboxylate transporters (MCT) to be consumed by neurons. Physiological (phys.) and experimentally increased (exp.) blood lactate levels are indicated. (B) Under artificially increased blood pyruvate levels, pyruvate enters brain cells from extracellular space via MCTs, forcing the extrusion of lactate. Pyruvate entry and concurrent lactate exit via MCTs requires relatively high intracellular lactate levels.

In summary, the genetically encoded lactate sensor *Laconic* in combination with 2PLSM was successfully applied to investigate brain energy metabolism at the single cell level *in vivo* for the first time. We demonstrate that neurons and astrocytes readily take up blood-borne lactate. Our data suggest a significantly lower baseline lactate level in neurons in comparison to astrocytes. Our findings

furthermore support the concept of compartmentalized lactate pools with a lactate flux from astrocytes to neurons.

Experimental Procedures

Viral constructs of the lactate sensor *Laconic* and the pyruvate sensor *Pyronic*

Genetically-encoded FRET sensors for lactate ('*Laconic';* San Martín et al., 2013), and pyruvate ('*Pyronic*'; San Martín et al., 2014), were cloned into adeno-associated viral (AAV) plasmids for astrocyte and neuron specific expression. The astrocyte-specific construct included a minimal GFAP promoter ($GfaABC_1D$, sGFAP; kindly provided by Dr. M. Brenner, Department of Neurobiology, University of Alabama) (Lee et al., 2008), a beta-globin intron, and a poly-adenylation signal. The neuronal construct included a human synapsin-1 (SYN) promoter, a Woodchuck Hepatitis Virus (WHP) Post-transcriptional Regulatory Element (WPRE) and a poly-adenylation signal (Glover et al., 2002; Kügler et al., 2001). The four different shuttle plasmids (pAAV-SYN-*Laconic*, pAAV-GFAP-*Laconic*, pAAV-SYN-*Pyronic*, and pAAV-GFAP-*Pyronic*) were used to generate AAV serotype 6 (SYN constructs) or AAV serotype 9 (GFAP constructs) viral particles, by co-transfecting the shuttle plasmid with the pDP6 and pDF9 helper plasmids in HEK293-AAV cells (Agilent Technologies, Santa Clara, CA). Viral particles were isolated from the cell lysates, using iodixanol step gradients and HPLC purification on heparin-binding (AAV6) and ion exchange (AAV9) columns. The number of viral genomic copies (VG) was measured by TaqMan real-time PCR, with primers amplifying specific sequences in the human beta-globin intron or WPRE element.

Animals

All experimental procedures were approved by the local veterinary authorities in Zurich and conformed to the guidelines of the Swiss Animal Protection Law, Veterinary Office, Canton of Zurich (Act of Animal Protection 16 December 2005 and Animal Protection Ordinance 23 April 2008). Surgery was performed in female wild type mice (*C57BL/6J*; Charles River) of 8 to 10 weeks of age (20 to 25 gram bodyweight). The mice had free access to water and food and an inverted 12-hour light/dark cycle.

Anesthesia

The animals were anesthetized with a mixture of fentanyl (0.05 mg per kg bodyweight; *Sintenyl,* Sintetica, Switzerland), midazolam (5 mg per kg bodyweight; *Dormicum*, Roche, Switzerland) and medetomidine (0.5 mg per kg bodyweight; *Domitor*, Orion Pharma, Finland) intraperitoneally and anesthesia was maintained with midazolam (5 mg per kg bodyweight) subcutaneously after 50 minutes. To prevent hypoxaemia, a face mask provided 300 mL/min of 100% oxygen. Core

temperature was kept constant at 37°C using a homeothermic blanket heating system during all surgical and experimental procedures (Harvard Apparatus, Holliston, MA, USA). The head was fixed in a stereotaxic apparatus and the eyes were kept wet with ointment (vitamin A eye cream; Bausch & Lomb, Switzerland).

Virus injection

A 4x4 mm craniotomy was performed above the somatosensory cortex using a dental drill (Bien-Air, Bienne, Switzerland) and solutions containing virus vector were injected into the primary somatosensory cortex at a close distance to achieve neighboring, but non-overlapping, sensor protein expression: 75 nL of AAV9-GFAP-*Laconic* (titer 3.1E12 VG/mL); 150 nL of AAV6-SYN-*Laconic* (titer 1.02E13 VG/mL) (San Martín et al., 2013); 75 nL of AAV9-GFAP-*Pyronic* (titer 1.6E12 VG/mL); 150 nL of AAV6-SYN-*Pyronic* (titer 1.15E12 VG/mL) (San Martín et al., 2014). Large vessels were avoided to prevent bleeding and the absorption of light by hemoglobin during imaging. A square cover slip (3x3 mm, UQG Optics Ltd, UK) was placed on the exposed dura mater and fixed to the skull with dental cement, according to published protocols (Holtmaat et al., 2009).

Head-post implantation

A bonding agent (*Gluma Comfort Bond*; Heraeus Kulzer, Hanau, Germany) was applied to the cleaned skull and polymerized with a handheld blue light source (600 mW/cm^2; Demetron LC, Switzerland). A custom-made aluminium head post was connected with dental cement (*EvoFlow*; Ivoclar Vivadent AG, Liechtenstein) to the bonding agent for later reproducible animal fixation in the microscopic setup. The skin lesion was treated with antibiotic ointment (Neomycin, *Cicatrex*; Janssen-Cilag AG, Switzerland) and closed with acrylic glue (*Histoacryl*, B. Braun, Germany). After surgery the animals were kept warm and provided with analgesics (metamizole 0.2 mg/g bodyweight; Sintetica, Switzerland) and an antibiotic was added to the drinking water (enrofloxacin, 200 mg/l drinking water; *Baytril*, Bayer, Germany). Sensor protein expression was checked using a fluorescence stereomicroscope (*Leica MZ16 FA*) two to three weeks after virus injection and prior to imaging.

Intracellular lactate measurements

The mice were imaged using a custom-built two-photon laser scanning microscope (2PLSM) with a tunable pulsed laser (*MaiTai eHP DS* system, Spectra-Physics, CA, USA) at 870 nm wavelength and equipped with a 20x water immersion objective (W-Plan-Apochromat 20x/1.0 differential interference contrast, Zeiss, Germany). During measurements the animals were head-fixed and kept under the anesthesia described above. The galvo-mirrors and a motorized objective were used to cycle through two to four individual fields of view. Unidirectional frame scans at 0.1 Hz and 512x512 pixels resolution were acquired with *ScanImage* (r3.8.1; Janelia Research Campus; Pologruto et al., 2003)). Lactate

concentration in cultured cells were measured with the use of *Laconic* as previously described (Sotelo-Hitschfeld et al., 2015).

Extracellular lactate measurements

Extracellular lactate measurements were performed with a commercially available recording system (*Pinnacle Inc.*, Lawrence, KS, USA). Mice were fixed in a stereotactic frame under anesthesia (isoflurane 1.5%; Abbott, North Chicago, IL, USA), the skull was opened with a dental drill, and a guide cannula (Part 7032, Pinnacle Technology, Lawrence, KS, USA) was implanted into the primary somatosensory cortex (from bregma: A/P +1.41, M/L -2.8, D/V -1.0) and fixed with dental cement to an anchor screw (Part 8209, Pinnacle Technology, Lawrence, KS, USA). After a recovery period of two weeks, the pre-calibrated lactate biosensor was inserted into the guide cannula (Naylor et al., 2012). A tail vein catheter was inserted for saline, lactate and pyruvate infusions. Recording started after one hour of signal stabilization.

Blood lactate level measurements

The femoral artery was exposed and cannulated with fine bore polyethylene tubing (0.28 mm ID, 0.61 mm OD, Portex, Smith medical, UK) to measure blood lactate level. Blood drops were removed from the cannula and every fourth drop was used for an enzymatic lactate assay (*Lactate Pro 2*, Arkray, Japan). After each blood sample analysis, the tubing was rinsed with heparinized (50 IU/ml) 0.9% saline solution.

Intervention protocols

For intravenous interventions, a 30 Gauge needle was connected to fine bore polyethylene tubing (0.28 mm ID, 0.61 mm OD, Portex, Smith medical, UK), filled with 0.9% saline solution and inserted into one of the tail veins. Before imaging, the tubing was connected via an X connector (model *SC25*, Instech, USA) to peristaltic pumps (*Reglo digital ISM 831*, Ismatec SA, Germany), which were operated via custom written *Matlab* codes. A 500 mM solution of sodium chloride (*S7653*, Sigma-Aldrich, MO, USA), sodium L-lactate (*L7022*, Sigma, MO, USA) or sodium pyruvate (*P2256*, Sigma-Aldrich, MO, USA) at 4 mmol per kg bodyweight was injected during 3 minutes.

Immunohistochemistry

Four mice expressing astrocytic and neuronal *Laconic* sensors and one mouse intraperitoneally injected with 2 mg per kg bodyweight lipopolysaccharides (Fontana et al., 1981) were anesthetized with pentobarbital (*Nembutal*, >50 mg/kg) intraperitoneally and transcardially perfused with 2% paraformaldehyde to assess immunohistochemical alterations. Brains were post-fixed in 4% paraformaldehyde, rinsed with phosphate-buffered saline (PBS), and cryoprotected with 30 % sucrose in PBS. The frozen brains were then cut into 40 µm sections with a sliding microtome and fluorescent

regions were identified with a fluorescence stereomicroscope (*Leica MZ16 FA*; Leica Microsystems, Germany). Free-floating sections were incubated with rabbit anti-Glial fibrillary acidic protein (GFAP) antibody (*Z0334*; DakoCytomation, DK), rabbit anti-fibrinogen antibody (*A0080*; DakoCytomation, DK) or rat anti-CD68 antibody (*MCA1957GA*; AbD Serotec) and stained with red-fluorescent secondary antibody (goat anti-rabbit and goat anti-rat Cy3; Jackson Immuno Research Laboratories Inc.). Images of the sections were collected with a laser-scanning confocal microscope (*LSM510-Meta*; Zeiss, Germany).

Cell culture experiments

All animal procedures for the *cell culture* experiments were approved by the *Institutional Animal Care and Use Committee* of the *Centro de Estudios Científicos*. Mixed cortical cultures of neuronal and glial cells were prepared from 1-3 day-old neonates (*C57BL/6J*) as detailed previously (Bittner, 2010). For *Laconic* sensor expression, cultures were exposed to 5 x 10^6 PFU of *Ad Laconic* and studied after 48 h (culture day 8-10). The co-culture cells were imaged with an upright *Olympus FV1000* confocal microscope and a 440 nm solid-state laser as detailed previously (Sotelo-Hitschfeld et al., 2015). Masked ratio images were generated from background-subtracted images using *ImageJ* software.

Data analysis and statistics

Astrocytic domains and neuronal cytoplasm of individual cells of cortical layers L2/3 (150-250 µm below the dura) were outlined using ImageJ (1.46r; National Institutes of Health, USA). The mTFP channel (with bandpass filter 475/64; Semrock, USA) was divided by the Venus channel (with bandpass filter 542/50; Semrock, USA) and the ratio was normalized to the corresponding baseline or as indicated in the figure legend using Matlab (MathWorks, USA). Time acquisition curves are filtered with a moving average of five frames and indicated as mean ± standard deviation. Effects in multiple animals were compared using t-tests in R (R Core Team, 2014). P values < 0.05 were taken as significance limit.

Author contributions

P.M. performed the in vivo two-photon experiments. M.E. and P.M. performed the extracellular lactate measurements. P.M., A.F.C., V.K., M.T.W., R.G. and M.Z. helped establish in vivo and in vitro experimental protocols. I.R.-G. and F.B.-L. performed cell culture experiments. A.S.M. and F.B. created the sensors *Laconic* and *Pyronic*. J.S., S.L. and B.S. prepared the viral vectors. P.M., M.T.W., F.B, J.S. and B.W. wrote the manuscript. P.M., M.T.W., P.J.M., F.B. and B.W. conceived and designed experiments. P.A., P.J.M., F.B. and B.W. provided laboratory infrastructure and financial support. All authors discussed the data and critically revised the manuscript.

Acknowledgements

This research was partly supported by the Swiss National Science Foundation, the Hartmann Müller-Stiftung, and the Swiss Foundation for Excellence in Biomedical Research. BW is a member of the Clinical Research Priority Program of the University of Zurich on Molecular Imaging. LFB is partly funded by the Fondecyt Grant 1130095. The Centro de Estudios Científicos CECs is funded by the Chilean Government through the Centers of Excellence Basal Financing Program of CONICYT.

References

Barros, L.F. (2013). Metabolic signaling by lactate in the brain. Trends Neurosci. *36*, 396–404.

Barros, L.F., and Deitmer, J.W. (2010). Glucose and lactate supply to the synapse. Brain Res. Rev. *63*, 149–159.

Bélanger, M., Allaman, I., and Magistretti, P.J. (2011). Brain Energy Metabolism: Focus on Astrocyte-Neuron Metabolic Cooperation. Cell Metab. *14*, 724–738.

Van den Berg, C.J., Krzalić, L., Mela, P., and Waelsch, H. (1969). Compartmentation of glutamate metabolism in brain. Evidence for the existence of two different tricarboxylic acid cycles in brain. Biochem. J. *113*, 281–290.

Bittar, P.G., Charnay, Y., Pellerin, L., Bouras, C., and Magistretti, P.J. (1996). Selective Distribution of Lactate Dehydrogenase Isoenzymes in Neurons and Astrocytes of Human Brain. J. Cereb. Blood Flow Metab. *16*, 1079–1089.

Bittner, C.X. (2010). High resolution measurement of the glycolytic rate. Front. Neuroenergetics *2*.

Boretius, S., Tammer, R., Michaelis, T., Brockmöller, J., and Frahm, J. (2013). Halogenated volatile anesthetics alter brain metabolism as revealed by proton magnetic resonance spectroscopy of mice in vivo. NeuroImage *69*, 244–255.

Boumezbeur, F., Petersen, K.F., Cline, G.W., Mason, G.F., Behar, K.L., Shulman, G.I., and Rothman, D.L. (2010). The Contribution of Blood Lactate to Brain Energy Metabolism in Humans Measured by Dynamic 13C Nuclear Magnetic Resonance Spectroscopy. J. Neurosci. *30*, 13983–13991.

Bouzier-Sore, A.-K., Voisin, P., Bouchaud, V., Bezancon, E., Franconi, J.-M., and Pellerin, L. (2006). Competition between glucose and lactate as oxidative energy substrates in both neurons and astrocytes: a comparative NMR study. Eur. J. Neurosci. *24*, 1687–1694.

Brooks, G.A., Dubouchaud, H., Brown, M., Sicurello, J.P., and Butz, C.E. (1999). Role of mitochondrial lactate dehydrogenase and lactate oxidation in the intracellular lactate shuttle. Proc. Natl. Acad. Sci. *96*, 1129–1134.

Brown, A.M., and Ransom, B.R. (2007). Astrocyte glycogen and brain energy metabolism. Glia *55*, 1263–1271.

Brown, M.A., and Brooks, G.A. (1994). Trans-Stimulation of Lactate Transport from Rat Sarcolemmal Membrane Vesicles. Arch. Biochem. Biophys. *313*, 22–28.

Cremer, J.E., Cunningham, V.J., Pardridge, W.M., Braun, L.D., and Oldendorf, W.H. (1979). Kinetics of Blood-Brain Barrier Transport of Pyruvate, Lactate and Glucose in Suckling, Weanling and Adult Rats. J. Neurochem. *33*, 439–445.

Debernardi, R., Pierre, K., Lengacher, S., Magistretti, P.J., and Pellerin, L. (2003). Cell-specific expression pattern of monocarboxylate transporters in astrocytes and neurons observed in different mouse brain cortical cell cultures. J. Neurosci. Res. *73*, 141–155.

Denk, W., Strickler, J.H., and Webb, W.W. (1990). Two-photon laser scanning fluorescence microscopy. Science *248*, 73–76.

Dienel, G.A. (2012). Brain lactate metabolism: the discoveries and the controversies. J. Cereb. Blood Flow Metab. *32*, 1107–1138.

Fishbein, W.N., Foellmer, J.W., Davis, J.I., Fishbein, T.M., and Armbrustmacher, P. (1988). Clinical assay of the human erythrocyte lactate transporter: I. Principles, procedure, and validation. Biochem. Med. Metab. Biol. *39*, 338–350.

Fontana, A., Bosshard, R., Dahinden, C., Grob, P., and Grieder, A. (1981). Glia cell response to bacterial lipopolysaccharide: Effect on nucleotide synthesis, its genetic control and definition of the active principle. J. Neuroimmunol. *1*, 343–352.

Fünfschilling, U., Supplie, L.M., Mahad, D., Boretius, S., Saab, A.S., Edgar, J., Brinkmann, B.G., Kassmann, C.M., Tzvetanova, I.D., Möbius, W., et al. (2012). Glycolytic oligodendrocytes maintain myelin and long-term axonal integrity. Nature *485*, 517–521.

Garcia, C.K., Goldstein, J.L., Pathak, R.K., Anderson, R.G.W., and Brown, M.S. (1994). Molecular characterization of a membrane transporter for lactate, pyruvate, and other monocarboxylates: Implications for the Cori cycle. Cell *76*, 865–873.

Giaume, C., Leybaert, L., C. Naus, C., and C. Sáez, J. (2013). Connexin and pannexin hemichannels in brain glial cells: properties, pharmacology, and roles. Front. Pharmacol. *4*.

Glenn, T.C., Martin, N.A., Horning, M.A., McArthur, D.L., Hovda, D.A., Vespa, P., and Brooks, G.A. (2015). Lactate: Brain Fuel in Human Traumatic Brain Injury: A Comparison with Normal Healthy Control Subjects. J. Neurotrauma *32*, 820–832.

Glover, C.P.J., Bienemann, A.S., Heywood, D.J., Cosgrave, A.S., and Uney, J.B. (2002). Adenoviral-Mediated, High-Level, Cell-Specific Transgene Expression: A SYN1-WPRE Cassette Mediates Increased Transgene Expression with No Loss of Neuron Specificity. Mol. Ther. *5*, 509–516.

Gonzalez, S.V., Nguyen, N.H.T., Rise, F., and Hassel, B. (2005). Brain metabolism of exogenous pyruvate. J. Neurochem. *95*, 284–293.

Grienberger, C., and Konnerth, A. (2012). Imaging Calcium in Neurons. Neuron *73*, 862–885.

Halestrap, A.P. (2013). Monocarboxylic acid transport. Compr. Physiol. *3*, 1611–1643.

Halestrap, A.P., and Wilson, M.C. (2012). The monocarboxylate transporter family—Role and regulation. IUBMB Life *64*, 109–119.

van Hall, G., Stromstad, M., Rasmussen, P., Jans, O., Zaar, M., Gam, C., Quistorff, B., Secher, N.H., and Nielsen, H.B. (2009). Blood lactate is an important energy source for the human brain. J Cereb Blood Flow Metab *29*, 1121–1129.

Herzog, R.I., Jiang, L., Herman, P., Zhao, C., Sanganahalli, B.G., Mason, G.F., Hyder, F., Rothman, D.L., Sherwin, R.S., and Behar, K.L. (2013). Lactate preserves neuronal metabolism and function following antecedent recurrent hypoglycemia. J. Clin. Invest. *123*, 1988–1998.

Holtmaat, A., Bonhoeffer, T., Chow, D.K., Chuckowree, J., De Paola, V., Hofer, S.B., Hübener, M., Keck, T., Knott, G., Lee, W.-C.A., et al. (2009). Long-term, high-resolution imaging in the mouse neocortex through a chronic cranial window. Nat. Protoc. *4*, 1128–1144.

Horn, T., and Klein, J. (2010). Lactate levels in the brain are elevated upon exposure to volatile anesthetics: A microdialysis study. Neurochem. Int. *57*, 940–947.

Hu, Y., and Wilson, G.S. (1997). A Temporary Local Energy Pool Coupled to Neuronal Activity: Fluctuations of Extracellular Lactate Levels in Rat Brain Monitored with Rapid-Response Enzyme-Based Sensor. J. Neurochem. *69*, 1484–1490.

Hung, Y.P., Albeck, J.G., Tantama, M., and Yellen, G. (2011). Imaging Cytosolic NADH-NAD+ Redox State with a Genetically Encoded Fluorescent Biosensor. Cell Metab. *14*, 545–554.

Klein, J.R., and Olsen, N.S. (1947). Distribution of Intravenously Injected Glutamate, Lactate, Pyruvate, and Succinate Between Blood and Brain. J. Biol. Chem. *167*, 1–5.

Kügler, S., Meyn, L., Holzmüller, H., Gerhardt, E., Isenmann, S., Schulz, J.B., and Bähr, M. (2001). Neuron-Specific Expression of Therapeutic Proteins: Evaluation of Different Cellular Promoters in Recombinant Adenoviral Vectors. Mol. Cell. Neurosci. *17*, 78–96.

Laughton, J.D., Charnay, Y., Belloir, B., Pellerin, L., Magistretti, P.J., and Bouras, C. (2000). Differential messenger RNA distribution of lactate dehydrogenase LDH-1 and LDH-5 isoforms in the rat brain. Neuroscience *96*, 619–625.

Lee, Y., Messing, A., Su, M., and Brenner, M. (2008). GFAP promoter elements required for region-specific and astrocyte-specific expression. Glia *56*, 481–493.

Lerchundi, R., Fernández-Moncada, I., Contreras-Baeza, Y., Sotelo-Hitschfeld, T., Mächler, P., Wyss, M.T., Stobart, J., Baeza-Lehnert, F., Alegría, K., Weber, B., et al. (2015). NH4+ triggers the release of astrocytic lactate via mitochondrial pyruvate shunting. Proc. Natl. Acad. Sci. 201508259.

Lin, A.-L., Fox, P.T., Hardies, J., Duong, T.Q., and Gao, J.-H. (2010). Nonlinear coupling between cerebral blood flow, oxygen consumption, and ATP production in human visual cortex. Proc. Natl. Acad. Sci. *107*, 8446–8451.

Magistretti, P.J., and Allaman, I. (2015). A Cellular Perspective on Brain Energy Metabolism and Functional Imaging. Neuron *86*, 883–901.

Martinez-Hernandez, A., Bell, K.P., and Norenberg, M.D. (1977). Glutamine Synthetase: Glial Localization in Brain. Science *195*, 1356–1358.

Mathiisen, T.M., Lehre, K.P., Danbolt, N.C., and Ottersen, O.P. (2010). The perivascular astroglial sheath provides a complete covering of the brain microvessels: An electron microscopic 3D reconstruction. Glia *58*, 1094–1103.

McCaslin, A.F.H., Chen, B.R., Radosevich, A.J., Cauli, B., and Hillman, E.M.C. (2011). In vivo 3D morphology of astrocyte-vasculature interactions in the somatosensory cortex: implications for neurovascular coupling. J. Cereb. Blood Flow Metab. *31*, 795–806.

Miller, L.P., and Oldendorf, W.H. (1986). Regional Kinetic Constants for Blood–Brain Barrier Pyruvic Acid Transport in Conscious Rats by the Monocarboxylic Acid Carrier. J. Neurochem. *46*, 1412–1416.

Mosienko, V., Teschemacher, A.G., and Kasparov, S. (2015). Is L-lactate a novel signaling molecule in the brain? J. Cereb. Blood Flow Metab. *35*, 1069–1075.

Naylor, E., Aillon, D.V., Barrett, B.S., Wilson, G.S., Johnson, D.A., Johnson, D.A., Harmon, H.P., Gabbert, S., and Petillo, P.A. (2012). Lactate as a Biomarker for Sleep. Sleep *35*, 1209–1222.

Oberheim, N.A., Takano, T., Han, X., He, W., Lin, J.H.C., Wang, F., Xu, Q., Wyatt, J.D., Pilcher, W., Ojemann, J.G., et al. (2009). Uniquely Hominid Features of Adult Human Astrocytes. J. Neurosci. *29*, 3276–3287.

Pellerin, L., and Magistretti, P.J. (1994). Glutamate uptake into astrocytes stimulates aerobic glycolysis: a mechanism coupling neuronal activity to glucose utilization. Proc. Natl. Acad. Sci. *91*, 10625–10629.

Pellerin, L., Bergersen, L.H., Halestrap, A.P., and Pierre, K. (2005). Cellular and subcellular distribution of monocarboxylate transporters in cultured brain cells and in the adult brain. J. Neurosci. Res. *79*, 55–64.

Pierre, K., and Pellerin, L. (2005). Monocarboxylate transporters in the central nervous system: distribution, regulation and function. J. Neurochem. *94*, 1–14.

Pologruto, T.A., Sabatini, B.L., and Svoboda, K. (2003). ScanImage: Flexible software for operating laser scanning microscopes. Biomed. Eng. OnLine *2*, 13.

Prichard, J., Rothman, D., Novotny, E., Petroff, O., Kuwabara, T., Avison, M., Howseman, A., Hanstock, C., and Shulman, R. (1991). Lactate rise detected by 1H NMR in human visual cortex during physiologic stimulation. Proc. Natl. Acad. Sci. *88*, 5829–5831.

Provent, P., Kickler, N., Barbier, E.L., Bergerot, A., Farion, R., Goury, S., Marcaggi, P., Segebarth, C., and Coles, J.A. (2007). The ammonium-induced increase in rat brain lactate concentration is rapid and reversible and is compatible with trafficking and signaling roles for ammonium. J. Cereb. Blood Flow Metab. *27*, 1830–1840.

Quistorff, B., Secher, N.H., and Lieshout, J.J.V. (2008). Lactate fuels the human brain during exercise. FASEB J. *22*, 3443–3449.

Rasmussen, P., Wyss, M.T., and Lundby, C. (2011). Cerebral glucose and lactate consumption during cerebral activation by physical activity in humans. FASEB J. *25*, 2865–2873.

R Core Team (2014). R: A Language and Environment for Statistical Computing (Vienna, Austria: R Foundation for Statistical Computing).

Sada, N., Lee, S., Katsu, T., Otsuki, T., and Inoue, T. (2015). Targeting LDH enzymes with a stiripentol analog to treat epilepsy. Science *347*, 1362–1367.

San Martín, A., Ceballo, S., Ruminot, I., Lerchundi, R., Frommer, W.B., and Barros, L.F. (2013). A Genetically Encoded FRET Lactate Sensor and Its Use To Detect the Warburg Effect in Single Cancer Cells. PLoS ONE *8*, e57712.

San Martín, A., Ceballo, S., Baeza-Lehnert, F., Lerchundi, R., Valdebenito, R., Contreras-Baeza, Y., Alegría, K., and Barros, L.F. (2014). Imaging Mitochondrial Flux in Single Cells with a FRET Sensor for Pyruvate. PLoS ONE *9*, e85780.

Sappey-Marinier, D., Calabrese, G., Fein, G., Hugg, J.W., Biggins, C., and Weiner, M.W. (1992). Effect of Photic Stimulation on Human Visual Cortex Lactate and Phosphates Using 1H and 31P Magnetic Resonance Spectroscopy. J. Cereb. Blood Flow Metab. *12*, 584–592.

Schurr, A. (2002). Lactate, glucose and energy metabolism in the ischemic brain (Review). Int. J. Mol. Med. *10*, 131–136.

Sickmann, H.M., Schousboe, A., Fosgerau, K., and Waagepetersen, H.S. (2005). Compartmentation of Lactate Originating from Glycogen and Glucose in Cultured Astrocytes. Neurochem. Res. *30*, 1295–1304.

Sotelo-Hitschfeld, T., Niemeyer, M.I., Mächler, P., Ruminot, I., Lerchundi, R., Wyss, M.T., Stobart, J., Fernández-Moncada, I., Valdebenito, R., Garrido-Gerter, P., et al. (2015). Channel-Mediated Lactate Release by K+-Stimulated Astrocytes. J. Neurosci. *35*, 4168–4178.

Stobart, J.L., and Anderson, C.M. (2013). Multifunctional role of astrocytes as gatekeepers of neuronal energy supply. Front. Cell. Neurosci. *7*.

Suzuki, A., Stern, S.A., Bozdagi, O., Huntley, G.W., Walker, R.H., Magistretti, P.J., and Alberini, C.M. (2011). Astrocyte-Neuron Lactate Transport Is Required for Long-Term Memory Formation. Cell *144*, 810–823.

Tang, F., Lane, S., Korsak, A., Paton, J.F.R., Gourine, A.V., Kasparov, S., and Teschemacher, A.G. (2014). Lactate-mediated glia-neuronal signalling in the mammalian brain. Nat. Commun. *5*.

Tekkök, S.B., Brown, A.M., Westenbroek, R., Pellerin, L., and Ransom, B.R. (2005). Transfer of glycogen-derived lactate from astrocytes to axons via specific monocarboxylate transporters supports mouse optic nerve activity. J. Neurosci. Res. *81*, 644–652.

Weber, B., and Barros, L.F. (2015). The Astrocyte: Powerhouse and Recycling Center. Cold Spring Harb. Perspect. Biol. a020396.

Wyss, M.T., Jolivet, R., Buck, A., Magistretti, P.J., and Weber, B. (2011). In Vivo Evidence for Lactate as a Neuronal Energy Source. J. Neurosci. *31*, 7477–7485.

Yang, J., Ruchti, E., Petit, J.-M., Jourdain, P., Grenningloh, G., Allaman, I., and Magistretti, P.J. (2014). Lactate promotes plasticity gene expression by potentiating NMDA signaling in neurons. Proc. Natl. Acad. Sci. *111*, 12228–12233.

Supplemental Figures

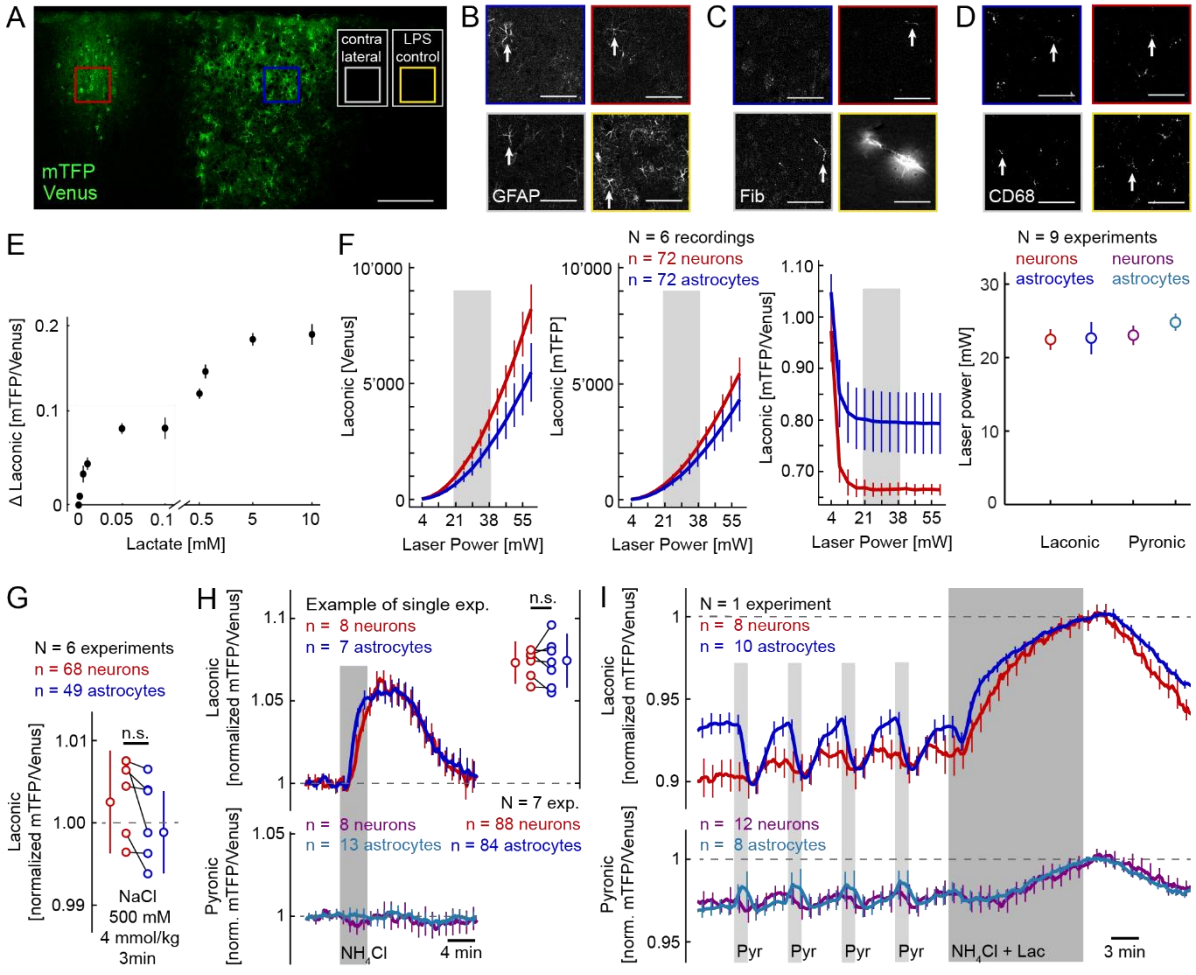

Figure S1. *Laconic* immunohistochemistry and specificity. Related to Figure 1, 3 and 4.

(A) Neuronal (left) and astrocytic (middle) *Laconic* fluorescence acquired *post mortem* using confocal microscopy. Cortical area without virus injection (right). Scale bar: 200 µm. (B) Both, astrocytic (blue frame) and neuronal (red frame) *Laconic* expressing tissue showed sparsely GFAP-positive astrocytes (arrows) without an increase compared to contralateral (gray frame) layer 2/3 cortex (image sections correspond to frame selections in panel A). The same GFAP staining was positive in mice injected with lipopolysaccharide (LPS, yellow frame), which is known to induce cortical inflammation (Fontana et al., 1981). (C) Fibrinogen staining was restricted to vessels (arrows) without any sign of blood brain barrier leakage as in LPS treated mice. (D) Staining for CD68 did not indicate an increased number or reactivity of microglia as with LPS treatment (arrows). Scale bars in figures B-D: 50 µm. (E) The *in vitro* calibration curve of *Laconic* shows the substrate binding kinetics of lactate at 25° celsius (San Martín et al., 2013). (F) Increasing the output laser power from 4 to 59 mW (measured under the objective) increased the fluorescence intensity in the *Venus* and *mTFP* channel, but did not affect ratio values at laser intensities used in this study (20 to 40 mW, grey bar). In the rightmost subpanel, laser power values measured in a set of experiments with pyruvate infusions are indicated. (G) The intravenous injection of sodium chloride (4 mmol per kg bodyweight in three minutes, 500 mM solution) did not show different signal changes in astrocytes and neurons (n.s. = $p > 0.05$). (H) Ammonium chloride (NH_4Cl) infusions over four minutes (2.5 mmol/kg bodyweight) increased *Laconic* signals in neurons and astrocytes (7.3 ± 1.3% vs.

7.4 ± 1.6%, respectively, normalization to baseline, mean of peak amplitudes, n.s. = $p > 0.05$). (I) Repetitive infusions of pyruvate (2 mmol per kg bodyweight in 1.5 minutes, 500 mM solution) were followed by the *Laconic* saturation protocol (ammonium chloride 4 mmol per kg bodyweight 500 mM solution mixed with lactate 8 mmol per kg bodyweight 1 M solution in 15 minutes). Normalization to the sensor's saturation point demonstrates the convergence of astrocytic and neuronal *Laconic* under pyruvate induced trans-acceleration (upper traces). The simultaneous measurement of the pyruvate sensor *Pyronic* demonstrates the specificity of *Laconic* to lactate (lower traces). Data are represented as mean ± SD.

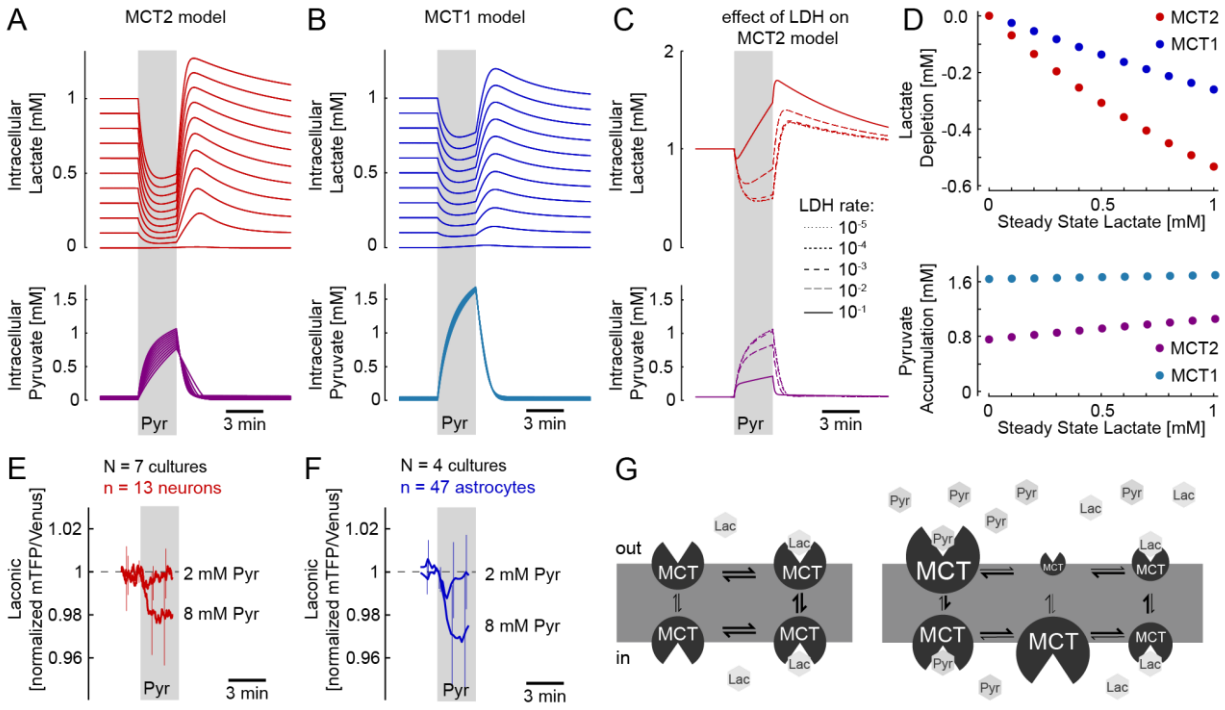

Figure S2. In silico modeling of trans-acceleration and *in vitro* controls. Related to Figure 2 and 5.

Lactate and pyruvate are transported in and out of cells through monocarboxylate transporters (MCTs). Competition between the two substrates for the shared binding site in the transporter and the fact that the binding site trans-locates more efficiently when complexed with a substrate leads to trans-acceleration (also known as accelerated exchange (Garcia et al., 1994), that is the enhancement of transport of a substrate located at the opposite side of the membrane. Trans-acceleration can be explained with the following kinetic model: (A) Simulation results of intracellular lactate and pyruvate concentrations using kinetic parameters of the MCT 2 (4 µM; symmetrically distributed; pH 7.4; K_{off} lactate 7.6 x 10^6 s^{-1} and K_{off} pyruvate 7.6 x 10^5 s^{-1}) during an extracellular 2 mM pyruvate challenge. Each line represents a different steady state lactate concentration from 0 to 1 mM at baseline. The rate of LDH is set to 10^{-4} s^{-1} and the reverse reaction 20 times lower, putting the ratio lactate/pyruvate to 20. (B) The same model as before but with the kinetic parameters of MCT 1 (20 µM; symmetrically distributed; pH 7.4; K_{off} lactate 7.6 x 10^7 s^{-1} and K_{off} pyruvate 7.6 x 10^6 s^{-1}). (C) The contribution of LDH activity on pyruvate induced transients in the MCT 2 model is demonstrated for a wide range of LDH rates. (D) In the two MCT models, the amplitude of lactate depletion after 20 s depends linearly on the baseline lactate level and is larger with MCT 2 than MCT 1 (top). Pyruvate accumulates more in the MCT1 model (bottom). (E) Cultured neurons expressing *Laconic* showed pyruvate dose dependent lactate depletion (cells in a Krebs Ringer Hepes Bicarbonate buffer with 2 mM glucose and 1 mM lactate). (F) Cultured astrocytes in the same buffer solution showed similar *Laconic* transients. Data are represented as mean ± SD. (G) Under physiological conditions pyruvate concentrations are too low to compete with lactate at MCTs (left). After a rise in extracellular pyruvate (right part), the transporters bind pyruvate, which results in a reduced binding site availability for lactate and a reduction of lactate influx. Then the binding site trans-locates from outward-facing to inward-facing configuration. If there is lactate within the cell, the increased number of inward-facing sites subsequently causes an increased lactate efflux. The combination of reduced lactate influx and increased lactate efflux results in a drop of intracellular lactate concentration. This increase of lactate flux by pyruvate in this example is analogous to the extrusion of calcium by sodium in the Na^+-Ca^{2+} exchanger.

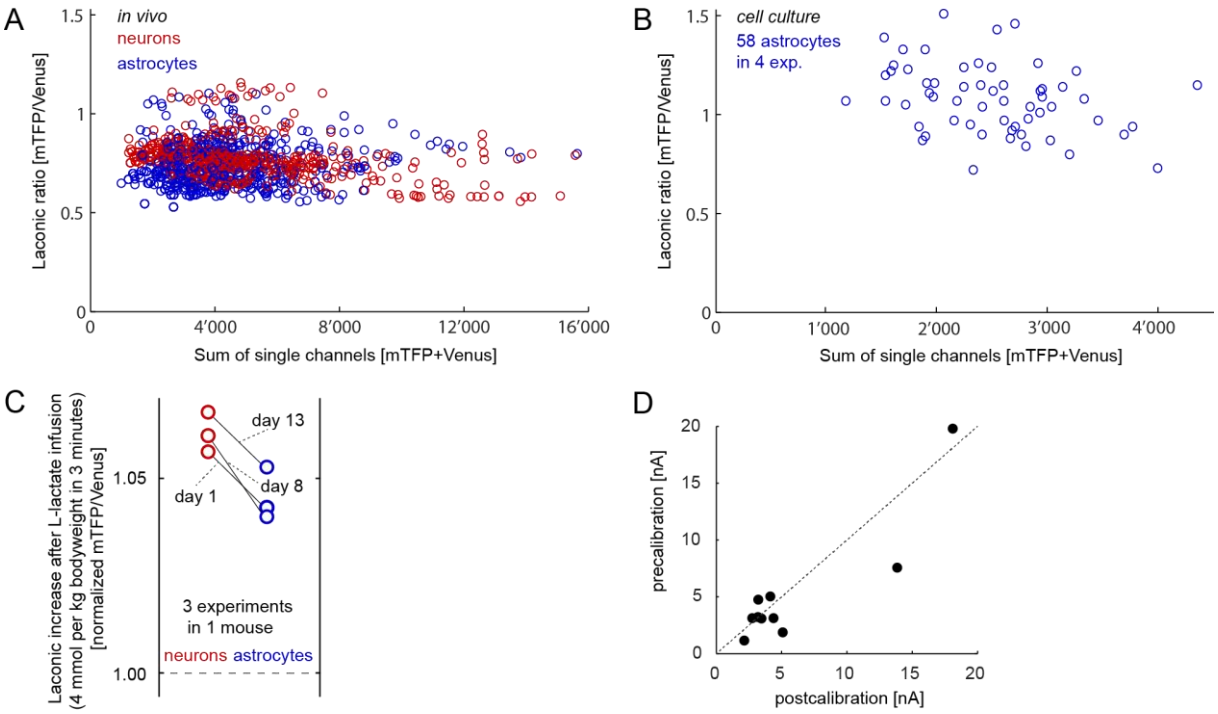

Figure S3. Characterization of intracellular and extracellular lactate measurements. Related to Figure 2, 3, 4 and 5.

(A) and (B) demonstrate that the Laconic FRET ratio is independent from sensor expression levels. (A) A sample measurement from baseline (frame 10) from each cell imaged in this study was taken and the sum of the two channels was plotted against their ratio. (B) The same plot is given for cultured astrocytes. (C) Demonstration of reproducibility over different imaging sessions. Repetitive lactate infusions in a single mouse on day 1, 8 and 13 increased *Laconic* signals in variable populations of layer 2/3 neocortical neurons and astrocytes. (D) Comparison of the *in vitro* pre- and post- calibration values from the extracellular lactate biosensors used *in vivo* demonstrates that the sensitivity of the sensor was preserved within an experiment.

Supplemental References

Fontana, A., Bosshard, R., Dahinden, C., Grob, P., and Grieder, A. (1981). Glia cell response to bacterial lipopolysaccharide: Effect on nucleotide synthesis, its genetic control and definition of the active principle. J. Neuroimmunol. *1*, 343–352.

Garcia, C.K., Goldstein, J.L., Pathak, R.K., Anderson, R.G.W., and Brown, M.S. (1994). Molecular characterization of a membrane transporter for lactate, pyruvate, and other monocarboxylates: Implications for the Cori cycle. Cell *76*, 865–873.

San Martín, A., Ceballo, S., Ruminot, I., Lerchundi, R., Frommer, W.B., and Barros, L.F. (2013). A Genetically Encoded FRET Lactate Sensor and Its Use To Detect the Warburg Effect in Single Cancer Cells. PLoS ONE *8*, e57712.

Publication II: *In vivo* stimulation of *Laconic*

Channel-mediated lactate release by K^+-stimulated astrocytes

[1,3]Sotelo-Hitschfeld T., [1]Niemeyer M.I., [2]Mächler, P., [1]Ruminot, I., [1,3]Lerchundi, R., [2]Wyss, M., [2]Stobart, J.,[1,3]Fernández-Moncada, I., [1]Valdebenito, R., [1,3]Garrido-Gerter, P., [1,3]Contreras-Baeza, Y., [4]Schneider, B., [4]Langacher, S., [1,3]San Martín, A., [5]Bonvento, G., [4]Magistretti, P.J., [1]Sepúlveda, F.V., [2]Weber, B., [1]Barros, L.F

[1] Centro de Estudios Científicos (CECs), Valdivia, Chile.

[2] Institute of Pharmacology & Toxicology, University of Zürich, Switzerland.

[3] Universidad Austral de Chile, Valdivia, Chile.

[4] École polytechnique fédérale de Lausanne (EPFL), Lausanne, Switzerland.

[5] Molecular Imaging Research Center (MIRCen), CEA, Fontenay-aux-Roses, France.

Corresponding author: L. Felipe Barros, Centro de Estudios Científicos (CECs), Casilla 1469, Valdivia, Chile.

Cellular/Molecular

Channel-Mediated Lactate Release by K^+-Stimulated Astrocytes

Tamara Sotelo-Hitschfeld,[1,4] María I. Niemeyer,[1] Philipp Mächler,[2,3] Iván Ruminot,[1] Rodrigo Lerchundi,[1,4] Matthias T. Wyss,[2,3] Jillian Stobart,[2,3] Ignacio Fernández-Moncada,[1,4] Rocío Valdebenito,[1] Pamela Garrido-Gerter,[1,4] Yasna Contreras-Baeza,[1,4] Bernard L. Schneider,[5] Patrick Aebischer,[5] Sylvain Lengacher,[5] Alejandro San Martín,[1,4] Juliette Le Douce,[6] Gilles Bonvento,[6] Pierre J. Magistretti,[5,7] Francisco V. Sepúlveda,[1] Bruno Weber,[2,3] and L. Felipe Barros[1]

[1]Centro de Estudios Científicos, Valdivia 5110466, Chile, [2]Institute of Pharmacology and Toxicology, University of Zürich, 8057 Zürich, Switzerland, [3]Neuroscience Center Zürich, University and ETH Zürich, 8092 Zürich, Switzerland, [4]Universidad Austral de Chile, Valdivia, Chile, [5]Brain Mind Institute, École Polytechnique Fédérale de Lausanne, CH-1015 Lausanne, Switzerland, [6]Commissariat à l'Energie Atomique, Institut d'Imagerie Biomédicale, Molecular Imaging Research Center and Centre National de la Recherche Scientifique, Université Paris-Sud, Université Paris-Saclay, UMR 9199, F-92265 Fontenay-aux-Roses, France, and [7]Division of Biological and Environmental Sciences and Engineering, Kaust, Saudi Arabia

Excitatory synaptic transmission is accompanied by a local surge in interstitial lactate that occurs despite adequate oxygen availability, a puzzling phenomenon termed aerobic glycolysis. In addition to its role as an energy substrate, recent studies have shown that lactate modulates neuronal excitability acting through various targets, including NMDA receptors and G-protein-coupled receptors specific for lactate, but little is known about the cellular and molecular mechanisms responsible for the increase in interstitial lactate. Using a panel of genetically encoded fluorescence nanosensors for energy metabolites, we show here that mouse astrocytes in culture, in cortical slices, and *in vivo* maintain a steady-state reservoir of lactate. The reservoir was released to the extracellular space immediately after exposure of astrocytes to a physiological rise in extracellular K^+ or cell depolarization. Cell-attached patch-clamp analysis of cultured astrocytes revealed a 37 pS lactate-permeable ion channel activated by cell depolarization. The channel was modulated by lactate itself, resulting in a positive feedback loop for lactate release. A rapid fall in intracellular lactate levels was also observed in cortical astrocytes of anesthetized mice in response to local field stimulation. The existence of an astrocytic lactate reservoir and its quick mobilization via an ion channel in response to a neuronal cue provides fresh support to lactate roles in neuronal fueling and in gliotransmission.

Key words: **fluorescence microscopy; genetically encoded nanosensor; gliotransmission; membrane depolarization**

Introduction

The discovery of surface lactate receptors in neurons and other brain cells (Bozzo et al., 2013; Lauritzen et al., 2013; Tang et al., 2014) has rekindled interest in the local extracellular lactate rise that develops within seconds of neural activation (Prichard et al., 1991; Hu and Wilson, 1997; Barros, 2013). Some of us have recently proposed a mechanism contributing to the lactate transient that is based on the observation that a rise in extracellular K^+ ($[K^+]_o$), such as that recorded during neural activity, stimulates an astrocytic glucose consumption in culture and in brain slices, which also occurs within seconds (Bittner et al., 2011; Ruminot et al., 2011). Exposure of astrocytes to elevated $[K^+]_o$ was found to augment extracellular lactate, but, given the limited temporal resolution of standard biochemical techniques, it was not possible to ascertain whether K^+-stimulated astrocytes were able to release lactate within seconds, the time frame of the interstitial lactate transient observed *in vivo*. Genetically encoded nanosensors specific for nicotinamide adenine dinucleotide (NADH), lactate, and pyruvate, which were used here to map the fate of glucose and lactate during the first seconds of K^+ stimulation, have been developed since then (Hung et al., 2011; San Martín et al., 2013, 2014a). We report that astrocytes *in vitro* and *in vivo* maintain a cytosolic reservoir of lactate, which, in response to plasma membrane depolarization, is immediately released to the extracellular space via an ion channel that conducts lactate and is positively modulated by lactate itself.

Received Dec. 11, 2014; revised Jan. 9, 2015; accepted Jan. 13, 2015.

Author contributions: T.S.-H., M.I.N., M.T.W., F.V.S., B.W., and L.F.B. designed research; T.S.-H., M.I.N., P.M., I.R., R.L., M.T.W., I.F.-M., R.V., P.G.-G., Y.C.-B., A.S.M., and J.L.D. performed research; J.S., B.L.S., P.A., S.L., A.S.M., J.L.D., G.B., P.J.M., B.W., and L.F.B. contributed unpublished reagents/analytic tools; T.S.-H., M.I.N., P.M., I.R., R.L., M.T.W., I.F.-M., R.V., P.G.-G., Y.C.-B., A.S.M., F.V.S., B.W., and L.F.B. analyzed data; T.S.-H., F.V.S., B.W., and L.F.B. wrote the paper.

This research was partly funded by Fondecyt Grant 1130095 (to L.F.B.) and a joint grant from the Comisión Nacional de Investigación Científica y Tecnológica (CONICYT)-Chile and the Deutsche Forschungsgemeinschaft to L.F.B. and Joachim W. Deitmer, TU Kaiserslautern, Germany (DFG-12, DE 231/25-1). B.W. is partly supported by the Clinical Research Priority Program of the University of Zurich on Molecular Imaging. We also thank the Evaluation-orientation de la Coopération Scientifique-Sud program (Grant C10S04 to G.B. and L.F.B.) and the French National Research Agency ANR (Grant 2011 MALZ 003-02 to G.B.). The Centro de Estudios Científicos is funded by the Chilean Government through the Centers of Excellence Basal Financing Program of CONICYT. We thank Pablo Cid for helpful discussions, Karin Alegría for expert technical assistance, and Karen Everett for critical reading of the manuscript.

The authors declare no competing financial interests.

Correspondence should be addressed to L. Felipe Barros, Centro de Estudios Científicos (CECs), Valdivia 5110466, Chile. E-mail: fbarros@cecs.cl.

DOI:10.1523/JNEUROSCI.5036-14.2015

 0270-6474/15/354168-11$15.00/0

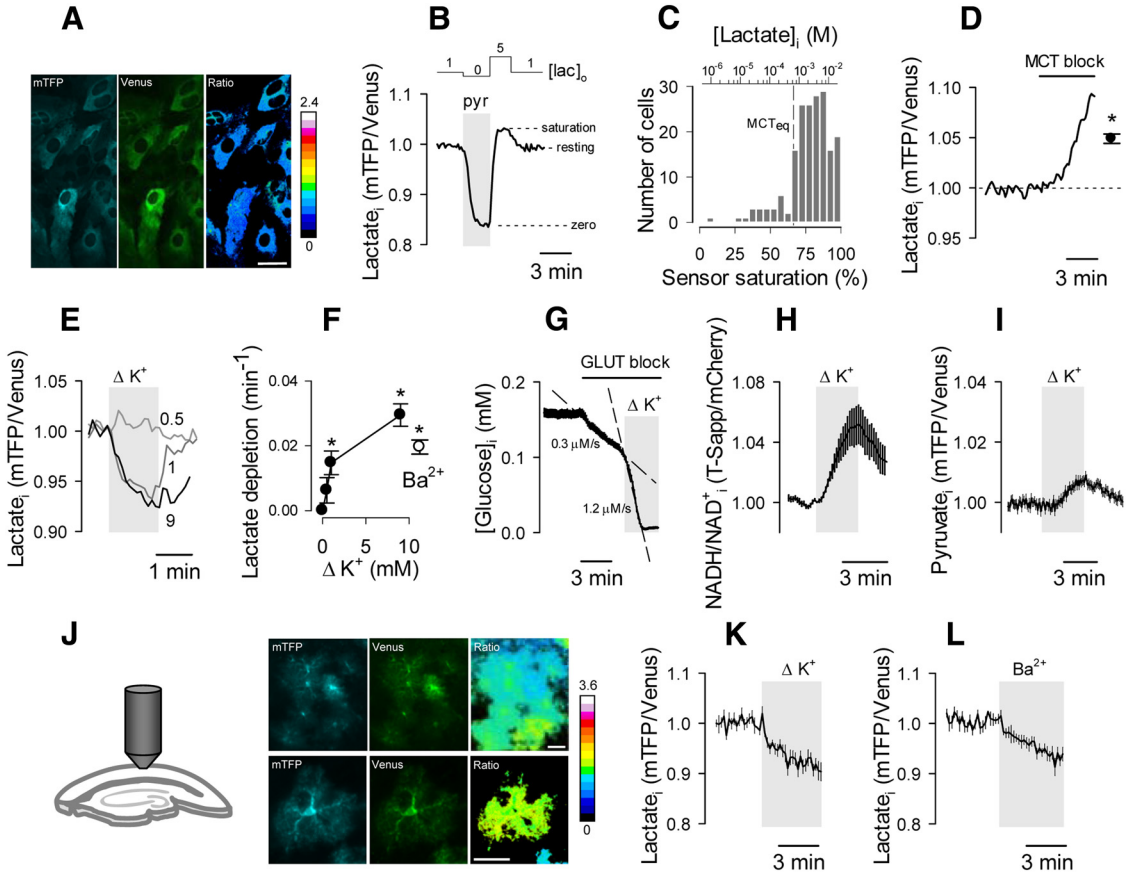

Figure 1. Astrocytes maintain a cytosolic lactate reservoir that is depleted in the short term by high $[K^+]_o$. ***A***, The FRET lactate sensor Laconic expressed in the cytosol of cultured astrocytes, showing mTFP (blue), Venus (green), and the ratio between mTFP and Venus. Scale bar, 20 μm. ***B***, Laconic was first depleted of lactate by superfusion with 10 mM pyruvate (pyr), and then saturated with 5 mM lactate and 2 mM glucose (San Martín et al., 2013). ***C***, Resting lactate level in 183 cells (17 experiments), estimated with the protocol in ***B***. The top *x*-axis indicates lactate concentration, according to the kinetic parameters estimated *in vitro*. Equilibrium concentration (MCT_{eq}) of the monocarboxylate transporters. ***D***, Response of intracellular lactate to 1 μM AR-C155858. The closed symbol represents the average change after 5 min of MCT blockage. ***E***, Effect of 0.5, 1, and 9 mM $[K^+]_o$ additions on the lactate level of an astrocyte. Resting $[K^+]_o = 3$ mM. ***F***, Initial rates of K^+-induced lactate depletion. The open symbol represents the initial rate of lactate depletion after exposure to 3 mM Ba^{2+}. ***G–I***, Effect of a 9 mM $[K^+]_o$ rise on glucose consumption (***G***), cytosolic $NADH/NAD^+$ ratio (***H***), and cytosolic pyruvate level (***I***). ***J***, Protoplasmic astrocytes expressing Laconic observed in an acute cortical slice at low (top) and high (bottom) magnification. Scale bar, 20 μm. ***K***, ***L***, The effects of increasing $[K^+]_o$ by 9 mM (***K***) or by adding 3 mM Ba^{2+} (***L***) on the lactate level of protoplasmic astrocytes are shown.

Materials and Methods

Standard reagents and inhibitors were acquired from Sigma. AR-C155858 was purchased from Haoyuan Chemexpress. Plasmids encoding the sensors FLII ^{12}Pglu700$\mu\Delta$6 (Takanaga et al., 2008), Peredox (Hung et al., 2011), Laconic (San Martín et al., 2013), and Pyronic (San Martín et al., 2014a) are available from Addgene (www.addgene.org). Ad Laconic, Ad Pyronic, and Ad FLII ^{12}Pglu700$\mu\Delta$6 (all serotype 5) were custom made by Vector Biolabs. The adeno-associated virus (AAV9) expressing Laconic under the control of the short gfaABC$_1$D promoter was generated at the École Polytechnique Fédérale de Lausanne. Design, production, and titration of the AAV9 vector for transgene expression in astrocytes have been described previously (Dirren et al., 2014).

Animals

Animal procedures in Valdivia were approved by the Centro de Estudios Científicos Animal Care and Use Committee, following the recommendations of the *Guide for the Care and Use of Laboratory Animals*, Institute of Laboratory Animal Resources, National Research Council. Animals used were mixed F1 male mice (C57BL/6J6CBA/J), kept in an animal room under specific pathogen-free conditions at a room temperature of 20 ± 2°C, in a 12 h light/dark cycle with free access to food and water. Surgical and experimental procedures in Zürich were approved by the local veterinary authorities, conforming to the guidelines of the Swiss Animal Protection Law, Veterinary Office, Canton Zürich (Act of Animal Protection 16 December 2005 and Animal Protection Ordinance 23 April 2008). Wild-type mice (C57BL/6J; Harlan Laboratories) 10 weeks of age and with a body weight of 20 g were housed in single cages, with water and food available *ad libitum*.

Experimental preparations

Culture cells. Mixed cortical cultures of neuronal and glial cells were prepared from 1- to 3-d-old neonates (Loaiza et al., 2003). HEK293 cells were cultured as previously described (San Martín et al., 2013). HEK cells and astrocytes were plasmid transfected (0.5 μg/ml) using Lipofectamine 2000 or 3000 (Life Technologies). Alternatively, astrocytes were exposed to 5×10^6 pfu of Ad Laconic, Ad Pyronic, or Ad FLII ^{12}Pglu700$\mu\Delta$6, and were studied after 48 h (culture days 8–10). Extracellular lactate levels were measured with the BioVision Lactate Assay Kit according to the instructions of the manufacturer.

Brain slices. Neonatal mice (days 1–3) were removed from the mother and anesthetized by hypothermia over 15 min. Animals were positioned upon a stage and injected with 1 μl of AAV9 (titer 3.1E12 VG/ml) into the skull (Davidson et al., 2010) using a Fusion 100 syringe pump (Chemyx). After injection, the animals were positioned on a temperate bed until they recovered and then returned to the mother. After 4 weeks, animals were killed by cervical dislocation and coronal brain sections (200 μm in thickness) were prepared as described previously (Jakoby et al., 2014).

Somatosensory cortex in vivo. Animals were anesthetized with an intraperitoneally injected mixture of fentanyl (0.05 mg/kg body weight; Sintenyl, Sintetica), midazolam (5 mg/kg body weight; Dormicum, Roche), and medetomidine (0.5 mg/kg body weight; Domitor, Orion Pharma), and again after 50 min with midazolam only (5 mg/kg body weight). If

necessary, anesthesia was prolonged with isoflurane (0.5%; Abbott). The animal head was fixed in a stereotaxic apparatus (David Kopf Instruments), and the eyes were kept wet with an ointment (vitamin A eye cream; Bausch & Lomb). A 4 × 4 mm craniotomy was performed using a surgical drill (Osseodoc) and 200 nl of recombinant AAV9 (titer 3.1E12 VG/ml), carrying the genetically encoded lactate sensor Laconic, was injected into the primary somatosensory cortex. A square coverslip (3 × 3 mm, UQG Optics Ltd) was lightly pressed onto the exposed brain and fixed with dental cement to the skull. A bonding agent (Gluma Comfort Bond, Heraeus Kulzer) was applied to the cleaned skull and was polymerized with a handheld blue light source (600 mW/cm^2; Demetron LC). A custom-made aluminum headpost was fixed to the bonding agent with dental cement (Tetric EvoFlow, Ivoclar Vivadent). The open skin was treated with an antibiotic ointment (Cicatrex, Janssen-Cilag) and closed with acrylic glue (Histoacryl, B. Braun). After surgery the animals were kept warm and given analgesics (Novaminsulfon, 50%, Sintetica), and the antibiotic enrofloxacin was added to the drinking water for 5 d (200 mg/L drinking water; Baytril, Bayer).

Fluorescence imaging

Detailed protocols for the use of the fluorescent sensors are available (Hou et al., 2011; Tantama et al., 2012; Barros et al., 2014; San Martín et al., 2014b). In the article describing the lactate sensor Laconic (San Martín et al., 2013), data were presented showing some sensitivity to pH in the alkaline range and also to citrate in the millimolar range. However, further characterization has shown that the sensitivities to pH and citrate were not a property of the sensor itself but *in vitro* artifacts respectively due to protein instability at room temperature in a noncellular milieu and divalent chelation by citrate. These results will be presented in detail in a separate manuscript (San Martin et al., manuscript in preparation). Measurements in cultured cells were performed at room temperature (22–24°C) in a 95% air/5% CO_2-gassed solution of the following composition (in mM): 112 NaCl, 3 KCl, 1.25 CaCl2, 1.25 MgCl2, 1–2 glucose, 10 HEPES, and 24 NaHCO3, pH 7.4. Slice measurements were performed at room temperature (22–24°C) in a 95% O_2/5% CO_2-gassed solution of the following composition (in mM): 126 NaCl, 3 KCl, 1.25 NaH_2PO_4, 1.25 CaCl2, 1.25 MgCl2, 10 glucose, and 26 NaHCO3, at pH 7.4. Cells and slices were imaged with an upright Olympus FV1000 confocal microscope equipped with a 20× water-immersion objective (numerical aperture, 1.0) and a 440 nm solid-state laser. Alternatively, cells were imaged with Olympus IX70 or BX51 microscopes equipped with Cairn Research monochromators and Optosplits, and either a Hamamatsu Orca or Rollera camera. FLII ^{12}Pglu700$\mu\Delta$6, Laconic, and Pyronic were excited at 430 nm for 0.2–0.8 s, and were detected at 485/40 nm [cyan fluorescent protein or monomeric teal fluorescent protein (mTFP)] and 535/30 nm (Citrine or Venus). Peredox-mCherry was imaged at 410 nm excitation and 485/40 emission (T-sapphire), and 570 nm excitation and 610/50 nm emission (mCherry). Masked ratio images were generated from background-subtracted images using ImageJ software. The H^+-sensitive dye 2′,7′-bis-(2-carboxyethyl)-5-(and-6)-carboxyfluorescein (BCECF) was ester loaded at 0.1 μM for 3–4 min, and the signal was calibrated by exposing the cultures to solutions of different pH after permeabilizing the cells with 10 μg/ml nigericin and 20 μg/ml gramicidin in an intracellular buffer. BCECF was sequentially excited at 440 and 490 nm (0.05 s), and imaged at 535/30 nm. Calcein was ester loaded at 0.1 μM for 20 min and then imaged using confocal microscopy.

After 3 weeks of sensor expression, living mice were imaged with a custom-built two-photon laser-scanning microscope using a tunable pulsed (Mai Tai eHP DS system, Spectra-Physics) at a wavelength of 870 nm using a 20× water-immersion objective (W Plan-Apochromat 20×/1.0 differential interference contrast, Zeiss). The animals were head fixed and kept under anesthesia, as described above. Body temperature was kept constant with a feedback-controlled heating pad (37°C; Harvard Apparatus). Frame scans were acquired with ScanImage (r3.8.1; Janelia Research Campus; Pologruto et al., 2003) at 1.63 Hz and 512 × 512 pixels resolution. Single astrocytes of cortical layers L2/3 (150–250 μm below the dura) were outlined using ImageJ (1.46r; National Institutes of Health) and the mTFP channel (with bandpass filter 475/64; Semrock)

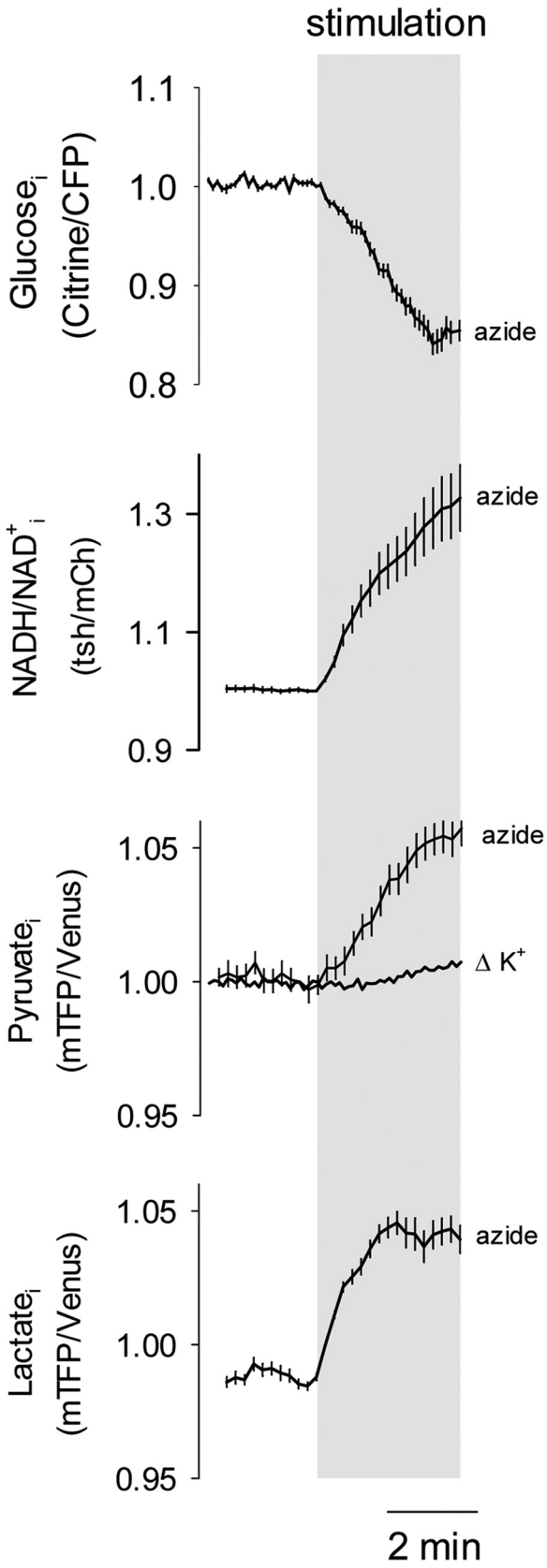

Figure 2. Intracellular lactate accumulation in response to OXPHOS inhibition. Astrocytes were exposed to 5 mM azide while measuring glucose, NADH/NAD $^+$ ratio, pyruvate or lactate. The effect of 12 mM $[K^+]_o$ on pyruvate levels (from Fig. 1*I*) is shown for comparison.

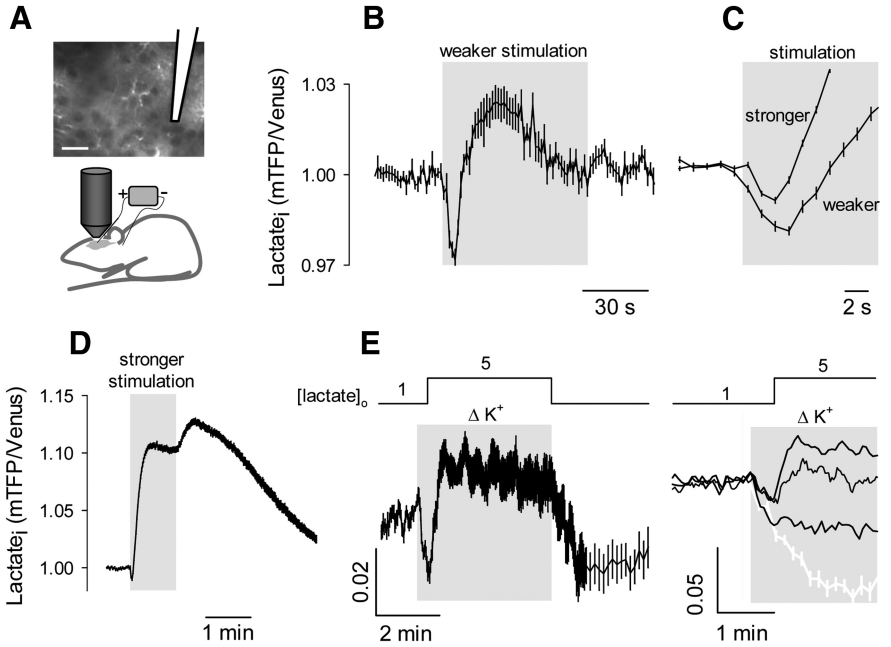

Figure 3. Early depletion of astrocytic lactate during local electrical stimulation *in vivo*. The strength of electrical stimulation was modulated by varying the distance between cells and the tip of the stimulation pipette, giving a weaker stimulation at 300–500 μm and a stronger stimulation at 20–200 μm. ***A***, Imaging of Laconic expressed in somatosensory cortex astrocytes. The location of the stimulation pipette is indicated. Scale bar, 20 μm. ***B***, Data from a single experiment. ***C***, Early response to weaker ($n = 3$ experiments) and stronger stimulation ($n = 7$ experiments). ***D***, Extended time course for stronger stimulation ($n = 7$ experiments) ***E***, Left, Intracellular lactate level in cultured astrocytes exposed first to a 9 mM increase in $[K^+]_o$, and 30 s later, to a rise in extracellular lactate level from 1 to 5 mM. Right, Data from three cells from the same field (black) are compared with the average depletion elicited by a 9 mM $[K^+]_o$ increase at constant extracellular lactate concentration of 1 mM (white).

was divided by the Venus channel (with bandpass filter 542/50; Semrock), and the ratio was normalized to the corresponding baseline using Matlab (MathWorks). Glass capillaries (Science Products; GB120F-8P 0.69 × 1.20 × 80 mm with filament) were pulled to achieve an impedance of 1.5 MΩ at 1 kHz (P-87 pipette puller, Sutter Instrument Co.) and were filled with an artificial CSF solution of the following composition (in mM): 125 NaCl, 2.5 KCl, 2 CaCl2, 1 MgCl2, 25 glucose, 1.25 NaH_2PO_4, and 25 NaHCO3, pH 7.4 (Laboratorium Dr. Bichsel AG, Interlaken, Switzerland). The glass of the cranial window was split using a diamond glass cutter and was partially removed. The pipette was mounted on a manipulator (SM-5, Luigs & Neumann) inserted under visual control and left to rest for 60 min before imaging. Intracortical microstimulation was applied with a DC cathodal current of 100 μA for 1 min (1 Hz train frequency, 100 ms trains at 330 Hz, 0.26 ms pulse width) using a constant-current isolator (STG 4002, Multi Channel Systems).

Electrophysiology

Culture dishes containing cortical astrocytes were transferred to the stage of an inverted microscope for study. They were continuously superfused with a bathing solution containing the following (in mM): 136 NaCl, 3 KCl, 1.25 MgCl2, 1.25 CaCl2, 2.0 Glucose, 1.0 NaLactate, and 10 HEPES-Tris, at pH 7.4 and osmolality of 300 mOsm. The pipette solution contained the following (in mM): 145 NaLactate, 1.0 NaCl, 3.0 KCl, 3.0 BaCl2, and 10 HEPES-Tris 10 mM, at pH 7.4 and osmolality of 300 mOsm. Recordings of single channels in the cell-attached patch-clamp configuration were performed using 6- to 12-d-old astrocytes. Patch pipettes made from borosilicate glass were fire polished and covered in beeswax, and had a tip resistance of 3–4 MΩ (measured using the pipette solution described above). After obtaining GΩ seals, currents were measured using a List Medical L/M-EPC5 amplifier. An Ag/AgCl pellet acted as a bath ground and was connected to the bathing solution via a 0.5 M KCl agar bridge. Potentials were corrected for liquid junction shifts (Barry, 1994). Acquisition and analysis were performed with a Digidata 1200A analog-to-digital converter and Clampfit version 9.0 software (Molecular Devices). Acquisition was at 10 kHz with a filter (four-pole Bessel filter) at 3 kHz. Experiments were conducted at room temperature (20–24°C). NP_o, where N is the number of active channels in the membrane patch and P_o is the open probability, was calculated using the single-channel search and event statistics algorithms in pClamp version 9.0 software. The mean current I passing through the N channels present in the patch was estimated from current amplitude histograms. Single-channel conductance estimates were made on the assumption that astrocytes had a membrane potential E_m of −80 mV (Ruminot et al., 2011). Intracellular lactate concentration was assumed to be 1.4 mM. An intracellular chloride concentration of 30 mM was assumed (Bekar and Walz, 2002). We used these concentrations to calculate cell-attached patch reversal potential E_{rev} values of 27 and −116 mV, respectively, for chloride and lactate.

Data presentation and statistical analysis

Line traces represent individual cells. Unless otherwise stated, traces with error bars correspond to the mean ± SEM of eight or more cells ($n \geq 3$ experiments). Differences in mean values of paired samples were evaluated with the Student's t test. p values of <0.05 were considered significant and are indicated with an asterisk (*).

Results

Resting astrocytes maintain a standing lactate reservoir

Astrocyte lactate dynamics were monitored in real time with Laconic, the Forster resonance energy transfer (FRET) lactate nanosensor (San Martín et al., 2013; Fig. 1*A*). To estimate resting lactate levels in cultured astrocytes, cells were first emptied of lactate by accelerated exchange with pyruvate and then exposed to saturating levels of lactate, a two-point calibration protocol that has been described in detail previously (San Martín et al., 2013). With this approach, the sensor was found to be close to saturation in most astrocytes (Fig. 1*B*,*C*). Using the kinetic parameters obtained *in vitro* (San Martín et al., 2013), the average concentration of cytosolic lactate was estimated to be 1.4 ± 0.02 mM ($n = 183$ cells in 17 experiments). The transport of lactate across the astrocytic plasma membrane is mediated by monocarboxylate transporters (MCTs) that catalyze the electroneutral cotransport of a lactate anion and an H^+ ion. With 1 mM lactate in the superfusate at a pH of 7.4, and a mean intracellular pH of 7.2 ± 0.02 ($n = 43$ cells 3 experiments), MCTs in astrocytes are at thermodynamic equilibrium at 0.63 mM intracellular lactate ($[lactate]_o \times [H^+]_o = [lactate]_i \times [H^+]_i$). As shown in Figure 1*C*, 88% of the astrocytes maintained cytosolic lactate levels above equilibrium in the resting condition. MCT blockage with AR-C155858 (Ovens et al., 2010) led to further intracellular lactate accumulation (Fig. 1*D*), providing independent evidence that resting astrocytes are tonic lactate producers that keep lactate above the MCT equilibrium.

Depolarization by high $[K^+]_o$ depletes astrocytic lactate

A rise in $[K^+]_o$ has been reported to stimulate astrocytic glucose consumption, glycogen mobilization, and lactate production in cell cultures and in tissue slices (Hof et al., 1988; Bittner et al.,

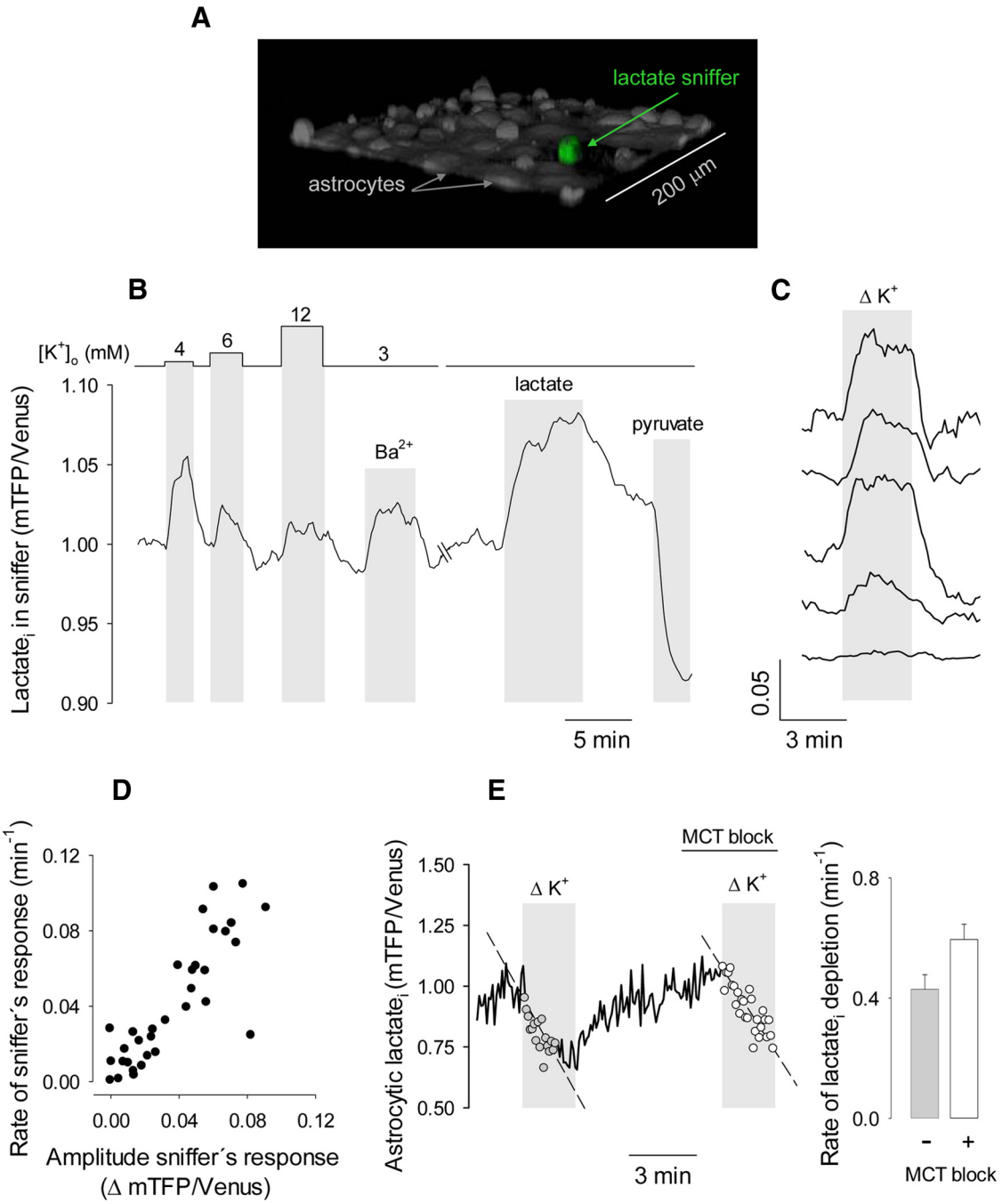

Figure 4. Fast astrocytic lactate release detected with a lactate sniffer. ***A***, HEK293 cells expressing Laconic (sniffers) were seeded on top of an astrocytic culture and imaged by 3D confocal microscopy (green). A second 3D reconstruction was performed after ester loading the culture with calcein (gray). ***B***, Response of a sniffer positioned on top of an astrocytic culture to increasing concentrations of $[K^+]_o$ (4, 6, and 12 mM), 3 mM Ba^{2+}, 1 mM lactate, and 10 mM pyruvate. The experiment was performed in 2 mM glucose and 0 mM lactate. ***C***, Typical response of sniffers to astrocytic culture exposure to 12 mM K^+. ***D***, Correlation between the amplitude and the initial rate of the response of the sniffer to 12 mM K^+. ***E***, Astrocytic lactate depletion by 12 mM K^+ in the absence (gray symbols and bars) and presence (white symbols and bars) of 1 μM AR-C155858.

2011; Ruminot et al., 2011; Choi et al., 2012; Sotelo-Hitschfeld et al., 2012). Therefore, we expected to find increased cytosolic lactate levels in K^+-stimulated astrocytes. Paradoxically, high $[K^+]_o$ led to depletion of the cytosolic lactate reservoir (Fig. 1*E*). The phenomenon was evoked with 4 mM K^+, a mere 1 mM over resting $[K^+]_o$ (Fig. 1*E*,*F*) and within the range reported in brain interstice during physiological neural activity (Fröhlich et al., 2008). The effect of K^+ was mimicked by Ba^{2+} (Fig. 1*F*), which depolarizes the plasma membrane by blocking K^+ channels (Ruminot et al., 2011). As reported (Bittner et al., 2011), the measurement of glucose consumption by applying a glucose transporter GLUT blocker (Bittner et al., 2010) to astrocytes expressing the glucose nanosensor FLII^{12}Pglu700$\mu\Delta$6 (Takanaga et al., 2008) showed that high $[K^+]_o$ stimulated glycolysis by >300% (Fig. 1*G*). Consistent with an increased glycolytic rate, Peredox (Hung et al., 2011) showed an increased NADH/NAD^+ ratio (Fig. 1*H*). However, Pyronic (San Martín et al., 2014a) revealed that cytosolic pyruvate concentrations increased slightly and only after a delay of ~30 s (Fig. 1*I*). The weak response of pyruvate to such strong glycolytic activation is consistent with the

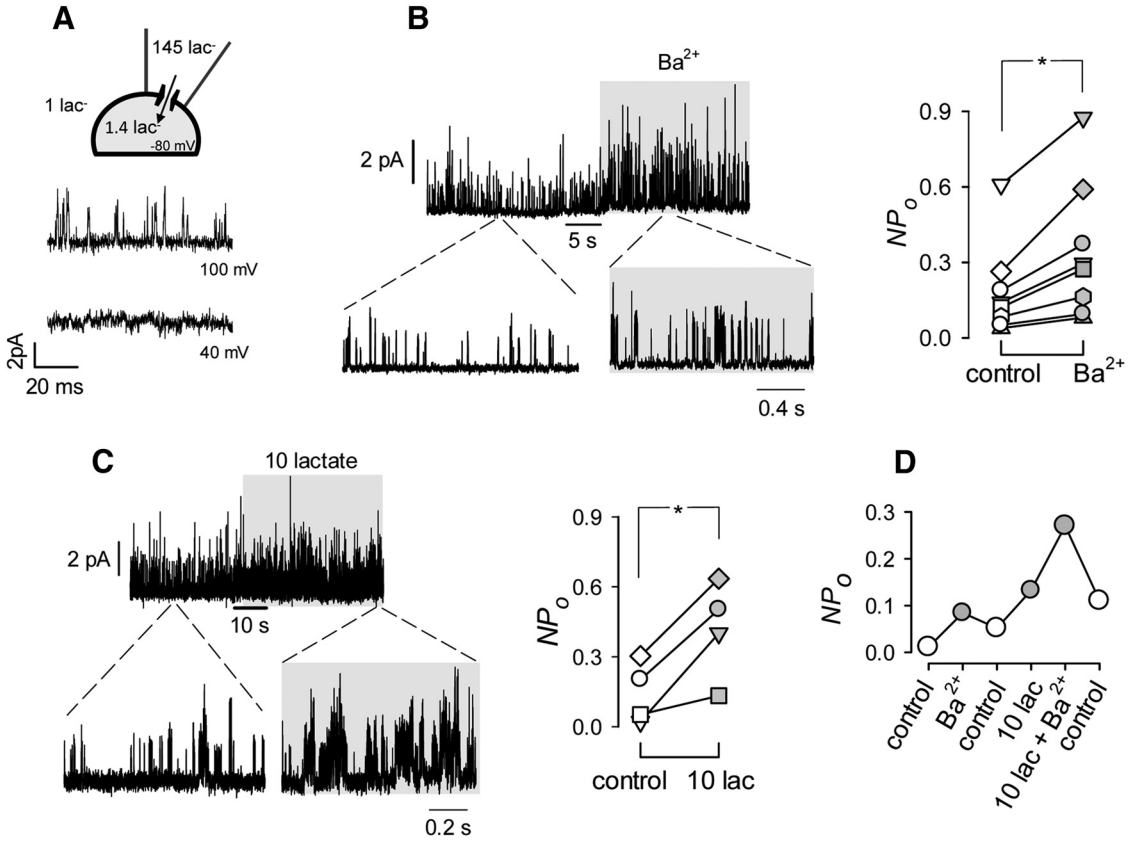

Figure 5. A lactate-permeable channel modulated by membrane depolarization and lactate. ***A***, Traces obtained under lactate-rich (145 mM) and chloride-low (10 mM) pipette conditions in the cell-attached mode at 100 and 40 mV applied potential. ***B***, Left, Recording from an astrocyte patch held at 0 mV (80 mV applied potential) before and during exposure of the cell to 3 mM Ba^{2+}. Right, The channel activity in eight similar experiments is illustrated as NP_o, the product of the number of channels in the patch and the open probability of each channel. ***C***, Left, Effect of increasing bath lactate concentration from 1 to 10 mM on channel activity. Right, Summary of four similar experiments. ***D***, A cell was sequentially bathed with 3 mM Ba^{2+} and/or 10 mM lactate for periods of 5 min as shown.

simultaneous operation of a lactate dehydrogenase (LDH)-mediated pyruvate sink driven by the lactate depletion and NADH increase. The phenomenon of lactate depletion seemed specific to high $[K^+]_o$, as the inhibition of oxidative phosphorylation (OXPHOS), which also stimulated glycolysis and increased the cytosolic NADH/NAD^+ ratio, led to the expected immediate accumulation of both pyruvate and lactate (Fig. 2). To study astrocytes in the tissue context, a recombinant adeno-associated virus coding for Laconic under the short $gfaABC_1D$ promoter was stereotaxically injected into the brain of neonatal mice, followed by cortical slice preparation and FRET determinations 4 weeks later. As illustrated in Figure 1*J–L*, when the slice was exposed to high $[K^+]_o$ or Ba^{2+}, protoplasmic astrocytes responded with a lactate depletion similar to that observed in culture. Considering the responses in cultured cells and in tissue slices of lactate, glucose, NADH/NAD^+ ratio, and pyruvate, we hypothesized that astrocytic depolarization by high $[K^+]_o$ stimulated lactate release to a larger extent than glycoytic lactate production.

Lactate dynamics *in vivo*

The lactate sensor was expressed in astrocytes of the primary somatosensory cortex of adult mice using the adeno-associated viral vector and was then imaged under anesthesia through a cranial window with two-photon microscopy (Fig. 3*A*). Local field stimulation that increases $[K^+]_o$ *in vivo* and depolarizes astrocytes within seconds (Chesler, 2003; Fröhlich et al., 2008) elicited a complex astrocytic lactate response. Immediately after the onset of stimulation, there was a fast transient decrease, followed by an overshoot and a secondary decrease despite continued stimulation (Fig. 3*B*). The lactate dip does not seem to arise from a stimulation artifact, as astrocytes located near the stimulation pipette showed a smaller dip (Fig. 3*C*). This stronger stimulation provoked a faster and larger overshoot that maintained cytosolic lactate above baseline levels long after stimulation had ended (Fig. 3*D*). Whereas electrical stimulation may affect metabolism by several mechanisms, a possible interpretation for the complex response observed *in vivo* is that the initial lactate dip is mediated by high $[K^+]_o$, as observed *in vitro*, and that the overshoot reflects the interstitial lactate buildup known to occur *in vivo*. Consistent with this explanation, both dip and overshoot could be mimicked in cultured astrocytes by elevating extracellular lactate levels a few seconds after the application of K^+ (Fig. 3*E*). The effect of adding lactate was variable from cell to cell, ranging from a slight decrease in the rate of lactate depletion to a proper overshoot (Fig. 3*E*). In view of the results described below, this is likely explained by variable balancing between MCT-mediated lactate influx and channel-mediated lactate efflux.

Astrocytes release lactate within seconds of membrane depolarization

Augmented lactate efflux in response to astrocyte depolarization was first confirmed with an enzymatic assay, which showed that a 1 min exposure of cultured astrocytes to 12 mM $[K^+]_o$ increased extracellular lactate by 69 ± 7%. For better temporal resolution,

a lactate-sniffer cell was engineered by expressing Laconic in wild-type HEK293 cells, which are MCT rich (San Martín et al., 2013, 2014a) and insensitive to glycolytic modulation by K^+ (Ruminot et al., 2011). To estimate lactate levels in the immediate vicinity of astrocytes, lactate sniffer cells were seeded on top of the astrocytic monolayer (Fig. 4*A*). Within seconds of exposing the cultures to elevated $[K^+]_o$ or Ba^{2+} level, the sniffers detected a higher extracellular lactate (Fig. 4*B*). The typical response was a rapid rise to a new steady state, which reverted to baseline levels after agonist removal, although we saw considerable cell-to-cell variability (Fig. 4*C*,*D*). Control experiments in the absence of astrocytes showed that intracellular lactate in HEK293 cells was insensitive to 12 mM $[K^+]_o$ or 3 mM Ba^{2+} (data not shown). These results indicate that astrocytes release lactate within seconds of membrane depolarization, thus explaining the intracellular depletion despite glycolytic stimulation. Next, we focused on the mechanisms underlying the lactate release, with first possible candidates being MCTs. However, the MCT blocker AR-C155858, which abrogates lactate permeation in these cells (San Martín et al., 2013, 2014a), had no apparent effect on the lactate depletion (Fig. 4*E*), pointing to the existence of an alternative release pathway.

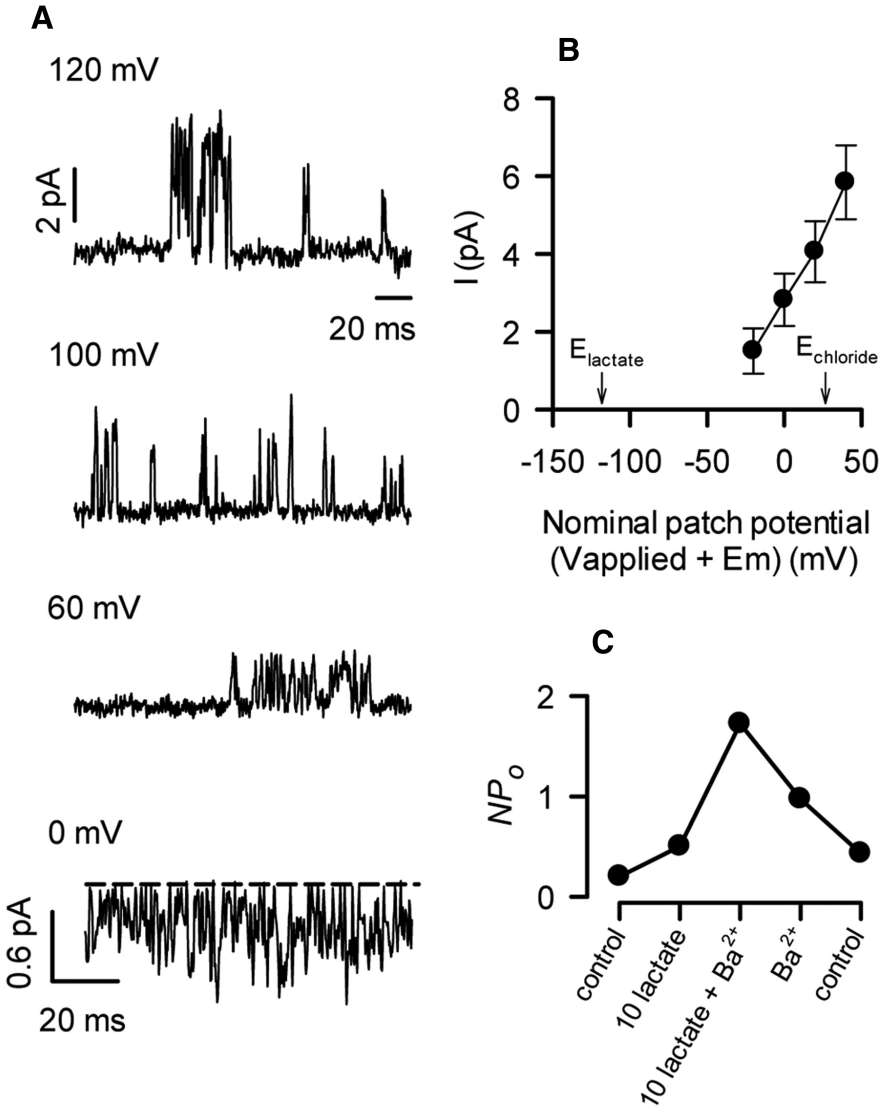

Figure 6. Further characterization of the lactate-permeable channel. ***A***, Traces obtained with a lactate-rich (145 mM), chloride-low (10 mM) medium, with pipette in the cell-attached mode at 120, 100, 60, and 0 applied potential. ***B***, Single-channel current obtained at increasing nominal patch potentials (calculated assuming an astrocytic membrane potential of −80 mV). The equilibrium potentials estimated for lactate and chloride are indicated. ***C***, A cell was sequentially bathed with 10 mM lactate and 3 mM Ba^{2+} for periods of 5 min as shown.

Channel-mediated lactate release by astrocytes

Our search for a lactate conductance started with whole-cell patch-clamp experiments, but no significant currents could be detected with a lactate-rich pipette at resting membrane potential or during depolarization ($n = 6$ experiments, data not shown). Experiments were therefore performed in the cell-attached configuration, a minimally invasive approach that leaves the intracellular milieu unperturbed, using a pipette solution rich in lactate, low in chloride, and supplemented with 3 mM Ba^{2+} to eliminate the potassium conductance (Ruminot et al., 2011). Assuming intracellular concentrations of 1.4 mM for lactate (see above) and of 30 mM for chloride (Bekar and Walz, 2002), approximate lactate reversal potential $E_{lactate}$ and chloride reversal potential E_{Cl} values are −116 and 27 mV, respectively. Records obtained under these conditions at an applied potential of 100 mV revealed transient outward currents consistent with ion channel activity (Fig. 5*A*). At an astrocytic membrane potential of −80 mV (Ruminot et al., 2011), this applied potential translates into a nominal patch potential of 20 mV, which is well above $E_{lactate}$ but below E_{Cl}. The only ion species capable of carrying this current is lactate, as chloride and sodium movements would generate inward currents. Accordingly, the currents became progressively smaller at more negative potentials (Figs. 5*A*, 6). Small inward currents were detected at a nominal patch potential of −80 mV (Fig. 6), suggesting that the channel also allows chloride to pass. For simplicity, we will use the term "lactate channel" to refer to this lactate-permeable channel. At a 40 mV nominal patch potential, the single-channel conductance of the lactate channel was 37 ± 6 pS ($n = 6$). Currents were detected in ~50% of the patches examined. It was not possible to test the effect of cell depolarization with high $[K^+]_o$, as this maneuver destabilized the patch and prevented reliable current determinations. However, cell depolarization by adding Ba^{2+} to the superfusate stabilized the patch, permitting prolonged experiments to be performed. Within seconds of exposure to Ba^{2+}, the open probability of the channel became significantly higher regardless of basal activity (Fig. 5*B*). Surprisingly, the activity of the channel was further increased when cells were superfused with a solution containing a higher concentration of lactate (Fig. 5*C*). The stimulatory effects of Ba^{2+} and lactate on channel activity were additive and reverted upon removal from the bathing solution, but

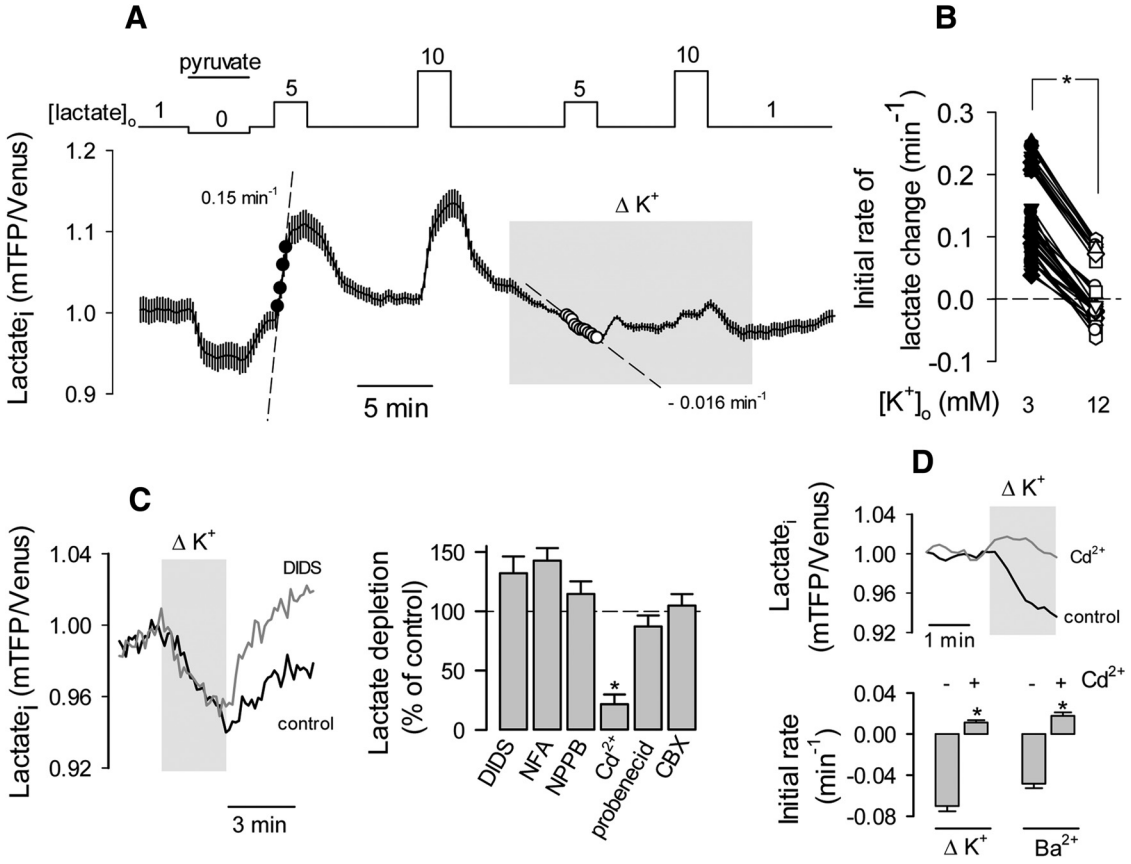

Figure 7. Stimulated astrocytes can extrude lactate against a lactate gradient. ***A***, Astrocytes were sequentially exposed to 10 mM pyruvate and then to 5 and 10 mM lactate in the presence of 3 or 12 mM $[K^+]_o$. ***B***, Summary of three similar experiments showing the initial rates of 5 mM lactate accumulation in 3 or 12 mM $[K^+]_o$. ***C***, Left, The effect of a 9 mM increase in $[K^+]_o$ on intracellular lactate was monitored in a single astrocyte before and during exposure to 200 μM DIDS. Right, Summary of similar experiments, with 200 μM DIDS, 500 μM NFA, 500 μM NPPB, 200 μM Cd^{2+}, 1 mM probenecid, or 10 μM CBX. Data are the rates of lactate depletion measured over 2 min ($n = 3$ experiments and 16–32 cells were used for each inhibitor). ***D***, Top, The effects of a 9 mM increase in $[K^+]_o$ or the addition of 3 mM Ba^{2+} on intracellular lactate level were monitored in single astrocytes before and during exposure to 200 μM Cd^{2+}. Bottom, Initial rates measured during the first minute of exposure to $[K^+]_o$ or 3 mM Ba^{2+} in the absence or presence of 200 μM Cd^{2+}.

this reversion was partial, at least over a period of minutes (Figs. 5*D*, 6).

MCTs are responsible for the lactate permeability of resting astrocytes (Barros and Deitmer, 2010; Bouzier-Sore and Pellerin, 2013; Stobart and Anderson, 2013). The high permeability of astrocytes to lactate is illustrated in Figure 7*A* as a rapid accumulation of cytosolic lactate in response to high extracellular lactate. However, when high lactate was applied in the presence of high $[K^+]_o$, the rise in lactate was smaller than that seen under resting conditions (Fig. 7*A*,*B*). In ~50% of cells, the 5 mM lactate pulse provoked intracellular lactate depletion (Fig. 7*A*,*B*). The latter result is highly informative as it means that despite high levels of extracellular lactate, efflux through the channel may still surpass influx through MCTs. It also means that the positive modulation of the channel by lactate, as described electrophysiologically, must occur at an extracellular site. The cell-attached configuration is not amenable to pharmacological characterization, so we used the initial depletion detected with the FRET nanosensor as a readout of channel activity. Considering the negative charge of lactate and the possible chloride current detected at 0 mV applied potential (Fig. 6), we tested a panel of anion channel blockers but found that only Cd^{2+} was able to inhibit K^+-induced lactate depletion to a significant extent (Fig. 7*C*). The pannexin channel blocker probenecid and the connexin hemichannel blocker CBX were not effective (Fig. 7*C*). On closer inspection, it became apparent that Cd^{2+} strongly inhibited lactate depletion immediately after the application of K^+ or Ba^{2+}, but that its effect became weaker over time (Fig. 7*D*). This suggests that there may be more than one pathway involved, and that the Cd^{2+}-sensitive channel is responsible for the early phase of the lactate release.

Discussion

The main finding of this study is that astrocytes release lactate via an ion channel in response to a small rise in extracellular K^+. The lactate-permeable channel was positively modulated by lactate itself. Resting astrocytes were found to accumulate lactate well above MCT thermodynamic equilibrium: a dynamic reservoir that was quickly mobilized in response to high $[K^+]_o$. Astrocytes are therefore equipped with a mechanism for the targeted delivery of lactate, which fits well to the emerging role of lactate as a signaling molecule (Fig. 8).

The transport of lactate across the plasma membrane of astrocytes and most other mammalian cells is mediated by H^+-coupled monocarboxylate transporters (Halestrap and Price, 1999; Barros and Deitmer, 2010; Bouzier-Sore and Pellerin, 2013; San Martín et al., 2013; Stobart and Anderson, 2013). Standard uptake assays based on isotopic tracers or pH-sensitive dyes show that lactate permeability of astrocytes is high, and no significant lactate gradients have been presumed to exist across the plasma membrane. With the FRET nanosensor, we were able to estimate lactate in the steady state and found that most astrocytes maintained lactate levels above thermodynamic equilibrium. In re-

sponse to high $[K^+]_o$ cytosolic lactate levels fell despite strong concurrent stimulation of glucose consumption. Pyruvate levels were almost unaffected, suggesting a close match between increased pyruvate production from glucose and pyruvate consumption by LDH, driven by a lower lactate level and an increased NADH/NAD^+ ratio. The K^+-dependent lactate depletion appears to be a robust phenomenon, as it was observed in both primary cultures and in protoplasmic astrocytes of adult brain slices. It has also been recorded in organotypical hippocampal slices (I. Ruminot and J.W. Deitmer, unpublished data). Also, within seconds of K^+ stimulation, a sniffer cell detected the release of lactate by astrocytes. Both lactate depletion and release were mimicked by Ba^{2+}, a maneuver that does not engage K^+ transporters (Gatto et al., 2007), suggesting that the phenomenon is chiefly mediated by membrane depolarization. In living animals, electrical stimulation of the somatosensory cortex triggered a complex astrocytic lactate response, with an initial dip and a delayed overshoot. As lactate modulates astrocytic glycolysis within seconds (Sotelo-Hitschfeld et al., 2012), the lactate dip may contribute to the stimulation of glycolysis by high $[K^+]_o$. Although the depletion phase of the lactate dip observed in protoplasmic astrocytes *in vivo* correlates with the K^+-dependent depletion observed in cultured astrocytes and in protoplasmic astrocytes *in vitro*, and we could mimic both dip and overshoot under culture conditions, the extent to which the lactate dip *in vivo* is mediated by K^+ is not clear at this stage. Electrical stimulation increases interstitial K^+ and depolarizes astrocytes (Fröhlich et al., 2008), but also mobilizes other mediators that may affect lactate metabolism. The combination of cytosolic depletion and release is evidence of increased lactate permeability, an outcome that could not be ascribed to the MCTs, as pharmacological MCT blockage failed to prevent lactate depletion. Both the depletion of cytosolic lactate by high $[K^+]_o$ and the further depletion during a lactate pulse could be explained by the electrophysiological detection of a lactate-permeable ion channel, having an open probability increased by plasma membrane depolarization and by lactate. The lactate channel was not detected in the whole-cell configuration, suggesting the need for an intact intracellular milieu. Considering that the application of high lactate concentrations to K^+-stimulated cells caused a decrease in intracellular lactate levels, the modulation of the channel by lactate seems to occur at the cell surface. One possible explanation may be direct gating of the channel by the permeant ion, a phenomenon that has already been described for anion channels (Pusch and Jentsch, 1994; Catalán et al., 2004).

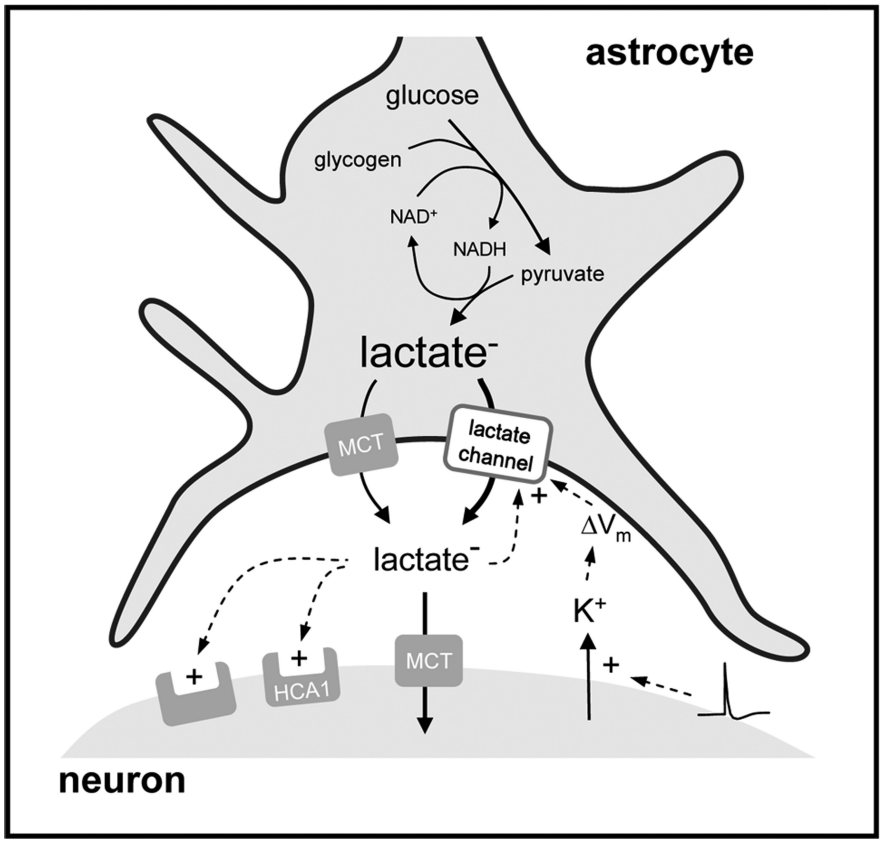

Figure 8. Activity-dependent channel-mediated lactate release by astrocytes. Resting astrocytes maintain a standing reservoir of cytosolic lactate, the result of a dynamic balance between glycolytic production and MCT-mediated lactate export. Active neurons release K^+, which depolarizes the astrocytic plasma membrane (ΔV_m) and activates the lactate-permeable channel, resulting in lactate release, leading to higher $[lactate]_o$ and further lactate release through a positive feedback. Neurons may sense lactate through HCA1 (Bozzo et al., 2013; Lauritzen et al., 2013) and other surface lactate receptors (Tang et al., 2014), or after internalization of lactate via MCTs.

To the best of our knowledge, there are no previous reports of lactate-permeable ion channels in astrocytes. The lactate-permeable channel of astrocytes was insensitive to 4,4′-diisothiocyano-2,2′-stilbenedisulfonic acid (DIDS), niflumic acid (NFA), 5-nitro-2-(3-phenylpropylamino)benzoic acid (NPPB), probenecid, and carbenoxolone (CBX), but was partially inhibited by Cd^{2+}, a nonspecific ion channel inhibitor. Anion channels are notoriously insensitive to inhibitors (Kimelberg et al., 2006), which has made it very difficult to link functionally identified anion channels to their molecular counterparts (Jentsch et al., 2002). However, a breakthrough was made recently with the molecular identification of the volume-regulated anion channel VRAC (Qiu et al., 2014; Voss et al., 2014). Anion channels in astrocytes are stimulated by ATP, cell swelling, shape changes, and other stimuli (Kimelberg et al., 2006), but we found no information on astrocytic anion channels activated by cell depolarization. This may be because electrophysiological measurements are normally performed in whole-cell voltage clamp, a configuration in which the lactate channel did not appear. It was, however, readily found in the cell-attached patch-clamp configuration, suggesting the need for a cytosolic factor that may be lost during dialysis. The main substrate of anion channels is chloride, but some of these channels may also transport large zwitterionic polyions such as taurine (125 Da; Qiu et al., 2014; Voss et al., 2014), and are therefore likely to transport lactate, a smaller monovalent anion (88 Da). Lactate has not been routinely included in selectivity studies of anion channels. The maxi-anion channel is present in astrocytes (Kimelberg et al., 2006), but its conductance seems too large (>300 pS for chloride, and presumably >100 pS for lactate) to account for the lactate permeability described here. Conductance may also be invoked

against connexins and pannexins (>200 pS; Giaume et al., 2013), together with the observed insensitivity of the lactate channel to carbenoxolone and probenecid, and the fact that connexins and pannexins are permeable to cations.

An activity-dependent lactate channel in astrocytes has consequences for brain lactate dynamics. There are fundamental differences between the standard transport of lactate via MCTs and transport via an ion channel; one of these is vectorial flux. Lactate is a monovalent anion, and at the resting membrane potential of astrocytes (−80 mV) lactate will flow through the channel against a 20-fold chemical gradient. At 12 mM $[K^+]_o$, the membrane potential of a "depolarized" astrocyte is still −60 mV (Ruminot et al., 2011), a voltage at which channel-mediated efflux will occur against a 10-fold chemical gradient. This explains how an imposed fivefold rise in extracellular lactate failed to increase intracellular lactate levels in K^+-stimulated astrocytes (Fig. 3*E*). In contrast, MCT-mediated transport is electroneutral and may only extrude lactate if there is a favorable combined chemical gradient for lactate and H^+. During neural activity, astrocytes become more alkaline and neurons acidify (Chesler, 2003), a combination that works against the transfer of lactate from astrocytes to neurons (Barros and Deitmer, 2010). Using a pathway that is H^+ independent and sensitive to membrane potential, astrocytes may push lactate toward neurons regardless of the pH gradient, even if lactate has accumulated in the interstice. Another relevant property of channels is their unmatched throughput rate. Assuming linear dose dependence, we can calculate that a single 37 pS channel (adjusted at 1.4 mM and −60 mV) conducts $>10^5$ lactate molecules per second, about a thousand times faster than the maximum turnover number of MCT1 (Ovens et al., 2010). Astrocytic lactate has been proposed to serve as an energy substrate for active neurons, a mechanism known as the astrocyte-to-neuron lactate shuttle (ANLS; Pellerin and Magistretti, 1994; Bouzier-Sore and Pellerin, 2013; Stobart and Anderson, 2013). In its standard version, ANLS is mediated by MCTs, and therefore the direction of flux is determined by the lactate gradient between both cells, which is unknown (Barros and Deitmer, 2010). The lactate channel strengthens the ANLS by providing obligatory vectorial flux (energized by the astrocytic membrane potential), activity dependence (mediated by $[K^+]_o$), and a much higher throughput rate.

In addition to a role in neurometabolic coupling, the lactate channel may contribute to intercellular signaling. The G_i-protein-coupled receptor for lactate HCA1 (GPR81) was recently described in synaptic regions, perivascular locations, and glia (Bergersen and Gjedde, 2012; Lauritzen et al., 2013), whereas the engagement of HCA1 in cortical neurons in culture reduced their spontaneous activity (Bozzo et al., 2013). In the locus ceruleus, astrocytic lactate was found to excite neurons, a phenomenon mediated by a different surface lactate receptor (Tang et al., 2014). After entering neurons, lactate affects pH, the NADH/NAD^+ ratio, and the energy status, modulating enzyme catalysis, gene expression, and higher-order brain functions like memory consolidation (Gilbert et al., 2006; Suzuki et al., 2011; Barros, 2013; Yang et al., 2014). Because of the delicate geometry of protoplasmic astrocytes, their membrane potential is thought to be a local parameter, exquisitely sensitive to fluctuations in $[K^+]_o$ (Kofuji and Newman, 2004; Fröhlich et al., 2008; Witthoft et al., 2013). Depending on location, the lactate channel may sense the local rise in $[K^+]_o$ that accompanies excitatory neurotransmission and perhaps the activity of the nodes of Ranvier, which are contacted by astrocytic processes. A single channel may deliver lactate transiently as a localized jet, permitting accurate homing of targets in neighboring cells and/or in autocrine fashion. The amplification conferred by the positive feedback modulation of the channel by lactate is expected to make the release even more abrupt. Astrocytes detect synaptic activity through metabotropic and ionotropic glutamate receptors, leading to the release of glutamate, ATP, and D-serine, small neuromodulators that are collectively termed gliotransmitters (Araque et al., 2014). Astrocytes can also detect synaptic activity through changes in local $[K^+]_o$. The neuromodulatory roles of lactate, its steady-state reservoir in astrocytes, and its fast release in response to K^+, suggest that lactate may also qualify as a gliotransmitter.

References

Araque A, Carmignoto G, Haydon PG, Oliet SH, Robitaille R, Volterra A (2014) Gliotransmitters travel in time and space. Neuron 81:728–739. CrossRef Medline

Barros LF (2013) Metabolic signaling by lactate in the brain. Trends Neurosci 36:396–404. CrossRef Medline

Barros LF, Deitmer JW (2010) Glucose and lactate supply to the synapse. Brain Res Rev 63:149–159. CrossRef Medline

Barros LF, Baeza-Lehnert F, Valdebenito R, Ceballo S, Alegría K (2014) Fluorescent nanosensor based flux analysis: overview and the example of glucose. In: Springer protocols: brain energy metabolism (Waagepetersen HS, Hirrlinger J, eds), pp 145–159. Berlin: Springer.

Barry PH (1994) JPCalc, a software package for calculating liquid junction potential corrections in patch-clamp, intracellular, epithelial and bilayer measurements and for correcting junction potential measurements. J Neurosci Methods 51:107–116. CrossRef Medline

Bekar LK, Walz W (2002) Intracellular chloride modulates A-type potassium currents in astrocytes. Glia 39:207–216. CrossRef Medline

Bergersen LH, Gjedde A (2012) Is lactate a volume transmitter of metabolic states of the brain? Front Neuroenergetics 4:5. CrossRef Medline

Bittner CX, Loaiza A, Ruminot I, Larenas V, Sotelo-Hitschfeld T, Gutiérrez R, Córdova A, Valdebenito R, Frommer WB, Barros LF (2010) High resolution measurement of the glycolytic rate. Front Neuroenergetics 2:26. CrossRef Medline

Bittner CX, Valdebenito R, Ruminot I, Loaiza A, Larenas V, Sotelo-Hitschfeld T, Moldenhauer H, San Martín A, Gutiérrez R, Zambrano M, Barros LF (2011) Fast and reversible stimulation of astrocytic glycolysis by K^+ and a delayed and persistent effect of glutamate. J Neurosci 31:4709–4713. CrossRef Medline

Bouzier-Sore AK, Pellerin L (2013) Unraveling the complex metabolic nature of astrocytes. Front Cell Neurosci 7:179. CrossRef Medline

Bozzo L, Puyal J, Chatton JY (2013) Lactate modulates the activity of primary cortical neurons through a receptor-mediated pathway. PLoS One 8:e71721. CrossRef Medline

Catalán M, Niemeyer MI, Cid LP, Sepúlveda FV (2004) Basolateral ClC-2 chloride channels in surface colon epithelium: regulation by a direct effect of intracellular chloride. Gastroenterology 126:1104–1114. CrossRef Medline

Chesler M (2003) Regulation and modulation of pH in the brain. Physiol Rev 83:1183–1221. CrossRef Medline

Choi HB, Gordon GR, Zhou N, Tai C, Rungta RL, Martinez J, Milner TA, Ryu JK, McLarnon JG, Tresguerres M, Levin LR, Buck J, MacVicar BA (2012) Metabolic communication between astrocytes and neurons via bicarbonate-responsive soluble adenylyl cyclase. Neuron 75:1094–1104. CrossRef Medline

Davidson S, Truong H, Nakagawa Y, Giesler GJ Jr (2010) A microinjection technique for targeting regions of embryonic and neonatal mouse brain in vivo. Brain Res 1307:43–52. CrossRef Medline

Dirren E, Towne CL, Setola V, Redmond DE Jr, Schneider BL, Aebischer P (2014) Intracerebroventricular injection of adeno-associated virus 6 and 9 vectors for cell type-specific transgene expression in the spinal cord. Hum Gene Ther 25:109–120. CrossRef Medline

Fröhlich F, Bazhenov M, Iragui-Madoz V, Sejnowski TJ (2008) Potassium dynamics in the epileptic cortex: new insights on an old topic. Neuroscientist 14:422–433. CrossRef Medline

Gatto C, Arnett KL, Milanick MA (2007) Divalent cation interactions with Na, K-ATPase cytoplasmic cation sites: implications for the para-nitrophenyl phosphatase reaction mechanism. J Membr Biol 216:49–59. CrossRef Medline

Giaume C, Leybaert L, Naus CC, Sáez JC (2013) Connexin and pannexin

hemichannels in brain glial cells: properties, pharmacology, and roles. Front Pharmacol 4:88. CrossRef Medline

Gilbert E, Tang JM, Ludvig N, Bergold PJ (2006) Elevated lactate suppresses neuronal firing in vivo and inhibits glucose metabolism in hippocampal slice cultures. Brain Res 1117:213–223. CrossRef Medline

Halestrap AP, Price NT (1999) The proton-linked monocarboxylate transporter (MCT) family: structure, function and regulation. Biochem J 343: 281–299. Medline

Hof PR, Pascale E, Magistretti PJ (1988) K^+ at concentrations reached in the extracellular space during neuronal activity promotes a Ca^{2+}-dependent glycogen hydrolysis in mouse cerebral cortex. J Neurosci 8:1922–1928. Medline

Hou BH, Takanaga H, Grossmann G, Chen LQ, Qu XQ, Jones AM, Lalonde S, Schweissgut O, Wiechert W, Frommer WB (2011) Optical sensors for monitoring dynamic changes of intracellular metabolite levels in mammalian cells. Nat Protoc 6:1818–1833. CrossRef Medline

Hu Y, Wilson GS (1997) A temporary local energy pool coupled to neuronal activity: fluctuations of extracellular lactate levels in rat brain monitored with rapid-response enzyme-based sensor. J Neurochem 69:1484–1490. CrossRef Medline

Hung YP, Albeck JG, Tantama M, Yellen G (2011) Imaging cytosolic NADH-NAD(+) redox state with a genetically encoded fluorescent biosensor. Cell Metab 14:545–554. CrossRef Medline

Jakoby P, Schmidt E, Ruminot I, Gutiérrez R, Barros LF, Deitmer JW (2014) Higher transport and metabolism of glucose in astrocytes compared with neurons: a multiphoton study of hippocampal and cerebellar tissue slices. Cereb Cortex 24:222–231. CrossRef Medline

Jentsch TJ, Stein V, Weinreich F, Zdebik AA (2002) Molecular structure and physiological function of chloride channels. Physiol Rev 82:503–568. CrossRef Medline

Kimelberg HK, Macvicar BA, Sontheimer H (2006) Anion channels in astrocytes: biophysics, pharmacology, and function. Glia 54:747–757. CrossRef Medline

Kofuji P, Newman EA (2004) Potassium buffering in the central nervous system. Neuroscience 129:1045–1056. CrossRef Medline

Lauritzen KH, Morland C, Puchades M, Holm-Hansen S, Hagelin EM, Lauritzen F, Attramadal H, Storm-Mathisen J, Gjedde A, Bergersen LH (2014) Lactate receptor sites link neurotransmission, neurovascular coupling, and brain energy metabolism. Cereb Cortex 10:2784–2795. CrossRef Medline

Loaiza A, Porras OH, Barros LF (2003) Glutamate triggers rapid glucose transport stimulation in astrocytes as evidenced by real-time confocal microscopy. J Neurosci 23:7337–7342. Medline

Ovens MJ, Davies AJ, Wilson MC, Murray CM, Halestrap AP (2010) AR-C155858 is a potent inhibitor of monocarboxylate transporters MCT1 and MCT2 that binds to an intracellular site involving transmembrane helices 7–10. Biochem J 425:523–530. CrossRef Medline

Pellerin L, Magistretti PJ (1994) Glutamate uptake into astrocytes stimulates aerobic glycolysis: a mechanism coupling neuronal activity to glucose utilization. Proc Natl Acad Sci U S A 91:10625–10629. CrossRef Medline

Pologruto TA, Sabatini BL, Svoboda K (2003) ScanImage: flexible software for operating laser scanning microscopes. Biomed Eng Online 2:13. CrossRef Medline

Prichard J, Rothman D, Novotny E, Petroff O, Kuwabara T, Avison M, Howseman A, Hanstock C, Shulman R (1991) Lactate rise detected by 1H NMR in human visual cortex during physiologic stimulation. Proc Natl Acad Sci U S A 88:5829–5831. CrossRef Medline

Pusch M, Jentsch TJ (1994) Molecular physiology of voltage-gated chloride channels. Physiol Rev 74:813–827. Medline

Qiu Z, Dubin AE, Mathur J, Tu B, Reddy K, Miraglia LJ, Reinhardt J, Orth AP, Patapoutian A (2014) SWELL1, a plasma membrane protein, is an essential component of volume-regulated anion channel. Cell 157:447–458. CrossRef Medline

Ruminot I, Gutiérrez R, Peña-Münzenmayer G, Añazco C, Sotelo-Hitschfeld T, Lerchundi R, Niemeyer MI, Shull GE, Barros LF (2011) NBCe1 mediates the acute stimulation of astrocytic glycolysis by extracellular K^+. J Neurosci 31:14264–14271. CrossRef Medline

San Martín A, Ceballo S, Ruminot I, Lerchundi R, Frommer WB, Barros LF (2013) A genetically encoded FRET lactate sensor and its use to detect the warburg effect in single cancer cells. PLoS One 8:e57712. CrossRef Medline

San Martín A, Ceballo S, Baeza-Lehnert F, Lerchundi R, Valdebenito R, Contreras-Baeza Y, Alegría K, Barros LF (2014a) Imaging mitochondrial flux in single cells with a FRET sensor for pyruvate. PLoS One 9:e85780. CrossRef Medline

San Martín A, Sotelo-Hitschfeld T, Lerchundi R, Fenandez-moncada I, Ceballo S, Valdebenito R, Baeza-Lehnert F, Alegria K, Contreras-Baeza Y, Garrido-Gerter P, Romero-Gomez I, Barros LF (2014b) Single-cell imaging tools for brain energy metabolism: a review. Neurophotonics 1:011004. CrossRef

Sotelo-Hitschfeld T, Fernández-Moncada I, Barros LF (2012) Acute feedback control of astrocytic glycolysis by lactate. Glia 60:674–680. CrossRef Medline

Stobart JL, Anderson CM (2013) Multifunctional role of astrocytes as gatekeepers of neuronal energy supply. Front Cell Neurosci 7:38. CrossRef Medline

Suzuki A, Stern SA, Bozdagi O, Huntley GW, Walker RH, Magistretti PJ, Alberini CM (2011) Astrocyte-neuron lactate transport is required for long-term memory formation. Cell 144:810–823. CrossRef Medline

Takanaga H, Chaudhuri B, Frommer WB (2008) GLUT1 and GLUT9 as major contributors to glucose influx in HepG2 cells identified by a high sensitivity intramolecular FRET glucose sensor. Biochim Biophys Acta 1778:1091–1099. CrossRef Medline

Tang F, Lane S, Korsak A, Paton JF, Gourine AV, Kasparov S, Teschemacher AG (2014) Lactate-mediated glia-neuronal signalling in the mammalian brain. Nat Commun 5:3284. CrossRef Medline

Tantama M, Hung YP, Yellen G (2012) Optogenetic reporters: fluorescent protein-based genetically encoded of signaling and metabolism in the brain. In: Progress in brain research (Knopfel T, Boyden E, eds), pp 235–263. Amsterdam: Elsevier.

Voss FK, Ullrich F, Münch J, Lazarow K, Lutter D, Mah N, Andrade-Navarro MA, von Kries JP, Stauber T, Jentsch TJ (2014) Identification of LRRC8 heteromers as an essential component of the volume-regulated anion channel VRAC. Science 344:634–638. CrossRef Medline

Witthoft A, Filosa JA, Karniadakis GE (2013) Potassium buffering in the neurovascular unit: models and sensitivity analysis. Biophys J 105:2046–2054. CrossRef Medline

Yang J, Ruchti E, Petit JM, Jourdain P, Grenningloh G, Allaman I, Magistretti PJ (2014) Lactate promotes plasticity gene expression by potentiating NMDA signaling in neurons. Proc Natl Acad Sci U S A 111:12228–12233. CrossRef Medline

Publication III: *In vivo* ammonium chloride effects on *Laconic*

NH+4 triggers the release of astrocytic lactate via mitochondrial pyruvate shunting

Rodrigo Lerchundi[a,b], Ignacio Fernández-Moncada[a,b], Yasna Contreras-Baeza[a,b], Tamara Sotelo-Hitschfeld[a,b], Philipp Mächler[c,d], Matthias T. Wyss[c,d], Jillian Stobart[c,d], Felipe Baeza-Lehnert[a], Karin Alegría[a], Bruno Weber[c,d] and L. Felipe Barros[a]

Author Affiliations

[a]Biological Laboratory, Centro de Estudios Científicos, 5110466 Valdivia, Chile;

[b]Universidad Austral de Chile, 5110566 Valdivia, Chile;

[c]Institute of Pharmacology and Toxicology, University of Zurich, 8057 Zurich, Switzerland;

[d]Neuroscience Center Zurich, Eidgenössische Technische Hochschule (ETH), and University of Zurich, 8057 Zurich, Switzerland

NH_4^+ triggers the release of astrocytic lactate via mitochondrial pyruvate shunting

Rodrigo Lerchundi[a,b], Ignacio Fernández-Moncada[a,b], Yasna Contreras-Baeza[a,b], Tamara Sotelo-Hitschfeld[a,b], Philipp Mächler[c,d], Matthias T. Wyss[c,d], Jillian Stobart[c,d], Felipe Baeza-Lehnert[a], Karin Alegría[a], Bruno Weber[c,d], and L. Felipe Barros[a,1]

[a]Biological Laboratory, Centro de Estudios Científicos, 5110466 Valdivia, Chile; [b]Universidad Austral de Chile, 5110566 Valdivia, Chile; [c]Institute of Pharmacology and Toxicology, University of Zurich, 8057 Zurich, Switzerland; and [d]Neuroscience Center Zurich, Eidgenössische Technische Hochschule (ETH), and University of Zurich, 8057 Zurich, Switzerland

Edited by Marcus E. Raichle, Washington University in St. Louis, St. Louis, MO, and approved July 29, 2015 (received for review April 28, 2015)

Neural activity is accompanied by a transient mismatch between local glucose and oxygen metabolism, a phenomenon of physiological and pathophysiological importance termed aerobic glycolysis. Previous studies have proposed glutamate and K^+ as the neuronal signals that trigger aerobic glycolysis in astrocytes. Here we used a panel of genetically encoded FRET sensors in vitro and in vivo to investigate the participation of NH_4^+, a by-product of catabolism that is also released by active neurons. Astrocytes in mixed cortical cultures responded to physiological levels of NH_4^+ with an acute rise in cytosolic lactate followed by lactate release into the extracellular space, as detected by a lactate-sniffer. An acute increase in astrocytic lactate was also observed in acute hippocampal slices exposed to NH_4^+ and in the somatosensory cortex of anesthetized mice in response to i.v. NH_4^+. Unexpectedly, NH_4^+ had no effect on astrocytic glucose consumption. Parallel measurements showed simultaneous cytosolic pyruvate accumulation and NADH depletion, suggesting the involvement of mitochondria. An inhibitor-stop technique confirmed a strong inhibition of mitochondrial pyruvate uptake that can be explained by mitochondrial matrix acidification. These results show that physiological NH_4^+ diverts the flux of pyruvate from mitochondria to lactate production and release. Considering that NH_4^+ is produced stoichiometrically with glutamate during excitatory neurotransmission, we propose that NH_4^+ behaves as an intercellular signal and that pyruvate shunting contributes to aerobic lactate production by astrocytes.

laconic | pyronic | peredox | FLII^{12}Pglu700μΔ6 | mitoSypHer

Brain tissue is almost exclusively energized by the oxidation of glucose. However, during neuronal activation, there is a larger increase in local glucose consumption relative to oxygen consumption (1). As this mismatch occurs in the presence of normal or augmented oxygen levels, it has been termed aerobic glycolysis, paralleling the signal detected by functional magnetic resonance imaging (2). Aerobic glycolysis and its associated lactate surge are causally linked to diverse functions of the brain in health and disease (3–10). Two signals are known to trigger aerobic glycolysis in brain tissue: glutamate and K^+, which are released by active neurons and stimulate glycolysis in astrocytes (11, 12).

Neurons produce as much NH_4^+ as they produce glutamate, both molecules being stoichiometrically linked in the glutamate-glutamine cycle (13). Brain tissue NH_4^+ increases within seconds of neural activation (14–16) and is quickly released to the interstitium (17, 18) to be captured by astrocytes through K^+ channels and transporters (19). It is well established that chronic exposure to pathological levels of NH_4^+ such as those observed during liver failure has a major impact on brain metabolism, but it is not known whether this molecule may affect energy metabolism at physiological levels, particularly within the time scale of synaptic transmission. A previous study showed a reversible rise in brain tissue lactate and cerebral blood flow within minutes of an i.v. infusion of NH_4^+. In view of this result, NH_4^+ was speculated to have signaling roles in the brain (20). The aim of the present work was to investigate this possibility.

Results

Increased Lactate Production and Release by Physiological NH_4^+. To investigate the acute effect of NH_4^+ on astrocytic metabolism, we chose 0.2 mM, a concentration within physiological levels in brain tissue (15, 21, 22). Experiments were carried out in cell cultures, in acute brain tissue slices and in the somatosensory cortex in vivo. First, the release of lactate by pure astrocytes in culture during a 1-min exposure to NH_4^+ was estimated using an enzymatic assay. Consistent with previous reports (20, 23), a significant increase in extracellular lactate was observed at 5 mM NH_4^+. However, the enzymatic assay was unable to detect significant lactate release at 0.2 or 0.5 mM NH_4^+ (Fig. 1*A*). To improve the sensitivity of detection, lactate was measured within cells using Laconic (24). All imaging of cultured astrocytes was performed on mixed cultures of astrocytes and neurons, in which astrocytes are better differentiated in terms of energy metabolism (25). Standard glucose and lactate concentrations in the superfusate were 1 and 0.5 mM, respectively. Exposure of astrocytes to 0.2 mM NH_4^+ induced a rapid and reversible increase in cytosolic lactate, a response that varied from cell to cell (Fig. 1*B*). The effect was reproducible (Fig. 1*C*) and dose dependent (Fig. 1 *D* and *E*). Cultured astrocytes are net lactate producers. To clarify whether the accumulation of lactate was due to increased production or impaired release, astrocytes were exposed to NH_4^+ in the presence of the monocarboxylate transporter (MCT) blocker AR-C155858 (26), which in these cells abrogates lactate transport (24). As shown in Fig. 1*F*, the increased rate of lactate accumulation in the presence of the MCT blocker demonstrates NH_4^+ stimulated lactate production. Lactate release was assessed independently by real-time estimation of lactate levels in the immediate vicinity of astrocytes using a lactate-sniffer HEK 293 cell (27). Seeded on a brain cell culture, lactate sniffers were observed to lie on top of the astrocytic monolayer (Fig. 1*G*). As

Significance

Aerobic glycolysis is important for synaptic growth, neuronal excitability, memory formation, and behavior and is also involved in neurodegeneration. Here we present evidence, obtained with novel optical tools, to show that NH_4^+ contributes to aerobic glycolysis by specifically inhibiting the mitochondrial consumption of pyruvate in astrocytes. NH_4^+, a waste product of excitatory neurotransmission, is therefore proposed to behave as an intercellular signal in brain tissue.

Author contributions: R.L., I.F.-M., Y.C.-B., T.S.-H., P.M., M.T.W., J.S., F.B.-L., B.W., and L.F.B. designed research; R.L., I.F.-M., Y.C.-B., T.S.-H., P.M., M.T.W., J.S., F.B.-L., and K.A. performed research; R.L., I.F.-M., Y.C.-B., T.S.-H., P.M., M.T.W., J.S., F.B.-L., K.A., B.W., and L.F.B. analyzed data; and R.L., B.W., and L.F.B. wrote the paper.

The authors declare no conflict of interest.

This article is a PNAS Direct Submission.

[1]To whom correspondence should be addressed. Email: fbarros@cecs.cl.

This article contains supporting information online at www.pnas.org/lookup/suppl/doi:10.1073/pnas.1508259112/-/DCSupplemental.

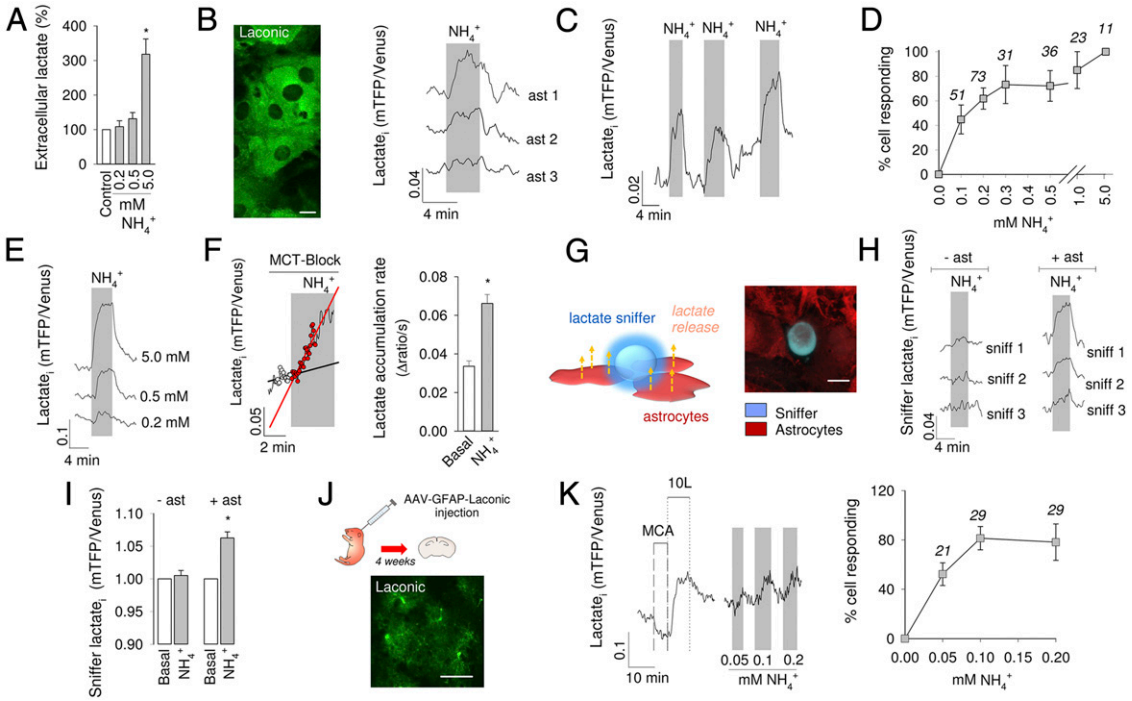

Fig. 1. NH_4^+ stimulates the production and release of lactate by astrocytes in vitro. (*A*) Extracellular lactate measurement with an enzymatic kit in pure astrocytic cultures. Cells were exposed for 1 min to 0.2, 0.5, or 5 mM NH_4^+. (*B*) (*Left*) Laconic expressed in the cytosol of astrocytes in culture. (Scale bar, 10 μm.) (*Right*) Effect of NH_4^+ on intracellular lactate is shown for 3 representative cells as the change of the mTFP/Venus ratio. (*C*) An astrocyte was exposed three times to 0.2 mM NH_4^+. (*D*) Dose dependence of the effect expressed as percentage of cells responding to NH_4^+ with an increase in lactate. Responding cells were distinguished from nonresponding cells by computing the average of five data points collected just before NH_4^+ exposure and the average of five data points at 3 min of exposure. The difference between the two values was considered significant if $P < 0.05$ (Mann-Whitney *u* test). The number of monitored cells is given. (*E*) Response of a single astrocyte to subsequent exposures to 0.2, 0.5, and 5 mM NH_4^+. (*F*) Astrocytes in glucose alone as energy substrate were first exposed to the MCT inhibitor AR-C155858 (1 μM) and 2 min later to 0.2 mM NH_4^+. Lines represent the rate of lactate accumulation before and during exposure to NH_4^+. Bars show averages. (*G*) (*Left*) Schematic representation of lactate sniffers above astrocytes. (*Right*) 3D confocal microscopy reconstruction of HEK 293 lactate sniffers (blue) and astrocytes loaded with Calcein orange (red). (*H*) Representative responses of sniffer cells exposed to 0.2 mM NH_4^+ in the absence and presence of astrocytes. (*I*) Bars show average changes in sniffer signal. (*J*) Protoplasmic astrocytes expressing Laconic in an acute hippocampal slice prepared 4 wk after AAV injection at P1. (Scale bar, 50 μm.) (*K*) (*Left*) Two-point calibration of Laconic with 50 mM monochloroacetate (MCA) and 10 mM lactate (10L), and response of a protoplasmic astrocyte to slice exposure to 0.05, 0.1, and 0.2 mM NH_4^+. (*Right*) Dose dependence of the effect expressed as percentage of cells responding to 0.2 mM NH_4^+ with an increase in lactate. Responding cells were identified as detailed in *D*. The number of monitored cells is given. $*P < 0.05$.

shown in Fig. 1 *H* and *I*, exposure of the cultures to NH_4^+ resulted in a rapid increase in sniffer signal that was variable in amplitude and reverted to baseline after NH_4^+ withdrawal. These results show that astrocytes increase their production and release of lactate within seconds of exposure to physiological levels of NH_4^+.

To verify if the response of astrocytes to NH_4^+ is detectable in brain tissue, lactate was measured in protoplasmic astrocytes of the hippocampus. For this purpose, a recombinant adeno-associated virus coding for Laconic under the short gfaABC$_1$D promoter was stereotactically injected into the brain of neonatal mice. After 4–5 wk, brain slices were prepared, and FRET measurements were made (Fig. 1*J*). Imaged in tissue slices, the sensor behaved as expected, with a decrease in signal on transacceleration of lactate export with the nonmetabolized MCT substrate monochloroacetate and an increase during exposure to 10 mM lactate (24). Addition of NH_4^+ to the slice caused a rapid increase in lactate in protoplasmic astrocytes, a response that could be detected even at 0.05 mM NH_4^+ (Fig. 1*K*). To approach astrocytic lactate in vivo, Laconic was expressed in astrocytes of the primary somatosensory cortex of adult mice and then imaged under anesthesia through a cranial window using two-photon microscopy (Fig. 2*A*). An i.v. bolus injection of NH_4^+ (2.5 mmol/kg body weight) provoked a quick rise in astrocytic lactate (Fig. 2*B*), followed by a rise in extracellular lactate, as detected by an enzyme-based microelectrode inserted into the brain tissue (Fig. 2*C*). Parallel measurements showed no apparent effects of the NH_4^+ bolus infusion on blood lactate levels (Fig. 2*D*), demonstrating that the changes detected in the brain were originated locally. Less NH_4^+ was also capable of increasing astrocytic lactate, with a lowest effective dose of 0.63 mmol/ kg (Fig. 2*E*). Considering that a bolus of 2.5 mmol/kg increased brain tissue NH_4^+ by 0.7 mM (20), the 0.63 mmol/kg bolus should have increased brain NH_4^+ by 0.17 mM. This calculated value, which is close to the physiological range, is probably an overestimate as it does not take into account NH_4^+ clearance by peripheral tissues and by astrocytes. Aerobic glycolysis may be triggered by stimulation of astrocytic glycolysis, such as that observed in response to glutamate or to high K^+ (11, 12). To assess glycolysis as a possible target for NH_4^+, astrocytic glucose was measured using the genetically encoded glucose nanosensor FLII^{12}Pglu700μΔ6 (28). As shown in Fig. S1, exposure to physiological NH_4^+ levels had no apparent effect on cytosolic glucose concentration nor on the rate of glucose consumption measured with a transport block protocol (29). We conclude that physiological NH_4^+ does not stimulate glucose consumption in astrocytes.

Mitochondrial Flux Inhibition by Physiological NH_4^+. In lactate producers like astrocytes, most NADH is produced in glycolysis. Measurements with the genetically encoded fluorescent nanosensor Peredox (30) showed a decrease in cytosolic NADH in response to NH_4^+ (Fig. 3*A*), a result that is consistent with the lack of effect of NH_4^+ on glucose consumption and that also rules out glycogen as a putative source of lactate. Thus, we focused on

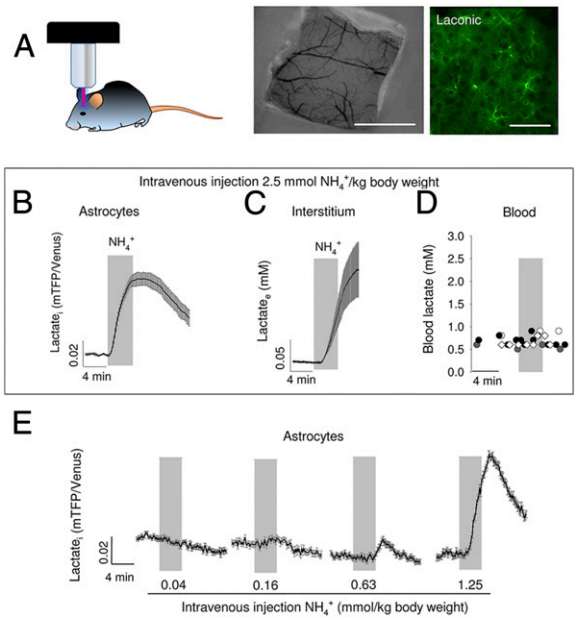

Fig. 2. NH_4^+ increases astrocytic lactate in vivo. (*A*) Schematic representation of an in vivo experiment. (*Left*) Anesthetized mouse previously injected with AAV9-GFAP-Laconic is positioned in the two-photon microscope setup for measurement of astrocytic lactate. (*Center*) Cranial window exposing the somatosensory cortex. (Scale bar, 1 mm.) (*Right*) Protoplasmic astrocytes expressing Laconic in the somatosensory cortex, layer II/III. (Scale bar, 50 μm.) A bolus of NH_4^+ (2.5 mmol/kg body weight) was injected i.v. while monitoring astrocytic lactate with Laconic (*B*), extracellular lactate with an inserted biosensor (*C*), or blood lactate with an enzymatic assay (*D*). Symbols in *D* represent data from four separate experiments. (*E*) Response of astrocytic lactate to sequential i.v. injections of increasing doses of NH_4^+.

mitochondrial inhibition as the possible mechanism for the lactate surge. Measurements with the FRET nanosensor Pyronic (31) supported this hypothesis by showing a rapid increase of cytosolic pyruvate in response to NH_4^+, which could be observed even at 0.05 mM (Fig. 3*B*). Next, mitochondrial pyruvate consumption was monitored using a transport block protocol (31). Briefly, astrocytes were first incubated with pyruvate alone as energy substrate and then were exposed to a mixture of surface pyruvate transport blockers, a condition under which the rate of cytosolic pyruvate depletion represents the rate of mitochondrial pyruvate consumption. In our culture conditions, the uptake of pyruvate is partly mediated by a pathway sensitive to AR-C155858 and by a pathway sensitive to probenecid. As shown in Fig. 3*C*, NH_4^+ markedly decreased mitochondrial pyruvate consumption. To further characterize the dynamics of mitochondrial inhibition, cells were simultaneously exposed to NH_4^+ and pyruvate transport blockers during high-frequency data acquisition. During the first seconds of exposure, the rate of pyruvate depletion was similar to that observed in the absence of NH_4^+, but then the depletion came to a stop and pyruvate levels began to recover. A numerical model of pyruvate dynamics could be fitted to the data, indicating that NH_4^+ inhibited mitochondrial pyruvate uptake by 93%, with a delay of 30 s between surface transport block and mitochondrial inhibition (Fig. 3*D*). The resulting accumulation of pyruvate in the cytosol pushes the near-equilibrium LDH reaction toward NADH use and lactate production, thus accounting for the observed decrease in cytosolic NADH.

Mechanism of Mitochondrial Pyruvate Uptake Inhibition by NH_4^+. A robust cytosolic acidification was obtained with supraphysiological NH_4^+ (Fig. 3*E*), confirming that ammonium enters astrocytes mostly in the protonated form, a process known to be mediated by K^+ channels and transporters (19, 22). Exposure of astrocytes to physiological NH_4^+ caused a significant acidification of the mitochondrial matrix, as estimated with MitoSypHer, a genetically-encoded pH sensor (Fig. 3*F*). The mitochondrial acidification suggests that ammonium enters astrocytic mitochondria in the protonated form. We could not find information about the mechanisms of mitochondrial NH_4^+ transport in astrocytes. Preferential NH_4^+ over NH_3 uptake has previously been reported in liver mitochondria (32). Of note, although NH_3 is a gas, it diffusivity through biological membranes can be low, as reported in kidney cells (33). In contrast, physiological NH_4^+ did not acidify the cytosol to a significant extent (Fig. 3*E*). The absence of cytosolic acidification by low levels of ammonium is consistent with the higher pH and lower buffering capacity of the mitochondrial matrix relative to the cytosol (34), compounded by muffling from the high levels of cytosolic bicarbonate and carbonic anhydrase present in astrocytic cytosol (35). The uptake of pyruvate by mitochondria is mediated by the mitochondrial pyruvate carrier (MPC), which is an H^+-pyruvate cotransporter (36, 37). Therefore, the driving force for pyruvate uptake depends on the difference between the H^+ concentration in the cytosol and that in the more alkaline mitochondrial matrix (38). Because the MPC cotransports pyruvate with an H^+, the acidification of mitochondria by physiological NH_4^+ provides an explanation for the inhibition of pyruvate uptake by mitochondria. After entering mitochondria, most of the pyruvate is metabolized via the Krebs cycle. This pathway may be inhibited by NH_3 at α-ketoglutarate dehydrogenase (21), a possible downstream target for NH_4^+ after deprotonation. NH_4^+ had no apparent effect on mitochondrial membrane potential (Fig. 3*G*). A stable mitochondrial potential in the face of matrix acidification has been previously ascribed to Ca^{2+} efflux (39), but we could not find a detectable increase in cytosolic Ca^{2+} in astrocytes exposed to NH_4^+ (Fig. S2). An alternative explanation for the constancy of mitochondrial potential may be inhibition of ATP synthase mediated by the H^+-sensitive modulator IF1 (40).

Discussion

This article describes a previously unidentified mechanism of aerobic glycolysis. We found that physiological levels of NH_4^+ induce a rapid and reversible increase in lactate production and release by astrocytes, a robust phenomenon observed in cultured cells, brain tissue slices, and in the somatosensory cortex in vivo. In contrast to the metabolic roles of glutamate and K^+, the NH_4^+-dependent lactate surge was not due to glycolytic stimulation but to pyruvate shunting, explained by acidification of the mitochondrial matrix. As NH_4^+ is produced by neurons in an activity-dependent manner, the present mechanism suggests that NH_4^+ diverts lactate from astrocytes to neurons (Fig. 4).

NH_4^+ as a Marker for Neurotransmission. Astrocytes capture glutamate released during excitatory neurotransmission and send it back to neurons in the form of glutamine. Within neurons, glutamine is reconverted to glutamate with the stoichiometric production of NH_4^+ (13). The physiological concentration of NH_4^+ in brain tissue of several species has been estimated at about 0.2 mM (15, 21), with a more recent 0.45 mM measured in mouse brain interstitium with a double barreled electrode (22). An increase in nervous tissue NH_4^+ during neural activity has been reported in several animal models, including frog sciatic nerve (14), rat brain slices (15), and slices of the bee retina (17). Using a rapid freezing technique, a transient increase in brain tissue NH_4^+ was detected within 5 s of rat paw stimulation (16). It is not clear whether NH_4^+ is released together with glutamate during synaptic vesicle fusion (41) or alternatively through NH_4^+-permeable ion channels (42). NH_4^+ is rapidly captured by astrocytes via several pathways including K^+ channels and transporters (19, 22). Nitrogen may also be shuttled from neurons to astrocytes as

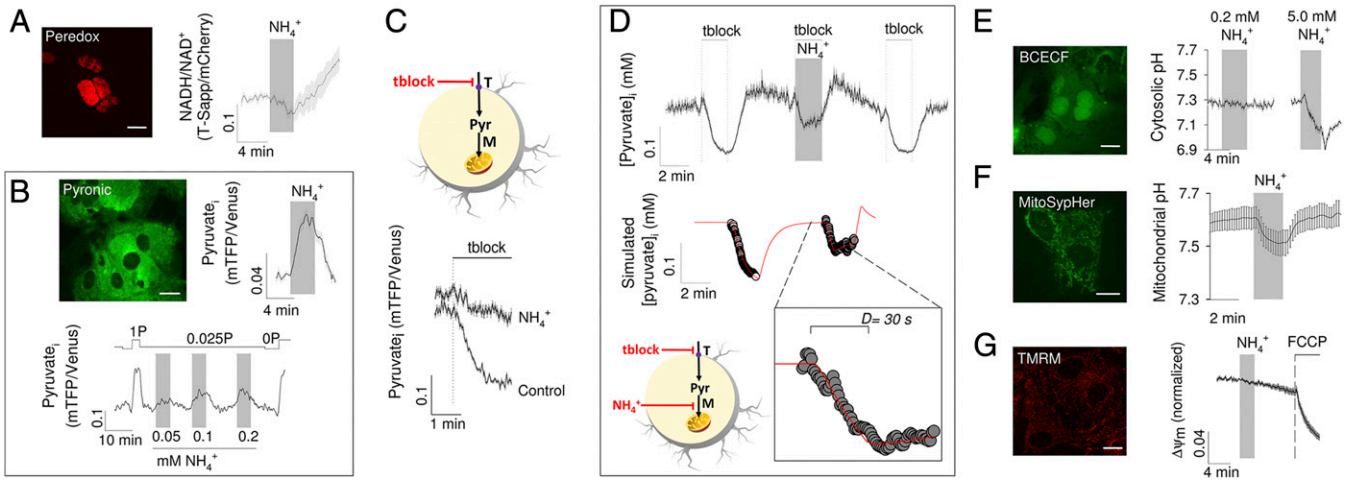

Fig. 3. Mitochondrial inhibition induced by NH_4^+. (*A*) Cultured astrocytes expressing the NADH/NAD^+ nanosensor Peredox in the nucleus. (Scale bar, 10 μm.) The graph shows the effect of 0.2 mM NH_4^+ on the NADH/NAD^+ ratio. (*B*) Cultured astrocytes expressing the pyruvate nanosensor Pyronic. (Scale bar, 10 μm.) The graph in the middle shows the effect of 0.2 mM NH_4^+ on astrocytic pyruvate. (*Right*) Response of a single astrocyte to subsequent exposures to 0.05, 0.1, and 0.2 mM NH_4^+. Pyruvate in the superfusate (P) was set at 0.025 mM during the stimulations or 0 and 1 mM for calibration purposes. (*C*) (*Upper*) Schematic representation of the method that estimates mitochondrial pyruvate consumption by inhibiting surface pyruvate transport (T) with 100 nM AR-C155858 and 1 mM probenecid (tblock). (*Lower*) Mitochondrial pyruvate consumption in cells that had been exposed for 3 min to 0.2 mM NH_4^+ and their controls. (*D*) (*Upper*) Surface pyruvate transport was blocked in the absence and presence of 0.2 mM NH_4^+. (*Lower*) Numerical model represented in the schematic was fitted (red line) to the pyruvate data (symbols) as described in the *SI Text*. (*Inset*) Delay in the onset of the NH_4^+ effect. (*E*) Effects of 0.2 and 5.0 mM NH_4^+ on astrocytic pH, estimated with BCECF. (*F*) Effect of 0.2 NH_4^+ on mitochondrial pH, estimated with mitoSypHer. (*G*) Effects of 0.2 NH_4^+ and 1 μM FCCP on mitochondrial membrane potential estimated with TMRM. (Scale bars, 10 μm.)

amino acids, but the extent of this indirect pathway seems to be less significant than direct transfer as NH_4^+ (18).

Mechanism of Lactate Production by NH_4^+. We observed that NH_4^+ acutely stimulated the production and release of lactate by astrocytes without affecting glycolysis. The phenomenon was detected even at 0.05 mM and coincided with a strong inhibition of pyruvate uptake by mitochondria. There was a coincidental decrease in cytosolic NADH, consistent with pyruvate to lactate conversion. NH_4^+ caused an acute acidification of the mitochondrial matrix but no detectable changes in cytosolic pH. The uptake of pyruvate by mitochondria is mediated by the H^+-coupled MPC (36, 37), and therefore the reduction of the transmitochondrial pH gradient by NH_4^+ provides a parsimonious explanation for the reduced uptake of pyruvate. There is increasing evidence that mitochondrial pH plays important physiological and pathological roles (43); for example, a recent study in astrocytes showed that glutamate inhibited oxygen consumption, a phenomenon ascribed to cytosolic acidification leading to mitochondrial acidification (34).

NH_4^+ Is a Signal for Aerobic Glycolysis. The control, by neurons, of astrocytic lactate release appears to involve several mechanisms acting within different temporal domains. In the short term (seconds), glutamate stimulates the glucose transporter GLUT1 via Na^+ and Ca^{2+} transients mediated by the Na^+-glutamate cotransporter (44, 45). Acting in parallel, K^+ stimulates glycolysis via the Na^+-HCO_3^- cotransporter NBCe1 (12, 46) and also opens a lactate permeable ion channel at the cell surface (27). By suppressing the uptake of pyruvate by astrocytic mitochondria within seconds, NH_4^+ adds an additional strategy for short-term induction of aerobic glycolysis. Acting on different targets, the three signals are likely to be synergic. The production of lactate by astrocytes is also stimulated by neuronal signals in the long term (minutes). Glutamate activates glycolysis via the Na^+-glutamate cotransporter (11, 12) and K^+ stimulates glycogen degradation via the HCO_3^--sensitive soluble adenylyl cyclase (47). Also within minutes, nitric oxide has been shown to stimulate astrocytic glycolysis through inhibition of cytochrome *c* oxidase leading to activation of 5′-AMP–activated protein kinase and PFKFB3 (48). It seems likely that NH_4^+ may also have long-term roles in the control of astrocytic glycolysis and similar mechanisms could be present in other glial cells. For example, retinal Müller cells have been shown to increase their production of lactate in response to NH_4^+, but only in the presence of glutamate (49). Cooperativity might also help to explain the present observation that astrocytes in brain slices, likely exposed to some glutamate, were found to be more sensitive to NH_4^+ than astrocytes in culture. Given the emerging importance of aerobic glycolysis and lactate for diverse

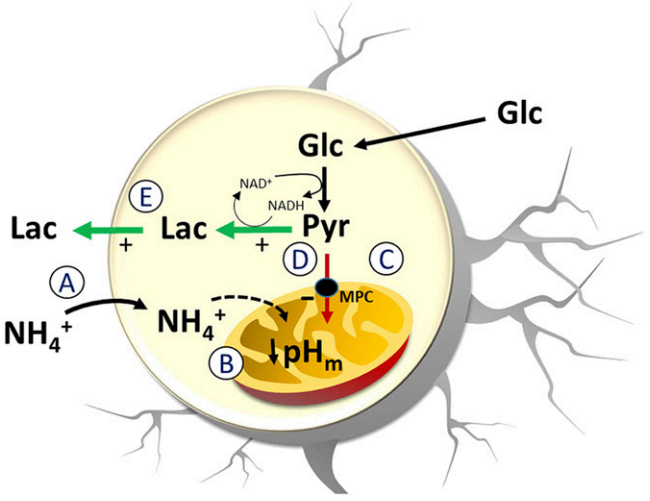

Fig. 4. Astrocytic lactate release in response to NH_4^+. The release of lactate by astrocytes exposed to NH_4^+ is explained by the following sequence of events. (*A*) NH_4^+ uptake by astrocytes through K^+ channels and transporters. (*B*) NH_4^+ entry into mitochondria leading to acidification of the mitochondrial matrix. (*C*) Inhibition of the H^+-coupled MPC. (*D*) Accumulation of pyruvate in the cytosol causing lactate accumulation and NADH depletion. (*E*) Increased lactate release.

local and higher functions of the brain (3–10, 50–55), we hope that the present findings will stimulate research on the physiological aspects of NH_4^+, particularly mitochondrial transport and neuronal release.

Materials and Methods

Standard reagents and inhibitors were acquired from Sigma or Merck. AR-C155858 was purchased from Haoyuan Chemexpress. The sensors FLII^{12}Pglu700μΔ6, Peredox, Laconic, Pyronic, and MitoSypHer are available from Addgene (www.addgene.org). Ad Laconic, Ad Pyronic, and Ad FLII^{12}Pglu700μΔ6 (serotype 5) were custom made by Vector Biolabs. The adeno-associated virus (AAV9) expressing Laconic under the control of the short gfaABC1D promoter was generated at the École Polytechnique Fédérale de Lausanne. Design, production, and titration of the AAV9 vector for transgene expression in astrocytes have been described previously (56). Fluo-4 AM, 2,7-bis-(2-carboxyethyl)-5-(and-6)-carboxyfluorescein (BCECF) AM, tetramethyl rhodamine methyl ester (TMRM), and Calcein AM were from Invitrogen. All NH_4^+ application were in the form of NH_4Cl. At pH 7.4 and 23 °C, 99% is in the ionized form (NH_4^+), and 1% is in the neutral form (NH_3).

Animals and Brain Cell Culture. All animal procedures for the in vitro experiments were approved by the Institutional Animal Care and Use Committee of the Centro de Estudios Científicos. Animals used for primary cultures and brain slices were mixed F1 male mice (C57BL/6J × CBA/J), kept in an animal room under SPF conditions at a room temperature of 20 ± 2 °C, in a 12/12-h light/dark cycle and with free access to water and food. Procedures for in vivo experiments were approved by the local veterinary authorities, conforming to the guidelines of the Swiss Animal Protection Law, Veterinary Office, Canton Zurich (Act of Animal Protection 16 December 2005 and Animal Protection Ordinance 23 April 2008). WT mice (C57BL/6J; Harlan Laboratories) 10 wk of age and with a body weight of 20 g were housed in single cages, with free access to water and food. Mixed brain cell primary cultures were prepared as detailed previously (46). To measure lactate release with an enzymatic method, pure astrocytic cultures were obtained by subculturing mixed cultures at day 14. After another 7 d in 24-well plates, cultures were exposed to experimental conditions in a 95% air/5% CO_2-gassed culture saline buffer (CSF) composed of (mM) 112 NaCl, 3 KCl, 1.25 $CaCl_2$, 1.25 $MgCl_2$, 2 glucose, 10 Hepes, and 24 $NaHCO_3$, pH 7.4, at room temperature. Extracellular lactate was measured using a fluorometric assay kit according to the manufacturer´s instructions (BioVision). For FRET sensor expression, cultures were exposed to 5×10^6 PFU of Ad Laconic, Ad Pyronic, or Ad FLII^{12}Pglu700μΔ6 and studied after 48 h (culture day 8–10). For plasmid expression of Peredox and mitoSypHer, cells were transfected using Lipofectamine 2000 or 3000 (Gibco) and studied after 48 h (culture day 8–10). The cytosolic and nuclear versions of Peredox responded similarly to NH_4^+, as expected from unrestricted movement of NADH and NAD^+ through the nuclear pore (30). However, the expression of nuclear Peredox was much stronger. Thus, we chose to illustrate NADH dynamics using nuclear Peredox. To generate lactate sniffers (27), HEK293 cells were first transfected with Laconic. After 24 h, the cells were detached with trypsin for 2 min, washed three times, and seeded on top of a mixed brain cell culture. The coculture was maintained with Neurobasal medium for 12–24 h until imaging.

Hippocampal Slices. Neonatal mice (postnatal days 1–2) were removed from the mother and anesthetized by hypothermia for 8 min. Animals were positioned on a stereotactic stage (57) and injected with 1 μL AAV9-GFAP-Laconic directly through the skull using a Fusion 100 Syringe Pump (Chemyx). After injection, animals were positioned on a temperate bed until recovery and returned to the mother. Four weeks after AAV injection, animals were killed by cervical dislocation, and 200-μm-thick coronal brain sections were prepared as described (58).

In Vivo Two-Photon Microscopy of Somatosensory Cortex. The protocol for in vivo determination of astrocytic lactate with Laconic has been detailed elsewhere (27). In brief, animals were anesthetized with an intraperitoneally injected mixture of fentanyl (0.05 mg/kg body weight; Sintenyl, Sintetica), midazolam (5 mg/kg body weight; Dormicum, Roche), and medetomidine (0.5 mg/kg body weight; Domitor, Orion Pharma) and again after 50 min with midazolam only (5 mg/kg body weight). The head was fixed in a stereotactic apparatus, and the eyes were kept wet with an ointment (vitamin A eye cream; Bausch & Lomb). A 4 × 4-mm craniotomy was drilled using a dental drill, and 75 nL AAV9-GFAP-Laconic (titer 3.1×10^{12} vg/mL) was injected into the primary somatosensory cortex. A square coverslip (3 × 3 mm; UQG Optics Ltd.) was lightly pressed on the exposed brain and fixed with dental cement to the skull. A bonding agent (Gluma Comfort Bond; Heraeus Kulzer) was applied to the cleaned skull and was polymerized with a handheld blue light source (600 mW/cm^2; Demetron LC, Kerr Corporation). The open skin was treated with an antibiotic ointment (Cicatrex; Janssen-Cilag AG) and closed with acrylic glue (Histoacryl; B. Braun). After surgery, the animals were kept warm and provided with analgesics (Novaminsulfon, 50%; Sintetica), and the antibiotic enrofloxacin was added to the drinking water (200 mg/L drinking water; Baytril, Bayer). For in vivo lactate measurements, mice were imaged with a custom-built two-photon laser-scanning microscope using a tunable pulsed (Mai Tai eHP DS system; Spectra-Physics) at a wavelength of 870 nm. The animals were head fixed and kept under anesthesia, as described above. Body temperature was kept constant with a feedback-controlled heating pad (37 °C; Harvard Apparatus). Extracellular lactate measurements were performed with the commercially available recording system from Pinnacle Technology. Mice were fixed in a stereotactic frame under anesthesia (isoflurane 1.5%; Abbott), the skull was opened with a dental drill, and a guide cannula (Part 7032; Pinnacle Technology) was implanted into the primary somatosensory cortex (A/P +1.41, M/L −2.8, D/V −1.0) and fixed with dental cement to an anchor screw (Part 8209; Pinnacle Technology). After a recovery period of 2 wk, the precalibrated lactate sensor was inserted into the guide cannula. A tail vein catheter was created for saline, lactate, and pyruvate infusions. Recording was started 1 h after signal stabilization. For blood lactate level measurements, the femoral artery was exposed and cannulated with fine bore polyethylene tubing (0.28 mm ID, 0.61 mm OD, Portex; Smiths Medical). Blood drops were removed from the cannula, and every fourth drop was used for an enzymatic lactate assay (Lactate Pro-2; Arkray). After each blood sample analysis, the tubing was rinsed with heparinized (50 IU/mL) 0.9% saline solution.

In Vitro Fluorescence Imaging. Detailed protocols for the use of the fluorescent sensors are available (59–62). Cells and slices were imaged with an upright Olympus FV1000 confocal microscope and a 440-nm solid-state laser. Alternatively, cells were imaged with Olympus IX70 or BX51 microscopes equipped with Cairn Research monochromators and Optosplits and either a Hamamatsu Orca or Rollera camera. Cells were superfused at 1 mL/min (chamber volume, 0.3 mL) at room temperature (22–24 °C): Cultures were superfused with a 95% air/5% CO_2-gassed CSF (1 mM glucose and 0.5 mM NaLactate), and tissue slices with a 95% O_2/5% CO_2-gassed solution composed of (mM) 126 NaCl, 3 KCl, 1.25 NaH_2PO_4, 1.25 $CaCl_2$, 1.25 $MgCl_2$, 10 glucose, and 26 $NaHCO_3$, at pH 7.4. Cell cultures were imaged approximately 30 min after Neurobasal removal; Typical time between animal killing and slice imaging was 2 h. Masked ratio images were generated from background-subtracted images using ImageJ software. Fluo4 was ester loaded at 4 μM for 15 min. BCECF was ester loaded at 0.1 μM for 3–4 min. Calcein orange was ester loaded at 1 μM for 30 min. BCECF and mitoSypHer were calibrated by exposing the cultures to different pH in the presence of 10 μg/mL nigericin and 20 μg/mL gramicidin in an intracellular buffer. The permeabilization procedure shifted the mitoSypHer signal, and therefore baseline mitochondrial pH was assumed to be 7.6 (34). For mitochondrial membrane potential imaging the cultures were loaded with the fluorescent dye TMRM for 30 min at 37 °C.

Data Presentation and Statistical Analysis: Line traces without errors represent individual cells. Traces with error bars correspond to mean ± SEM of eight or more cells ($n \geq 3$ experiments). Differences between two groups were evaluated with the Student *t* test or the Mann-Whitney *u* test, and differences between more groups were evaluated with the Kruskal–Wallis one-way ANOVA on ranks followed by Dunn´s test. $P < 0.05$ was considered significant. The computer simulation of pyruvate dynamics is described in *SI Text*.

ACKNOWLEDGMENTS. We thank Christine Rose for helpful suggestion and Karen Everett for critical reading of the manuscript. This research was partly funded by Fondecyt Grant 1130095 (to L.F.B.). B.W. is partly supported by the Swiss National Science Foundation and the Clinical Research Priority Program of the University of Zurich on Molecular Imaging. The Centro de Estudios Científicos is funded by the Chilean Government through the Centers of Excellence Basal Financing Program of the Comisión Nacional de Investigación Científica y Tecnológica (CONICYT).

1. Fox PT, Raichle ME, Mintun MA, Dence C (1988) Nonoxidative glucose consumption during focal physiologic neural activity. *Science* 241(4864):462–464.
2. Raichle ME, Mintun MA (2006) Brain work and brain imaging. *Annu Rev Neurosci* 29: 449–476.
3. Mintun MA, Vlassenko AG, Rundle MM, Raichle ME (2004) Increased lactate/pyruvate ratio augments blood flow in physiologically activated human brain. *Proc Natl Acad Sci USA* 101(2):659–664.
4. Wyss MT, Jolivet R, Buck A, Magistretti PJ, Weber B (2011) In vivo evidence for lactate as a neuronal energy source. *J Neurosci* 31(20):7477–7485.
5. Suzuki A, et al. (2011) Astrocyte-neuron lactate transport is required for long-term memory formation. *Cell* 144(5):810–823.
6. Goyal MS, Hawrylycz M, Miller JA, Snyder AZ, Raichle ME (2014) Aerobic glycolysis in the human brain is associated with development and neotenous gene expression. *Cell Metab* 19(1):49–57.
7. Barros LF (2013) Metabolic signaling by lactate in the brain. *Trends Neurosci* 36(7): 396–404.
8. Barros LF, Sierralta J, Weber B (2015) How doth the little busy bee: Unexpected metabolism. *Trends Neurosci* 38(1):1–2.
9. Chandrasekaran S, et al. (2015) Aggression is associated with aerobic glycolysis in the honey bee brain(1). *Genes Brain Behav* 14(2):158–166.
10. Bero AW, et al. (2011) Neuronal activity regulates the regional vulnerability to amyloid-β deposition. *Nat Neurosci* 14(6):750–756.
11. Pellerin L, Magistretti PJ (1994) Glutamate uptake into astrocytes stimulates aerobic glycolysis: A mechanism coupling neuronal activity to glucose utilization. *Proc Natl Acad Sci USA* 91(22):10625–10629.
12. Bittner CX, et al. (2011) Fast and reversible stimulation of astrocytic glycolysis by K^+ and a delayed and persistent effect of glutamate. *J Neurosci* 31(12):4709–4713.
13. Schousboe A, Bak LK, Waagepetersen HS (2013) Astrocytic Control of Biosynthesis and Turnover of the Neurotransmitters Glutamate and GABA. *Front Endocrinol (Lausanne)* 4:102.
14. Tashiro S (1922) Studies on alkaligenesis in tissues. *Am J Physiol* 60:519–543.
15. Richter D, Dawson RM (1948) The ammonia and glutamine content of the brain. *J Biol Chem* 176(3):1199–1210.
16. Tsukada Y, Takagaki G, Sugimoto S, Hirano S (1958) Changes in the ammonia and glutamine content of the rat brain induced by electric shock. *J Neurochem* 2(4): 295–303.
17. Coles JA, Marcaggi P, Véga C, Cotillon N (1996) Effects of photoreceptor metabolism on interstitial and glial cell pH in bee retina: Evidence of a role for NH4+. *J Physiol* 495(Pt 2):305–318.
18. Rothman DL, De Feyter HM, Maciejewski PK, Behar KL (2012) Is there in vivo evidence for amino acid shuttles carrying ammonia from neurons to astrocytes? *Neurochem Res* 37(11):2597–2612.
19. Kelly T, Rose CR (2010) Ammonium influx pathways into astrocytes and neurones of hippocampal slices. *J Neurochem* 115(5):1123–1136.
20. Provent P, et al. (2007) The ammonium-induced increase in rat brain lactate concentration is rapid and reversible and is compatible with trafficking and signaling roles for ammonium. *J Cereb Blood Flow Metab* 27(11):1830–1840.
21. Cooper AJ, Plum F (1987) Biochemistry and physiology of brain ammonia. *Physiol Rev* 67(2):440–519.
22. Rangroo Thrane V, et al. (2013) Ammonia triggers neuronal disinhibition and seizures by impairing astrocyte potassium buffering. *Nat Med* 19(12):1643–1648.
23. Kala G, Hertz L (2005) Ammonia effects on pyruvate/lactate production in astrocytes–interaction with glutamate. *Neurochem Int* 47(1-2):4–12.
24. San Martín A, et al. (2013) A genetically encoded FRET lactate sensor and its use to detect the Warburg effect in single cancer cells. *PLoS One* 8(2):e57712.
25. Mamczur P, et al. (2015) Astrocyte-neuron crosstalk regulates the expression and subcellular localization of carbohydrate metabolism enzymes. *Glia* 63(2):328–340.
26. Ovens MJ, Davies AJ, Wilson MC, Murray CM, Halestrap AP (2010) AR-C155858 is a potent inhibitor of monocarboxylate transporters MCT1 and MCT2 that binds to an intracellular site involving transmembrane helices 7-10. *Biochem J* 425(3):523–530.
27. Sotelo-Hitschfeld T, et al. (2015) Channel-mediated lactate release by K^+-stimulated astrocytes. *J Neurosci* 35(10):4168–4178.
28. Takanaga H, Chaudhuri B, Frommer WB (2008) GLUT1 and GLUT9 as major contributors to glucose influx in HepG2 cells identified by a high sensitivity intramolecular FRET glucose sensor. *Biochim Biophys Acta* 1778(4):1091–1099.
29. Bittner CX, et al. (2010) High resolution measurement of the glycolytic rate. *Front Neuroenergetics* 2:1–11.
30. Hung YP, Albeck JG, Tantama M, Yellen G (2011) Imaging cytosolic NADH-NAD(+) redox state with a genetically encoded fluorescent biosensor. *Cell Metab* 14(4): 545–554.
31. San Martín A, et al. (2014) Imaging mitochondrial flux in single cells with a FRET sensor for pyruvate. *PLoS One* 9(1):e85780.
32. Gutiérrez C, Beaty G, López-Vancell R, Estrada S (1987) Mechanism of ammonium translocation in rat liver mitochondria. Finger-printing of the translocator. *Acta Physiol Pharmacol Latinoam* 37(2):257–275.
33. Kikeri D, Sun A, Zeidel ML, Hebert SC (1989) Cell membranes impermeable to NH3. *Nature* 339(6224):478–480.
34. Azarias G, et al. (2011) Glutamate transport decreases mitochondrial pH and modulates oxidative metabolism in astrocytes. *J Neurosci* 31(10):3550–3559.
35. Deitmer JW, Rose CR (1996) pH regulation and proton signalling by glial cells. *Prog Neurobiol* 48(2):73–103.
36. Bricker DK, et al. (2012) A mitochondrial pyruvate carrier required for pyruvate uptake in yeast, Drosophila, and humans. *Science* 337(6090):96–100.
37. Herzig S, et al. (2012) Identification and functional expression of the mitochondrial pyruvate carrier. *Science* 337(6090):93–96.
38. Poburko D, Demaurex N (2012) Regulation of the mitochondrial proton gradient by cytosolic Ca^{2+} signals. *Pflugers Arch* 464(1):19–26.
39. Perry SW, Norman JP, Barbieri J, Brown EB, Gelbard HA (2011) Mitochondrial membrane potential probes and the proton gradient: A practical usage guide. *Biotechniques* 50(2): 98–115.
40. Campanella M, Parker N, Tan CH, Hall AM, Duchen MR (2009) IF(1): Setting the pace of the F(1)F(o)-ATP synthase. *Trends Biochem Sci* 34(7):343–350.
41. Marcaggi P (2006) An ammonium flux from neurons to glial cells. *Proc Physiol Soc* 3:SA16.
42. Marcaggi P, Coles JA (2001) Ammonium in nervous tissue: Transport across cell membranes, fluxes from neurons to glial cells, and role in signalling. *Prog Neurobiol* 64(2):157–183.
43. Santo-Domingo J, Demaurex N (2012) Perspectives on: SGP symposium on mitochondrial physiology and medicine: The renaissance of mitochondrial pH. *J Gen Physiol* 139(6):415–423.
44. Loaiza A, Porras OH, Barros LF (2003) Glutamate triggers rapid glucose transport stimulation in astrocytes as evidenced by real-time confocal microscopy. *J Neurosci* 23(19):7337–7342.
45. Porras OH, Ruminot I, Loaiza A, Barros LF (2008) Na(+)-Ca(2+) cosignaling in the stimulation of the glucose transporter GLUT1 in cultured astrocytes. *Glia* 56(1):59–68.
46. Ruminot I, et al. (2011) NBCe1 mediates the acute stimulation of astrocytic glycolysis by extracellular K^+. *J Neurosci* 31(40):14264–14271.
47. Choi HB, et al. (2012) Metabolic communication between astrocytes and neurons via bicarbonate-responsive soluble adenylyl cyclase. *Neuron* 75(6):1094–1104.
48. Almeida A, Moncada S, Bolaños JP (2004) Nitric oxide switches on glycolysis through the AMP protein kinase and 6-phosphofructo-2-kinase pathway. *Nat Cell Biol* 6(1): 45–51.
49. Poitry S, Poitry-Yamate C, Ueberfeld J, MacLeish PR, Tsacopoulos M (2000) Mechanisms of glutamate metabolic signaling in retinal glial (Müller) cells. *J Neurosci* 20(5): 1809–1821.
50. Gordon GR, Choi HB, Rungta RL, Ellis-Davies GC, MacVicar BA (2008) Brain metabolism dictates the polarity of astrocyte control over arterioles. *Nature* 456(7223):745–749.
51. Pellerin L, Magistretti PJ (2012) Sweet sixteen for ANLS. *J Cereb Blood Flow Metab* 32(7):1152–1166.
52. Lauritzen KH, et al. (2014) Lactate receptor sites link neurotransmission, neurovascular coupling, and brain energy metabolism. *Cereb Cortex* 24(10):2784–2795.
53. Bozzo L, Puyal J, Chatton JY (2013) Lactate modulates the activity of primary cortical neurons through a receptor-mediated pathway. *PLoS One* 8(8):e71721.
54. Tang F, et al. (2014) Lactate-mediated glia-neuronal signalling in the mammalian brain. *Nat Commun* 5:3284.
55. Yang J, et al. (2014) Lactate promotes plasticity gene expression by potentiating NMDA signaling in neurons. *Proc Natl Acad Sci USA* 111(33):12228–12233.
56. Dirren E, et al. (2014) Intracerebroventricular injection of adeno-associated virus 6 and 9 vectors for cell type-specific transgene expression in the spinal cord. *Hum Gene Ther* 25(2):109–120.
57. Davidson S, Truong H, Nakagawa Y, Giesler GJ, Jr (2010) A microinjection technique for targeting regions of embryonic and neonatal mouse brain in vivo. *Brain Res* 1307: 43–52.
58. Jakoby P, et al. (2014) Higher transport and metabolism of glucose in astrocytes compared with neurons: A multiphoton study of hippocampal and cerebellar tissue slices. *Cereb Cortex* 24(1):222–231.
59. Hou BH, et al. (2011) Optical sensors for monitoring dynamic changes of intracellular metabolite levels in mammalian cells. *Nat Protoc* 6(11):1818–1833.
60. Tantama M, Hung YP, Yellen G (2012) Optogenetic reporters: Fluorescent protein-based genetically encoded indicators of signaling and metabolism in the brain. *Progress in Brain Research*, eds Knopfel T, Boyden E (Elsevier, Amsterdam), pp 235–263.
61. Barros LF, Baeza-Lehnert F, Valdebenito R, Ceballo S, Alegría K (2014) *Springer Protocols: Brain Energy Metabolism*, eds Waagepetersen HS, Hirrlinger J (Springer, Berlin).
62. San Martín A, et al. (2014) Single-cell imaging tools for brain energy metabolism: a review. *Neurophotonics* 1(1):011004.

Supporting Information

Lerchundi et al. 10.1073/pnas.1508259112

SI Text

Mathematical Modeling. Cytosolic pyruvate dynamics in the absence of glucose were modeled using the minimal differential equation $dPyr/dt = \text{T-M}^*Pyr$, where $dPyr/dt$ is determined by the balance between surface pyruvate transport (T) and mitochondrial pyruvate metabolism, a function of cytosolic pyruvate concentration (Pyr) with the constant of proportionality M. As the steady-state cytosolic pyruvate concentration was measured at 0.2 mM (see Fig. 3*D*), the model could be simplified by assuming M = T*5. The differential equation was solved by numerical simulation using the Rosenbrock iteration procedure with the computer software Berkeley Madonna

$$dPyr/dt = \text{T} * [1 - \text{tblock} * \text{squarepulse}(\text{on}_1, \text{dur}_1)] * [1 - \text{tblock} * \text{squarepulse}(\text{on}_2, \text{dur}_2)] - \text{M} * pyr * [1 - \text{NH}_4^+\text{block} * \text{squarepulse}(\text{on}_2 + \text{D}, \text{dur}_3)]$$

where tblock is the degree of pharmacological inhibition of surface pyruvate transport; squarepulse(on_x, dur_x) is a function of value 0 except during the interval of duration dur_x starting at on_x, at which its value is 1; NH_4^+ block is the degree of inhibition of mitochondrial pyruvate uptake by NH_4^+; and squarepulse (on_2 + D, dur_3) is a function of value 0 except during the interval of duration dur_3 starting at on_2 + D, at which its value is 1. D represents the delay between the onset of the surface transport block and the onset of the mitochondrial block.

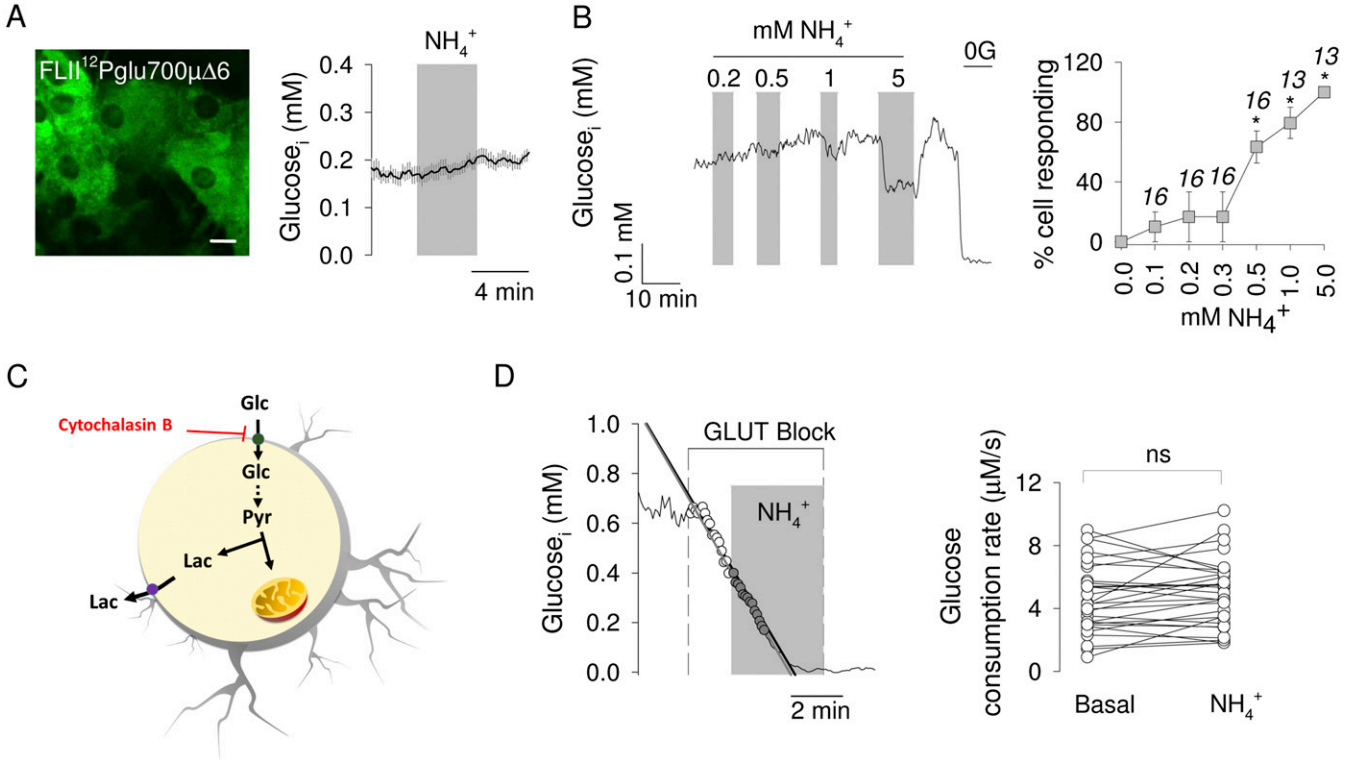

Fig. S1. Physiological NH_4^+ does not stimulate glucose consumption by astrocytes. (*A*) Cultured astrocytes expressing the glucose nanosensor FLII^{12}Pglu700μΔ6. (Scale bar, 10 μm.) The graph shows the effect of 0.2 mM NH_4^+ on cytosolic glucose. (*B*) (*Left*) Response of a single astrocyte to subsequent exposures to 0.2, 0.5, 1, and 5 mM NH_4^+. Glucose was removed (0G) at the end of the experiment for calibration purposes. (*Right*) Average effects expressed as percentage of cells responding to NH_4^+ with a decrease in cytosolic glucose. (*C*) Schematic representation of the method that estimates glucose consumption by inhibiting the glucose transporter GLUT1 with cytochalasin B. (*D*) (*Left*) Measurement of glucose consumption in a single astrocyte with 20 μM cytochalasin B before and during exposure to 0.2 mM NH_4^+. (*Right*) Glucose consumption rates estimated in several similar experiments. *$P < 0.05$.

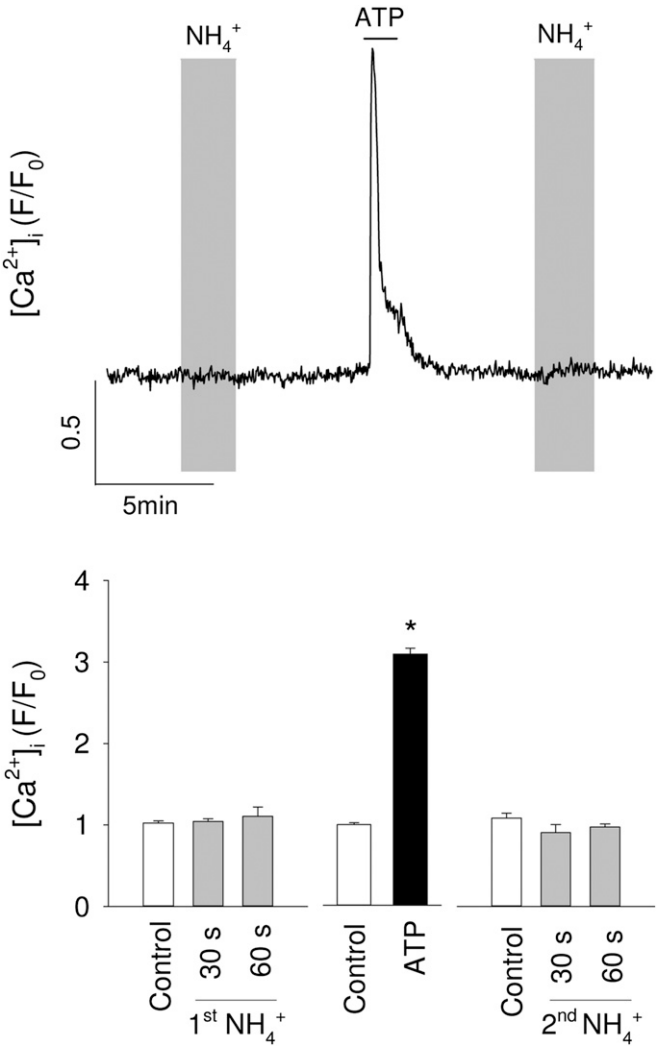

Fig. S2. No apparent effect of NH_4^+ on cytosolic $[Ca^{2+}]$ in astrocytes. Mixed brain cell cultures loaded with Fluo4 were sequentially exposed to 0.2 mM NH_4^+, to 50 μM ATP, and again to 0.2 mM NH_4^+. (*Upper*) Normalized data from a single astrocyte. (*Lower*) Data from 33 astrocytes in three separate experiments, showing average values of five data points recorded just before addition (control), after 30 and 60 s of NH_4^+ exposure and at the peak of the ATP response. $^*P < 0.05$.

General Discussion

Brain energy metabolism has been suggested to be highly compartmentalized on a cellular level in a way that astrocytes play a pivotal role in satisfying the neuronal energy need (for reviews see e.g. [11,59,148]). Glucose is the main fuel for the brain. However, according to the ANLS hypothesis, glucose is preferentially taken up by astrocytes, which then provide hungry neurons with energy rich substrates such as lactate. Even though sugar transport is a passive protein-mediated bidirectional process, some studies reported putatively disproportionate cellular glucose uptake in various neural tissue preparations using radiolabeled or fluorescent glucose derivatives: Vega et al. described disproportionally high 78% of glucose uptake into Schwann cells (glial cells of peripheral nerves)[149]. Likewise, in the central nervous system compartmentation of glucose uptake was shown with about 50% uptake in astrocytes[141], despite of neurons being the main energy consumers in the brain, as about 90% of ATP usage has been allocated to neurons[48,150]. In agreement, only few years ago, the first *in vivo* measurements tried to translate *in vitro* findings into the *in vivo* situation using the fluorescent dye 6-NBDG and two-photon microscopy, also pointing to primary glucose uptake in astrocytes[151]. However, this type of experiments is limited by the use of highly artificial surrogate markers for the measurement of processes related to the turnover of endogenous glucose. Another compartmentalized metabolite according to the ANLS hypothesis is lactate. The only method currently available that can measure cellular lactate levels is the fluorescent lactate sensor Laconic, which has only been used in artificial preparations like cell cultures so far[152]. However, lactate has been shown to be able to sustain neuronal activity during glucose deprivation[153,154] and to be used as brain energy substrates in patients with non-penetrating traumatic brain injuries[155].

During this project, the implementation of multiple FRET biosensors for *in vivo* brain imaging in mice on a cellular level using TPLSM was demonstrated. The new possibilities and also limitations of the individual sensors were presented to an academic field, which heads towards higher spatial and temporal resolutions and more physiological experimental settings.

We were able to demonstrate transitions of cellular metabolite concentrations during different interventions such as the application of glucose, lactate, pyruvate or ammonium concentration gradients from the blood to the brain tissue. However, FRET sensors hold the potential for absolute concentration measurements, but the necessary calibration of the sensors remains a major challenge: We suggested a calibration protocol for the glucose sensor *FLIPΔ6* and the lactate sensor *Laconic*, but we have limited tools to control the pyruvate sensor *Pyronic*. Nevertheless, we could demonstrate the

rate-limiting transport of glucose along the blood brain barrier and cellular membranes and the cellular compartmentation of resting lactate concentrations.

Implications, limitations and future directions

The projects presented in this doctoral thesis resulted in a novel FRET based methodology that allowed monitoring astrocytic and neuronal glucose, lactate and pyruvate concentrations in a semi-quantitative manner. So far, it was only possible to use this methodology in cell cultures and slices but not in the living mammal. Additionally, this methodology holds the potential to measure metabolite concentrations more quantitatively using the substrate binding kinetics of the sensor e.g. in experiments with two sensors with the same substrate specificity but different substrate affinities. Absolute metabolite levels in different cell-types can only be compared with FRET sensors, if the sensors could be calibrated in each ROI of each experiment individually. I presented above an *in vivo* calibration protocol for *Laconic* revealing higher baseline lactate levels in astrocytes. However, the reliable calibration of the glucose sensor *FLIPΔ6* is more complicated, as we only achieved partial glucose deprivation and filling in astrocytes and neurons in our experiments. So far, I lack a solid strategy to calibrate *Pyronic*, why it could only be used qualitatively as a control construct for *Laconic*. However, the use of intravenous oxamate, which accumulates in astrocytes and neurons and is sensed by *Pyronic* might allow a one-point calibration of *Pyronic* via saturation.

Interestingly, astrocytic and neuronal glucose levels were much more dependent on blood glucose levels than on neuronal activity. This can be explained by nicely balanced cellular glucose uptake and consumption rates under physiological conditions. The pronounced glucose transients in astrocytes compared to neurons can be explained by a higher capacity of astrocytes to increase glucose uptake and consumption. Therefore, astrocytes are more exposed to larger glucose transients in conditions of increased neuronal energy needs or extreme blood glucose levels, placing the astrocytic compartment between the vascular and the neuronal compartment, as it has been suggested by the ANLS[18]. By partially outsourcing glycolysis to astrocytes and relying on their lactate production for energy supply, neurons can might prefer the pentose phosphate pathway for glucose to protect themselves from excessive metabolic stress during depolarization[156].

An activation of transport across the predominant astrocytic glucose transporter GLUT1 upon stimulation has been shown *in vitro*[150], while neuronal glucose transport during activation has been shown to be rather inhibited[157,158]. Furthermore, a limited importance of neuronal glucose transport can also be suggested by the absence of a phenotype when GLUT3 was decreased by half[159]. The hypothesis of neurons being incompetent to upregulate glycolytic activity is supported by findings of

constant degradation of 6-phosphofructo-2-kinase/ fructose-2, 6-bisphosphatase-3[160]. This enzyme generates fructose-2,6-bisphosphate which regulates the activity of 6-phosphofructo-1-kinase, a rate determining enzyme in glycolysis which is necessary to increase the activity of the glycolytic pathway. It has been suggested that neurons may profit from a shuttling of glucose towards the pentose phosphate pathway at the expense of its use in the glycolytic pathway for regeneration of reduced glutathione to decrease oxidative stress[156]. Correspondingly, the silencing of enzymes of the glycolytic cascade in astrocytes but not in neurons did affect survival and behavior of drosophila flies[161]. However, systemically supplied lactate has been shown to be able to prevent neuronal damage during hypoglycemia[154,162]. Accordingly, astrocytes possess unique cytoarchitectural and phenotypic features that predestine them to fulfill such a metabolic gatekeeper function[163,164].

Our results may also help for a better understanding of deoxyglucose-based approaches often used in humans such as positron emission tomography[165]. However, the preferential site of glucose metabolism cannot be resolved by radiotracer-based methods with their limited spatial resolution. Other available techniques to determine processes related to cerebral energy metabolism *in situ* such as NMR spectroscopy, functional MRI or the just recently introduced MR technique based on glucose chemical exchange saturation transfer lack cellular resolution and may profit from deeper single cell-based insights for proper interpretation[166,167].

In the present work, we observed higher glucose transients upon changes of blood glucose levels in astrocytes compared to neurons. The pronounced glucose uptake in astrocytes despite lower global energy requirements compared to neurons supports the shuttle concept of energy-rich substrates such as lactate between astrocytes and neurons. Consistently, we observed a higher resting level of lactate in astrocytes under resting conditions[168]. This lactate in astrocytes could constitute an energy reservoir for neurons[169]. Indeed we observed during increased neuronal activity an early dip of astrocytic lactate followed by a large increase of neuronal and astrocytic lactate, which could represent an increase of lactate transport followed by increased lactate production[47]. This increase of astrocytic lactate production could be induced by ammonium released by activated neurons, a mechanism that we could mimic by injecting ammonium chloride in living mice[94].

The brain is in a very specific metabolic state under the anaesthetic protocol used. Brain metabolism is known to depend on systemic metabolic states in the blood compartment and the neuronal activity state. Therefore, brain energy metabolism needs to be investigated at variable physiological and pathological vegetative, cognitive and systemic metabolic states. For example, we found a profound increase of cellular lactate concentrations under Isoflurane but not triple anaesthesia, which are probably different from awake metabolic states. We found only minor glucose and lactate changes in

the somatosensory cortex upon physiological peripheral stimulation. The reason might be that physiological stimuli induce neuronal activity only in a small fraction of the neurons in the corresponding layer 2/3 cortex. To measure fast and localized changes in metabolite levels, the simultaneous measurement of neuronal calcium using TPLSM to correlate electrical with metabolic cellular events is necessary and in theory possible. Alternatively, silicate windows with slits were evaluated to repetitively apply intracortical microelectrode stimulation, which induced large *Laconic*, *Pyronic* and *FLIPΔ6* transients. Specifically, microstimulation revealed the lactate surge as a potential vasodilator during increased neuronal activation and possibly also isoflurane anaesthesia. If lactate mediates the vasodilation and brain edema induced by isoflurane, this could be prevented by lactate dehydrogenase blockage. To investigate the effect of the main astrocytic connexins 30 and 43 on cellular lactate levels and transients as it was part of the initial thesis proposal, an inducible knockout would be favorable and is now under evaluation. Cortical glucose consumption rates are altered under multiple pathological conditions such as brain tumors (Warburg effect), ischemia or Alzheimer's disease so that information about altered cellular metabolite levels could help for a better understanding of these pathologies. Other cell types such as oligodendrocytes have impaired energy metabolism in pathologies such as neurodegeneration[170] and could be specifically targeted using the FRET sensors presented in this work. To read out metabolic rates rather than concentrations using FRET sensors, specific and fast interventions such as with the ITM are necessary. However, it was not possible to apply the necessary blockers intra-cortically in sufficient speed and dosages in the living mouse during TPLSM.

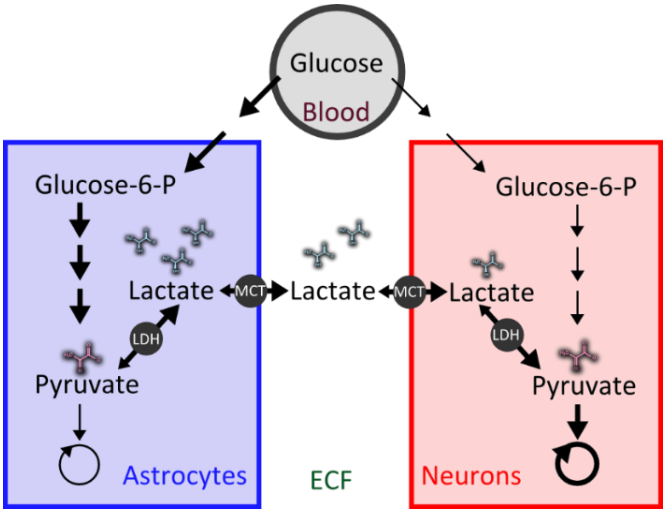

Figure i-9: Simplified ANLS model. A simplified model of brain energy metabolism with the compartments blood, extracellular space (ECF), astrocytes and neurons is given to illustrate the dependency of intercellular lactate flux from cellular lactate levels. In this thesis the levels of the key substrates glucose, lactate and pyruvate where investigated in astrocytes and neurons and glucose and lactate was also assessed in the blood and ECF compartments.

In summary, the possibilities and limitation of *in vivo* metabolic FRET imaging using TPLSM on cellular level are demonstrated in this work. Specifically, differences of glucose and lactate transients between the astrocytic and neuronal compartment provided *in vivo* evidence for the existence of an ANLS (Figure i-9). The methodology holds the potential of increased spatial, temporal and qualitative read-outs, which might further enlighten the role of metabolic signaling of varying brain states, brain regions, cellular compartments and pathologies.

Acknowledgements

I would like to thank the supervisor of my thesis Prof. Dr. Bruno Weber for giving me the opportunity to do a MD-PhD thesis at his laboratory and the continuous support throughout my project in various matters from writing program codes up to writing papers. I profited a lot from the profound technical know-how and the large investments in laboratory equipment during my projects. I am especially grateful for the opportunities to present my work to an international scientific community and becoming part of longstanding and productive collaborations.

Special thanks go to PD Dr. Dr. med. Matthias Wyss, who supported me in all aspects of my thesis including teaching me various methods, organizing experiments, preparing protocols, discussing results, reviewing documents and much more. His great experience kept the laboratory and my project running on every day matters and throughout big moves.

I would like to thank the members of my steering committee Prof. Dr. Markus Rudin and Prof. Dr. med. Alfred Buck for the productive progress meetings and for the scientific advice provided. I also thank Prof. Dr. med. Jürg Hodler for generously supporting my MD/PhD-application.

I thank Prof. Felipe Barros for providing essential plasmids and ideas for this work and the continuous scientific support and his hospitality in his laboratory in beautiful Valdivia, Chile. I also thank Prof. Dr. med. Pierre Magistretti for his constructive collaboration and feedback.

I would like to thank Prof. Jean-Marc Fritschy for his teaching and the opportunity to perform experiments in his laboratory.

I thank Dr. Maha Elsayed and Dr. Tina Notter for their extensive help with the Pinnacle biosensors and the immunohistochemistry, respectively.

I thank the master students Vincens Kälin and Alexandra von Faber-Castell for sharing their enthusiasm for our projects.

I thank Robin Gutierrez and Jill Stobart for being great colleagues, sharing their profound knowledge and contributing extensively to my projects. Special thanks also deserves the always kind, inspiring and supportive colleagues Novella, Johannes, Vida, Anand, Marc, Tilo, Geoff, Ladina, Max, Kim, Chaim, Johanna, Cari, Matthew, Aiman, Guillaume, Zoe, Inma and Anita.

I thank all my friends for their encouraging interest in my research and my family for supporting my education. I thank Prof. Dr. Sébastien Gagneux and Dr. Claudia Daubenberger at the Swiss Tropical and

Public Health Institute for giving me the opportunity to do my civilian service in great scientific and personal environments.

A thank beyond imagination goes to Federica for everything.

I am very grateful for financial support received from the Swiss National Science Foundation (SNSF, MD-PhD-Grant) and the Neuroscience Center Zurich (ZNZ, congress participation fees).

Curriculum vitae

Name	Philipp Mächler
Geburtsdatum:	20. Januar 1986
Bürgerort:	Zürich
Nationalität:	Schweiz

Ausbildung:

2011-2015	MD-PhD-Programm Zürich (Prof. Weber, Institut für Pharmakologie und Toxikologie Universität Zürich)
2010	Eidgenössisches Staatsexamen
2004 – 2010	Humanmedizin-Studium an der Universität Zürich und Université Catholique de Lille
2006 – 2009	Dissertation an der Klinik für Unfallchirurgie, Universität Zürich
2007	Aufnahme in die Schweizerische Studienstiftung
2004	Maturität MAR (Latein, Englisch und Physik)
1998 – 2004	Kantonsschule Realgymnasium Rämibühl Zürich
1992 – 1998	Primarschule in Erlenbach

Publications in peer reviewed journals

Mächler, P., Wyss, M.T., Elsayed, M., Stobart, J., Gutierrez, R., von Faber-Castell, A., Kaelin, V., Zuend, M., San Martín, A., Romero-Gómez, I., et al. **In Vivo Evidence for a Lactate Gradient from Astrocytes to Neurons.** Cell Metabolism, *in press*.

Mächler P., Wyss M.T., Zuend M., Gutierrez R., Lengacher S., Schneider B. , Magistretti P.J. , Barros F.L., Weber B. **Pronounced glucose dynamics in astrocytes compared to neurons.** *In preparation for J Neurosci.*

Sotelo-Hitschfeld, T., Niemeyer, M.I., Mächler, P., Ruminot, I., Lerchundi, R., Wyss, M.T., Stobart, J., Fernández-Moncada, I., Valdebenito, R., Garrido-Gerter, P., et al. (2015). **Channel-Mediated Lactate Release by K+-Stimulated Astrocytes.** J. Neurosci. *35*, 4168–4178.[47]

Lerchundi, R., Fernández-Moncada, I., Contreras-Baeza, Y., Sotelo-Hitschfeld, T., Mächler, P., Wyss, M.T., Stobart, J., Baeza-Lehnert, F., Alegría, K., Weber, B., et al. (2015). **NH4+ triggers the release of astrocytic lactate via mitochondrial pyruvate shunting.** PNAS 201508259.[94]

Mayrhofer, J.M., Haiss, F., Haenni, D., Weber, S., Zuend, M., Barrett, M.J.P., Ferrari, K.D., Maechler, P., Saab, A.S., Stobart, J.L., et al. (2015). **Design and performance of an ultra-flexible two-photon microscope for in vivo research.** Biomed. Opt. Express, BOE *6*, 4228–4237.

Posters and Talks

ZNZ Ph.D. Retreat 2011, Valens, Switzerland: Single cell investigation of brain glucose metabolism *in vivo*.

MD-PhD/-MSc retreat 2011, Wislikofen, Switzerland: The Neuroenergetic Role of Astrocytic Networks.

NCCR Neuro Concluding Symposium and ZNZ Annual Symposium 2012, Zurich, Switzerland: Single cell investigation of brain glucose metabolism *in vivo*. Mächler P., Wyss M.T., Zünd M., Lengacher S., Magistretti P.J., Barros F., Weber B.

Pharmacology & Toxicology Poster Day 2012, Zurich, Switzerland: *In vivo* imaging of glucose metabolism in single astrocytes using a genetically encoded FRET-nanosensor. Mächler P., Wyss M.T., Zünd M., Lengacher S., Magistretti PJ., Barros F., Weber B

MD-PhD/-MSc retreat 2012, Richisau, Switzerland: The Neuroenergetic Role of Astrocytic Networks.

Swiss Society for Neuroscience **symposium 2012**, Zurich, Switzerland: *In vivo* two-photon imaging of cerebral energy metabolism: Cellular compartmentation. Wyss M.T., Mächler P., Barros F., Magistretti P.J., Weber B.

Swiss Society for Neuroscience **symposium 2013**, Geneva, Switzerland: Investigating astrocytic and neuronal glucose concentration on the single cell level using novel FRET nanosensors. Mächler P., Wyss M.T., Gutierrez R., Zünd M., Lengacher S., Barros F., Weber B.

IBRO College 2013, Valdivia, Chile: Intrinsic optical imaging (IOI) and laser speckle imaging (LSI) in anaesthetized mice during neuronal stimulation.

Pharmacology Progress report seminar 12/3/2013, Zurich, Switzerland: FRET Sensors for Glucose and Lactate *in vivo.*

XI European Meeting on Glial Cells in Health and Disease 2013, Berlin, Germany: Estimation of glycolytic rates of single cells *in vivo.* Philipp Mächler, Matthias T. Wyss, Robin Gutierrez, Marc Zünd, Sylvain Lengacher, Bernard Schneider, Pierre Magistretti, Felipe Barros, Bruno Weber

European Molecular Imaging Meeting 2013, Turin, Italy: Two-photon imaging of single cell cerebral glucose concentration: Brain state dependence. Philipp Mächler, Matthias T. Wyss, Marc Zünd, Robin Gutierrez, Sylvain Lengacher, Bernard Schneider, Pierre Magistretti, Felipe Barros, Bruno Weber

Annual meeting of the Swiss Society of Neurosciences 2013, Geneva, Switzerland: Investigating astrocytic and neuronal glucose concentration on the single cell level using novel FRET nanosensors. Mächler P., Wyss M.T., Gutierrez R., Zünd M., Lengacher S., Barros F., Weber B.

ZNZ Annual Symposium 2013, Zurich, Switzerland: Estimation of glucose levels of single cells *in vivo*. Gutierrez R., Wyss M.T., Mächler P., Lengacher S., Magistretti P.J., Barros F., Weber B.

ICBEM International Conference on Brain Energy Metabolism 2014, Copenhagen, Denmark: Astrocyte - Neuron Lactate Gradient *in vivo*. Philipp Mächler, Matthias T. Wyss, Robin Gutierrez, Maha Elsayed, Sylvain Lengacher, Pierre Magistretti, Felipe Barros, Bruno Weber

International Astrocyte Meeting 1.-3.10.2014, Paris, France: Astrocyte-Neuron Lactate Gradient *in vivo.* Philipp Mächler, Matthias Wyss, Robin Gutierrez, Marc Zünd, Jillian Stobart, Sylvain Lengacher, Bernard Schneider, Pierre J Magistretti, Felipe Barros, Bruno Weber

European MD/PhD Meeting 2014, 11.-13.7.2014, Brunnen, Switzerland: Investigating astrocytic and neuronal glucose concentration on the single cell level using novel FRET nanosensors. Mächler P., Wyss M.T., Gutierrez R., Zünd M., Lengacher S., Barros F., Weber B.

Neuroscience Center Zurich *Symposium 2014*, 11.9.2014, Zurich, Switzerland: Astrocyte-neuron lactate gradient *in vivo*. Philipp Mächler, Matthias Wyss, R. Gutierrez, Sylvain Lengacher, Pierre J Magistretti, Felipe Barros, Bruno Weber

Pharmacology & Toxicology Poster Day 2014, 8.9.2014, Zurich, Switzerland: Astrocyte-Neuron Lactate Gradient *in vivo.* Philipp Mächler, Matthias Wyss, Robin Gutierrez, Marc Zünd, Jillian Stobart, Sylvain Lengacher, Pierre J Magistretti, Felipe Barros, Bruno Weber

Gordon Research Seminar Glial Biology, 28.2.2015 - 1.3.2015, Ventura CA, United States: *In vivo* evidence for compartmentalized brain lactate levels. Philipp Maechler, Matthias T. Wyss, Robin Gutierrez, Maha Elsayed, Jillian Stobart, Marc Zuend, Sylvain Lengacher, Bernard Schneider, Pierre Magistretti, Felipe Barros, Bruno Weber

Gordon Research Conference Glial Biology, 1.3.2015 – 6.3.2015, Ventura CA, United States: *In vivo* evidence for compartmentalized brain lactate levels. Philipp Maechler, Matthias T. Wyss, Robin Gutierrez, Maha Elsayed, Jillian Stobart, Marc Zuend, Sylvain Lengacher, Bernard Schneider, Pierre Magistretti, Felipe Barros, Bruno Weber

Neuroscience Center Zurich *Symposium 2015*, 11.9.2015, Zurich, Switzerland: Two-photon imaging of brain energy metabolites during cortical microstimulation. Philipp Mächler, Matthias Wyss, Jillian Stobart, Marc Zuend, Sylvain Lengacher, Bernard Schneider, Pierre Magistretti, Felipe Barros, Bruno Weber

Awards

SNF-Stipendium (MD-PhD-Programm)

Travel award and presentation of selected poster, ICBEM 2014, Copenhagen, Denmark

Best Poster Award (2014) European MD/PhD Meeting , Brunnen SZ, Switzerland

Poster Award (2014) Pharmacology & Toxicology POSTER DAY, Zürich Switzerland

References

1. Magistretti, P. J. in *In Fundamental Neuroscience* pp. 389–413 (San Diego: Academic Press, 1999).
2. Attwell, D. & Laughlin, S. B. An Energy Budget for Signaling in the Grey Matter of the Brain. *J. Cereb. Blood Flow Metab.* **21,** 1133–1145 (2001).
3. Virchow, R. L. K. *Die Cellularpathologie in ihrer Begründung auf physiologische und pathologische Gewebelehre*. (A. Hirschwald, 1859).
4. Lenhossék, M. *Der feinere Bau des Nervensystems: im Lichte neuester Forschungen*. (Fischer, 1893).
5. Kettenmann, H. & Verkhratsky, A. Neuroglia: the 150 years after. *Trends Neurosci.* **31,** 653–659 (2008).
6. Von Kölliker, A. Handbuch der Gewebelehre des Menschen. 6. Umgearbeitere Auflage. Erster Band: Die allgemeine Gewebelehre und die Systems der Haut, Knochen und Muskeln. *Leipz. Wilhelm Engelmann* (1889).
7. Andriezen, W. L. The Neuroglia Elements in the Human Brain. *Br. Med. J.* **2,** 227–230 (1893).
8. Iadecola, C. & Nedergaard, M. Glial regulation of the cerebral microvasculature. *Nat. Neurosci.* **10,** 1369–1376 (2007).
9. Oberheim, N. A. *et al.* Uniquely Hominid Features of Adult Human Astrocytes. *J. Neurosci.* **29,** 3276–3287 (2009).
10. Nedergaard, M., Ransom, B. & Goldman, S. A. New roles for astrocytes: Redefining the functional architecture of the brain. *Trends Neurosci.* **26,** 523–530 (2003).
11. Allaman, I., Bélanger, M. & Magistretti, P. J. Astrocyte-neuron metabolic relationships: for better and for worse. *Trends Neurosci.* **34,** 76–87 (2011).
12. Hawkins, R. A., Miller, A. L., Nielsen, R. C. & Veech, R. L. The acute action of ammonia on rat brain metabolism in vivo. *Biochem. J.* **134,** 1001–1008 (1973).

13. Ott, P. & Vilstrup, H. Cerebral effects of ammonia in liver disease: current hypotheses. *Metab. Brain Dis.* **29,** 901–911 (2014).

14. Stobart, J. L. & Anderson, C. M. Multifunctional role of astrocytes as gatekeepers of neuronal energy supply. *Front. Cell. Neurosci.* **7,** (2013).

15. Koehler, R. C., Roman, R. J. & Harder, D. R. Astrocytes and the regulation of cerebral blood flow. *Trends Neurosci.* **32,** 160–169 (2009).

16. Ogawa, S., Lee, T. M., Kay, A. R. & Tank, D. W. Brain magnetic resonance imaging with contrast dependent on blood oxygenation. *Proc. Natl. Acad. Sci. U. S. A.* **87,** 9868 –9872 (1990).

17. Kwong, K. K. *et al.* Dynamic magnetic resonance imaging of human brain activity during primary sensory stimulation. *Proc. Natl. Acad. Sci. U. S. A.* **89,** 5675 –5679 (1992).

18. Magistretti, P. J. Neuroscience: Energy on Demand. *Science* **283,** 496–497 (1999).

19. Nordberg, A., Rinne, J. O., Kadir, A. & Långström, B. The use of PET in Alzheimer disease. *Nat. Rev. Neurol.* **6,** 78–87 (2010).

20. Warburg, O. & others. On the origin of cancer cells. *Science* **123,** 309–314 (1956).

21. Feron, O. Pyruvate into lactate and back: From the Warburg effect to symbiotic energy fuel exchange in cancer cells. *Radiother. Oncol.* **92,** 329–333 (2009).

22. Matyash, V. & Kettenmann, H. Heterogeneity in astrocyte morphology and physiology. *Brain Res. Rev.* **63,** 2–10 (2010).

23. Zhang, Y. & Barres, B. A. Astrocyte heterogeneity: an underappreciated topic in neurobiology. *Curr. Opin. Neurobiol.* **20,** 588–594 (2010).

24. Halassa, M. M., Fellin, T., Takano, H., Dong, J.-H. & Haydon, P. G. Synaptic Islands Defined by the Territory of a Single Astrocyte. *J. Neurosci.* **27,** 6473–6477 (2007).

25. Bushong, E. A., Martone, M. E., Jones, Y. Z. & Ellisman, M. H. Protoplasmic Astrocytes in CA1 Stratum Radiatum Occupy Separate Anatomical Domains. *J. Neurosci.* **22,** 183–192 (2002).

26. Diamond, M. E., von Heimendahl, M., Knutsen, P. M., Kleinfeld, D. & Ahissar, E. 'Where' and 'what' in the whisker sensorimotor system. *Nat. Rev. Neurosci.* **9,** 601–612 (2008).

27. Houades, V., Koulakoff, A., Ezan, P., Seif, I. & Giaume, C. Gap Junction-Mediated Astrocytic Networks in the Mouse Barrel Cortex. *J. Neurosci.* **28,** 5207–5217 (2008).

28. Logothetis, N. K. What we can do and what we cannot do with fMRI. *Nature* **453,** 869–878 (2008).

29. Mathiisen, T. M., Lehre, K. P., Danbolt, N. C. & Ottersen, O. P. The perivascular astroglial sheath provides a complete covering of the brain microvessels: An electron microscopic 3D reconstruction. *Glia* **58,** 1094–1103 (2010).

30. Zonta, M. *et al.* Neuron-to-astrocyte signaling is central to the dynamic control of brain microcirculation. *Nat. Neurosci.* **6,** 43–50 (2002).

31. Gordon, G. R. J., Choi, H. B., Rungta, R. L., Ellis-Davies, G. C. R. & MacVicar, B. A. Brain metabolism dictates the polarity of astrocyte control over arterioles. *Nature* **456,** 745–749 (2008).

32. Haydon, P. G. & Carmignoto, G. Astrocyte Control of Synaptic Transmission and Neurovascular Coupling. *Physiol Rev* **86,** 1009–1031 (2006).

33. Rouach, N. *et al.* Gap junctions and connexin expression in the normal and pathological central nervous system. *Biol. Cell* **94,** 457–475 (2002).

34. Giaume, C., Koulakoff, A., Roux, L., Holcman, D. & Rouach, N. Astroglial networks: a step further in neuroglial and gliovascular interactions. *Nat Rev Neurosci* **11,** 87–99 (2010).

35. Rouach, N., Koulakoff, A., Abudara, V., Willecke, K. & Giaume, C. Astroglial Metabolic Networks Sustain Hippocampal Synaptic Transmission. *Science* **322,** 1551–1555 (2008).

36. Zlokovic, B. V. The Blood-Brain Barrier in Health and Chronic Neurodegenerative Disorders. *Neuron* **57,** 178–201 (2008).

37. Pardridge, W. M. & Oldendorf, W. H. Transport of Metabolic Substrates Through the Blood-Brain Barrier1. *J. Neurochem.* **28,** 5–12 (1977).

38. Martinez-Hernandez, A., Bell, K. P. & Norenberg, M. D. Glutamine Synthetase: Glial Localization in Brain. *Science* **195,** 1356–1358 (1977).

39. Van den Berg, C. J., Krzalić, L., Mela, P. & Waelsch, H. Compartmentation of glutamate metabolism in brain. Evidence for the existence of two different tricarboxylic acid cycles in brain. *Biochem. J.* **113,** 281–290 (1969).

40. Hertz, L. Functional interactions between neurons and astrocytes I. Turnover and metabolism of putative amino acid transmitters. *Prog. Neurobiol.* **13,** 277–323 (1979).

41. Pellerin, L. & Magistretti, P. J. Glutamate uptake into astrocytes stimulates aerobic glycolysis: a mechanism coupling neuronal activity to glucose utilization. *Proc. Natl. Acad. Sci. U. S. A.* **91,** 10625 –10629 (1994).

42. Pellerin, L. & Magistretti, P. J. Sweet sixteen for ANLS. *J. Cereb. Blood Flow Metab.* (2011). doi:10.1038/jcbfm.2011.149

43. Dienel, G. A. The metabolic trinity, glucose–glycogen–lactate, links astrocytes and neurons in brain energetics, signaling, memory, and gene expression. *Neurosci. Lett.* doi:10.1016/j.neulet.2015.02.052

44. Lundgaard, I. *et al.* Direct neuronal glucose uptake heralds activity-dependent increases in cerebral metabolism. *Nat. Commun.* **6,** (2015).

45. Barros, L. F. & Deitmer, J. W. Glucose and lactate supply to the synapse. *Brain Res. Rev.* **63,** 149–159 (2010).

46. Cerdán, S. *et al.* The redox switch/redox coupling hypothesis. *Neurochem. Int.* **48,** 523–530 (2006).

47. Sotelo-Hitschfeld, T. *et al.* Channel-Mediated Lactate Release by K+-Stimulated Astrocytes. *J. Neurosci.* **35,** 4168–4178 (2015).

48. Howarth, C., Gleeson, P. & Attwell, D. Updated energy budgets for neural computation in the neocortex and cerebellum. *J. Cereb. Blood Flow Metab.* **32,** 1222–1232 (2012).

49. Lennie, P. The Cost of Cortical Computation. *Curr. Biol.* **13,** 493–497 (2003).

50. Brown, A. M. & Ransom, B. R. Astrocyte glycogen as an emergency fuel under conditions of glucose deprivation or intense neural activity. *Metab. Brain Dis.* **30,** 233–239 (2014).

51. Attwood, P. V. & Cleland, W. W. Decarboxylation of oxalacetate by pyruvate carboxylase. *Biochemistry (Mosc.)* **25,** 8191–8196 (1986).

52. Duelli, R. & Kuschinsky, W. Brain Glucose Transporters: Relationship to Local Energy Demand. *Physiology* **16,** 71–76 (2001).

53. Barros, L. F., Bittner, C. X., Loaiza, A. & Porras, O. H. A quantitative overview of glucose dynamics in the gliovascular unit. *Glia* **55,** 1222–1237 (2007).

54. McEwen, B. S. & Reagan, L. P. Glucose transporter expression in the central nervous system: relationship to synaptic function. *Eur. J. Pharmacol.* **490,** 13–24 (2004).

55. Vannucci, S. J., Maher, F. & Simpson, I. A. Glucose transporter proteins in brain: Delivery of glucose to neurons and glia. *Glia* **21,** 2–21 (1997).

56. Brown, A. M. & Ransom, B. R. Astrocyte glycogen and brain energy metabolism. *Glia* **55,** 1263–1271 (2007).

57. Oz, G. *et al.* Human brain glycogen content and metabolism: implications on its role in brain energy metabolism. *Am J Physiol Endocrinol Metab* **292,** E946–951 (2007).

58. Brekke, E., Morken, T. S. & Sonnewald, U. Glucose metabolism and astrocyte–neuron interactions in the neonatal brain. *Neurochem. Int.* **82,** 33–41 (2015).

59. Hertz, L. Intercellular metabolic compartmentation in the brain: past, present and future. *Neurochem. Int.* **45,** 285–296 (2004).

60. Loaiza, A., Porras, O. H. & Barros, L. F. Glutamate Triggers Rapid Glucose Transport Stimulation in Astrocytes as Evidenced by Real-Time Confocal Microscopy. *J. Neurosci.* **23,** 7337–7342 (2003).

61. Bittner, C. X. *et al.* Fast and Reversible Stimulation of Astrocytic Glycolysis by K+ and a Delayed and Persistent Effect of Glutamate. *J. Neurosci.* **31,** 4709–4713 (2011).

62. Sibson, N. R. *et al.* Stoichiometric coupling of brain glucose metabolism and glutamatergic neuronal activity. *Proc. Natl. Acad. Sci.* **95,** 316–321 (1998).

63. Ruminot, I. *et al.* NBCe1 Mediates the Acute Stimulation of Astrocytic Glycolysis by Extracellular K+. *J. Neurosci.* **31,** 14264–14271 (2011).

64. Sotelo-Hitschfeld, T., FernáNdez-Moncada, I. & Barros, L. F. Acute feedback control of astrocytic glycolysis by lactate. *Glia* **60,** 674–680 (2012).

65. Chang, D. T. W., Honick, A. S. & Reynolds, I. J. Mitochondrial Trafficking to Synapses in Cultured Primary Cortical Neurons. *J. Neurosci.* **26,** 7035–7045 (2006).

66. Wong-Riley, M. T. T. Cytochrome oxidase: an endogenous metabolic marker for neuronal activity. *Trends Neurosci.* **12,** 94–101 (1989).

67. Gonzalez, S. V., Nguyen, N. H. T., Rise, F. & Hassel, B. Brain metabolism of exogenous pyruvate. *J. Neurochem.* **95,** 284–293 (2005).

68. Sada, N., Lee, S., Katsu, T., Otsuki, T. & Inoue, T. Targeting LDH enzymes with a stiripentol analog to treat epilepsy. *Science* **347,** 1362–1367 (2015).

69. Williamson, D. H., Lund, P. & Krebs, H. A. The redox state of free nicotinamide-adenine dinucleotide in the cytoplasm and mitochondria of rat liver. *Biochem. J.* **103,** 514–527 (1967).

70. Winkler, U. & Hirrlinger, J. Crosstalk of Signaling and Metabolism Mediated by the NAD+/NADH Redox State in Brain Cells. *Neurochem. Res.* 1–8 (2015). doi:10.1007/s11064-015-1526-0

71. Glancy, B. & Balaban, R. S. Role of Mitochondrial Ca2+ in the Regulation of Cellular Energetics. *Biochemistry (Mosc.)* **51,** 2959–2973 (2012).

72. Kasischke, K. A., Vishwasrao, H. D., Fisher, P. J., Zipfel, W. R. & Webb, W. W. Neural Activity Triggers Neuronal Oxidative Metabolism Followed by Astrocytic Glycolysis. *Science* **305,** 99–103 (2004).

73. Bittar, P. G., Charnay, Y., Pellerin, L., Bouras, C. & Magistretti, P. J. Selective Distribution of Lactate Dehydrogenase Isoenzymes in Neurons and Astrocytes of Human Brain. *J. Cereb. Blood Flow Metab.* **16,** 1079–1089 (1996).

74. Vesell, E. S. pH Dependence of Lactate Dehydrogenase Isozyme Inhibition by Substrate. *Nature* **210,** 421–422 (1966).

75. Chesler, M. & Kraig, R. P. Intracellular pH transients of mammalian astrocytes. *J. Neurosci.* **9,** 2011–2019 (1989).

76. O'Brien, J., Kla, K. M., Hopkins, I. B., Malecki, E. A. & McKenna, M. C. Kinetic Parameters and Lactate Dehydrogenase Isozyme Activities Support Possible Lactate Utilization by Neurons. *Neurochem. Res.* **32,** 597–607 (2006).

77. van Hall, G. *et al.* Blood lactate is an important energy source for the human brain. *J. Cereb. Blood Flow Metab.* **29,** 1121–1129 (2009).

78. Dienel, G. A. Brain lactate metabolism: the discoveries and the controversies. *J. Cereb. Blood Flow Metab.* **32,** 1107–1138 (2012).

79. Rasmussen, P., Wyss, M. T. & Lundby, C. Cerebral glucose and lactate consumption during cerebral activation by physical activity in humans. *FASEB J.* **25,** 2865–2873 (2011).

80. Quistorff, B., Secher, N. H. & Lieshout, J. J. V. Lactate fuels the human brain during exercise. *FASEB J.* **22,** 3443–3449 (2008).

81. Abi-Saab, W. M. *et al.* Striking Differences in Glucose and Lactate Levels Between Brain Extracellular Fluid and Plasma in Conscious Human Subjects: Effects of Hyperglycemia and Hypoglycemia. *J. Cereb. Blood Flow Metab.* **22,** 271–279 (2002).

82. Brooks, G. A. Cell–cell and intracellular lactate shuttles. *J. Physiol.* **587,** 5591–5600 (2009).

83. Swanson, R. A. & Benington, J. H. Astrocyte Glucose Metabolism under Normal and Pathological Conditions in vitro. *Dev. Neurosci.* **18,** 515–521 (1996).

84. Sickmann, H. M., Schousboe, A., Fosgerau, K. & Waagepetersen, H. S. Compartmentation of Lactate Originating from Glycogen and Glucose in Cultured Astrocytes. *Neurochem. Res.* **30,** 1295–1304 (2005).

85. Brooks, G. A. Lactate shuttles in Nature. *Biochem. Soc. Trans.* **30,** 258 (2001).

86. Pierre, K. & Pellerin, L. Monocarboxylate transporters in the central nervous system: distribution, regulation and function. *J. Neurochem.* **94,** 1–14 (2005).

87. Chiry, O. *et al.* Distribution of the monocarboxylate transporter MCT2 in human cerebral cortex: An immunohistochemical study. *Brain Res.* **1226,** 61–69 (2008).

88. Bergersen, L. H. Is lactate food for neurons? Comparison of monocarboxylate transporter subtypes in brain and muscle. *Neuroscience* **145,** 11–19 (2007).

89. Fishbein, W. N., Foellmer, J. W., Davis, J. I., Fishbein, T. M. & Armbrustmacher, P. Clinical assay of the human erythrocyte lactate transporter: I. Principles, procedure, and validation. *Biochem. Med. Metab. Biol.* **39,** 338–350 (1988).

90. Halestrap, A. P. Monocarboxylic acid transport. *Compr. Physiol.* **3,** 1611–1643 (2013).

91. Pellerin, L. *et al.* Activity-dependent regulation of energy metabolism by astrocytes: An update. *Glia* **55,** 1251–1262 (2007).

92. Nilsson, P., Hillered, L., Pontén, U. & Ungerstedt, U. Changes in Cortical Extracellular Levels of Energy-Related Metabolites and Amino Acids Following Concussive Brain Injury in Rats. *J. Cereb. Blood Flow Metab.* **10,** 631–637 (1990).

93. Choi, H. B. *et al.* Metabolic Communication between Astrocytes and Neurons via Bicarbonate-Responsive Soluble Adenylyl Cyclase. *Neuron* **75,** 1094–1104 (2012).

94. Lerchundi, R. *et al.* NH4+ triggers the release of astrocytic lactate via mitochondrial pyruvate shunting. *Proc. Natl. Acad. Sci.* 201508259 (2015). doi:10.1073/pnas.1508259112

95. Provent, P. *et al.* The ammonium-induced increase in rat brain lactate concentration is rapid and reversible and is compatible with trafficking and signaling roles for ammonium. *J. Cereb. Blood Flow Metab.* **27,** 1830–1840 (2007).

96. Bosoi, C. R. *et al.* Increased brain lactate is central to the development of brain edema in rats with chronic liver disease. *J. Hepatol.* **60,** 554–560 (2014).

97. Perea, G., Navarrete, M. & Araque, A. Tripartite synapses: astrocytes process and control synaptic information. *Trends Neurosci.* **32,** 421–431 (2009).

98. Barros, L. F. Metabolic signaling by lactate in the brain. *Trends Neurosci.* **36,** 396–404 (2013).

99. Bergersen, L. H. & Gjedde, A. Is lactate a volume transmitter of metabolic states of the brain? *Front. Neuroenergetics* **4,** (2012).

100. Tang, F. *et al.* Lactate-mediated glia-neuronal signalling in the mammalian brain. *Nat. Commun.* **5,** (2014).

101. Borg, M. A., Sherwin, R. S., Borg, W. P., Tamborlane, W. V. & Shulman, G. I. Local ventromedial hypothalamus glucose perfusion blocks counterregulation during systemic hypoglycemia in awake rats. *J. Clin. Invest.* **99,** 361–365 (1997).

102. Borg, M. A., Tamborlane, W. V., Shulman, G. I. & Sherwin, R. S. Local Lactate Perfusion of the Ventromedial Hypothalamus Suppresses Hypoglycemic Counterregulation. *Diabetes* **52,** 663–666 (2003).

103. Suzuki, A. *et al.* Astrocyte-Neuron Lactate Transport Is Required for Long-Term Memory Formation. *Cell* **144,** 810–823 (2011).

104. Mosienko, V., Teschemacher, A. G. & Kasparov, S. Is L-lactate a novel signaling molecule in the brain? *J. Cereb. Blood Flow Metab.* **35,** 1069–1075 (2015).

105. Angelova, P. R. *et al.* Functional Oxygen Sensitivity of Astrocytes. *J. Neurosci.* **35,** 10460–10473 (2015).

106. Calcinaghi, N. *et al.* Multimodal Imaging in Rats Reveals Impaired Neurovascular Coupling in Sustained Hypertension. *Stroke* (2013). doi:10.1161/STROKEAHA.111.000185

107. Hu, Y. & Wilson, G. S. Rapid Changes in Local Extracellular Rat Brain Glucose Observed with an In Vivo Glucose Sensor. *J. Neurochem.* **68,** 1745–1752 (1997).

108. Hu, Y. & Wilson, G. S. A Temporary Local Energy Pool Coupled to Neuronal Activity: Fluctuations of Extracellular Lactate Levels in Rat Brain Monitored with Rapid-Response Enzyme-Based Sensor. *J. Neurochem.* **69,** 1484–1490 (1997).

109. Helmchen, F. & Denk, W. Deep tissue two-photon microscopy. *Nat. Methods* **2,** 932–940 (2005).

110. Göppert-Mayer, M. Über Elementarakte mit zwei Quantensprüngen. *Ann. Phys.* **401,** 273–294 (1931).

111. Denk, W., Strickler, J. H. & Webb, W. W. Two-photon laser scanning fluorescence microscopy. *Science* **248,** 73–76 (1990).

112. Langer, D. *et al.* HelioScan: A software framework for controlling in vivo microscopy setups with high hardware flexibility, functional diversity and extendibility. *J. Neurosci. Methods* **215,** 38–52 (2013).

113. Mayrhofer, J. M. *et al.* Design and performance of an ultra-flexible two-photon microscope for in vivo research. *Biomed. Opt. Express* **6,** 4228–4237 (2015).

114. Pologruto, T. A., Sabatini, B. L. & Svoboda, K. ScanImage: Flexible software for operating laser scanning microscopes. *Biomed. Eng. OnLine* **2,** 13 (2003).

115. Holtmaat, A. *et al.* Long-term, high-resolution imaging in the mouse neocortex through a chronic cranial window. *Nat. Protoc.* **4,** 1128–1144 (2009).

116. Xu, C., Williams, R. M., Zipfel, W. & Webb, W. W. Multiphoton excitation cross-sections of molecular fluorophores. *Bioimaging* **4,** 198–207 (1996).

117. Nimmerjahn, A. & Helmchen, F. In Vivo Labeling of Cortical Astrocytes with Sulforhodamine 101 (SR101). *Cold Spring Harb. Protoc.* **2012,** pdb.prot068155 (2012).

118. Deuschle, K. *et al.* Construction and optimization of a family of genetically encoded metabolite sensors by semirational protein engineering. *Protein Sci.* **14,** 2304–2314 (2005).

119. Deuschle, K. *et al.* Genetically encoded sensors for metabolites. *Cytometry A* **64A,** 3–9 (2005).

120. Stosiek, C., Garaschuk, O., Holthoff, K. & Konnerth, A. In Vivo Two-Photon Calcium Imaging of Neuronal Networks. *Proc. Natl. Acad. Sci.* **100,** 7319–7324 (2003).

121. Mayrhofer, J. M., Haiss, F., Helmchen, F. & Weber, B. Sparse, reliable, and long-term stable representation of periodic whisker deflections in the mouse barrel cortex. *NeuroImage* **115,** 52–63 (2015).

122. Fehr, M., Lalonde, S., Lager, I., Wolff, M. W. & Frommer, W. B. In vivo imaging of the dynamics of glucose uptake in the cytosol of COS-7 cells by fluorescent nanosensors. *J. Biol. Chem.* **278,** 19127–19133 (2003).

123. Hou, B.-H. *et al.* Optical sensors for monitoring dynamic changes of intracellular metabolite levels in mammalian cells. *Nat. Protoc.* **6,** 1818–1833 (2011).

124. Takanaga, H., Chaudhuri, B. & Frommer, W. B. GLUT1 and GLUT9 as major contributors to glucose influx in HepG2 cells identified by a high sensitivity intramolecular FRET glucose sensor. *Biochim. Biophys. Acta BBA - Biomembr.* **1778,** 1091–1099 (2008).

125. Bittner, C. X. High resolution measurement of the glycolytic rate. *Front. Neuroenergetics* **2,** (2010).

126. John, S., Ottolia, M., Weiss, J. & Ribalet, B. Dynamic modulation of intracellular glucose imaged in single cells using a FRET-based glucose nanosensor. *Pflüg. Arch. Eur. J. Physiol.* **456,** 307–322 (2008).

127. Hung, Y. P., Albeck, J. G., Tantama, M. & Yellen, G. Imaging Cytosolic NADH-NAD+ Redox State with a Genetically Encoded Fluorescent Biosensor. *Cell Metab.* **14,** 545–554 (2011).

128. Okumoto, S. *et al.* Detection of glutamate release from neurons by genetically encoded surface-displayed FRET nanosensors. *Proc. Natl. Acad. Sci. U. S. A.* **102,** 8740–8745 (2005).

129. Gruenwald, K. *et al.* Visualization of glutamine transporter activities in living cells using genetically encoded glutamine sensors. *PloS One* **7,** e38591 (2012).

130. San Martín, A. *et al.* A Genetically Encoded FRET Lactate Sensor and Its Use To Detect the Warburg Effect in Single Cancer Cells. *PLoS ONE* **8,** e57712 (2013).

131. San Martín, A. *et al.* Imaging Mitochondrial Flux in Single Cells with a FRET Sensor for Pyruvate. *PLoS ONE* **9,** e85780 (2014).

132. Lee, Y., Messing, A., Su, M. & Brenner, M. GFAP promoter elements required for region-specific and astrocyte-specific expression. *Glia* **56,** 481–493 (2008).

133. Glover, C. P. J., Bienemann, A. S., Heywood, D. J., Cosgrave, A. S. & Uney, J. B. Adenoviral-Mediated, High-Level, Cell-Specific Transgene Expression: A SYN1-WPRE Cassette Mediates Increased Transgene Expression with No Loss of Neuron Specificity. *Mol. Ther.* **5,** 509–516 (2002).

134. Kügler, S. *et al.* Neuron-Specific Expression of Therapeutic Proteins: Evaluation of Different Cellular Promoters in Recombinant Adenoviral Vectors. *Mol. Cell. Neurosci.* **17,** 78–96 (2001).

135. Horn, T. & Klein, J. Lactate levels in the brain are elevated upon exposure to volatile anesthetics: A microdialysis study. *Neurochem. Int.* **57,** 940–947 (2010).

136. Boretius, S., Tammer, R., Michaelis, T., Brockmöller, J. & Frahm, J. Halogenated volatile anesthetics alter brain metabolism as revealed by proton magnetic resonance spectroscopy of mice in vivo. *NeuroImage* **69,** 244–255 (2013).

137. Dash, M. B., Bellesi, M., Tononi, G. & Cirelli, C. Sleep/wake dependent changes in cortical glucose concentrations. *J. Neurochem.* **124,** 79–89 (2013).

138. Naylor, E. *et al.* Lactate as a Biomarker for Sleep. *Sleep* **35,** 1209–1222 (2012).

139. Histed, M. H., Bonin, V. & Reid, R. C. Direct Activation of Sparse, Distributed Populations of Cortical Neurons by Electrical Microstimulation. *Neuron* **63,** 508–522 (2009).

140. Klein, J. R. & Olsen, N. S. Distribution of Intravenously Injected Glutamate, Lactate, Pyruvate, and Succinate Between Blood and Brain. *J. Biol. Chem.* **167,** 1–5 (1947).

141. Nehlig, A., Wittendorp-Rechenmann, E. & Lam, C. D. Selective Uptake of [14C]2-Deoxyglucose by Neurons and Astrocytes: High-Resolution Microautoradiographic Imaging by Cellular 14C-Trajectography Combined With Immunohistochemistry. *J. Cereb. Blood Flow Metab.* **24,** 1004–1014 (2004).

142. Fellows, L. K., Boutelle, M. G. & Fillenz, M. Extracellular Brain Glucose Levels Reflect Local Neuronal Activity: A Microdialysis Study in Awake, Freely Moving Rats. *J. Neurochem.* **59,** 2141–2147 (1992).

143. Carl-Heinrik, R. Intracerebral Microdialysis in Clinical Practice: Baseline V... : Neurosurgery. *LWW* Available at:

http://journals.lww.com/neurosurgery/Fulltext/2000/09000/Intracerebral_Microdialysis_in_Clinical_Practice_.35.aspx. (Accessed: 23rd November 2014)

144. Hertz, L. Astrocytic energy metabolism and glutamate formation–relevance for 13C-NMR spectroscopy and importance of cytosolic/mitochondrial trafficking. *Magn. Reson. Imaging* (2011).

145. Weber, B., Jolivet, R., Wyss, M. T. & Buck, A. in *Neural Metabolism In Vivo* (eds. Choi, I.-Y., Gruetter, R. & Lajtha, A.) **4,** 993–1003 (Springer US, 2012).

146. Sokoloff, L. *et al.* The [14c]deoxyglucose Method for the Measurement of Local Cerebral Glucose Utilization: Theory, Procedure, and Normal Values in the Conscious and Anesthetized Albino Rat1. *J. Neurochem.* **28,** 897–916 (1977).

147. Simpson, I. A., Carruthers, A. & Vannucci, S. J. Supply and demand in cerebral energy metabolism: the role of nutrient transporters. *J. Cereb. Blood Flow Metab.* **27,** 1766–1791 (2007).

148. Bélanger, M., Allaman, I. & Magistretti, P. J. Brain Energy Metabolism: Focus on Astrocyte-Neuron Metabolic Cooperation. *Cell Metab.* **14,** 724–738 (2011).

149. Véga, C., Martiel, J.-L., Drouhault, D., Burckhart, M.-F. & Coles, J. A. Uptake of locally applied deoxyglucose, glucose and lactate by axons and schwann cells of rat vagus nerve. *J. Physiol.* **546,** 551–564 (2003).

150. Harris, J. J., Jolivet, R. & Attwell, D. Synaptic Energy Use and Supply. *Neuron* **75,** 762–777 (2012).

151. Chuquet, J., Quilichini, P., Nimchinsky, E. A. & Buzsáki, G. Predominant enhancement of glucose uptake in astrocytes versus neurons during activation of the somatosensory cortex. *J. Neurosci.* **30,** 15298–15303 (2010).

152. Barros, L. F. Towards Single-Cell Real-Time Imaging of Energy Metabolism in the Brain. *Front. Neuroenergetics* **2,** (2010).

153. Schurr, A. Lactate, glucose and energy metabolism in the ischemic brain (Review). *Int. J. Mol. Med.* (2002). doi:10.3892/ijmm.10.2.131

154. Wyss, M. T., Jolivet, R., Buck, A., Magistretti, P. J. & Weber, B. In Vivo Evidence for Lactate as a Neuronal Energy Source. *J. Neurosci.* **31,** 7477–7485 (2011).

155. Glenn, T. C. *et al.* Lactate: Brain Fuel in Human Traumatic Brain Injury: A Comparison with Normal Healthy Control Subjects. *J. Neurotrauma* **32,** 820–832 (2015).

156. Bolaños, J. P., Almeida, A. & Moncada, S. Glycolysis: a bioenergetic or a survival pathway? *Trends Biochem. Sci.* **35,** 145–149 (2010).

157. Porras, O. H., Ruminot, I., Loaiza, A. & Barros, L. F. Na+-Ca2+ cosignaling in the stimulation of the glucose transporter GLUT1 in cultured astrocytes. *Glia* **56,** 59–68 (2008).

158. Porras, O. H., Loaiza, A. & Barros, L. F. Glutamate Mediates Acute Glucose Transport Inhibition in Hippocampal Neurons. *J. Neurosci.* **24,** 9669–9673 (2004).

159. Stuart, C. A. *et al.* Brain glucose transporter (Glut3) haploinsufficiency does not impair mouse brain glucose uptake. *Brain Res.* **1384,** 15–22 (2011).

160. Herrero-Mendez, A. *et al.* The bioenergetic and antioxidant status of neurons is controlled by continuous degradation of a key glycolytic enzyme by APC/C–Cdh1. *Nat. Cell Biol.* **11,** 747–752 (2009).

161. Volkenhoff, A. *et al.* Glial Glycolysis Is Essential for Neuronal Survival in Drosophila. *Cell Metab.* **22,** 437–447 (2015).

162. Herzog, R. I. *et al.* Lactate preserves neuronal metabolism and function following antecedent recurrent hypoglycemia. *J. Clin. Invest.* **123,** 1988–1998 (2013).

163. Weber, B. & Barros, L. F. The Astrocyte: Powerhouse and Recycling Center. *Cold Spring Harb. Perspect. Biol.* a020396 (2015). doi:10.1101/cshperspect.a020396

164. Iadecola, C. & Nedergaard, M. Glial regulation of the cerebral microvasculature. *Nat Neurosci* **10,** 1369–1376 (2007).

165. Barros, L. F., Porras, O. H. & Bittner, C. X. Why glucose transport in the brain matters for PET. *Trends Neurosci.* **28,** 117–119 (2005).

166. Magistretti, P. J. & Allaman, I. A Cellular Perspective on Brain Energy Metabolism and Functional Imaging. *Neuron* **86,** 883–901 (2015).

167. Hutchinson, L. Imaging: Novel glucose uptake imaging method. *Nat. Rev. Clin. Oncol.* **10,** 488–488 (2013).

168. Mächler, P. *et al.* In Vivo Evidence for a Lactate Gradient from Astrocytes to Neurons. *Cell Metab.* **0,**

169. Kasparov, S. Are Astrocytes the Pressure-Reservoirs of Lactate in the Brain? *Cell Metab.* **23,** 1–2 (2016).

170. Lee, Y. *et al.* Oligodendroglia metabolically support axons and contribute to neurodegeneration. *Nature* **487,** 443–448 (2012).